Nonlinear Static and Transient Analysis of Generally Laminated Beams

by

Andreas W. Obst

Thesis submitted to the Faculty of the

Virginia Polytechnic Institute and State University

in partial fulfillment of the requirements for the degree of

MASTER OF SCIENCE

in

Aerospace Engineering

APPROVED:

Rakesh K. Kapania, Chair

Eric R. Johnson

Efstratios Nikolaidis

Junuthula N. Reddy

December, 1991

Blacksburg, Virginia

NONLINEAR STATIC AND TRANSIENT ANALYSIS OF GENERALLY LAMINATED BEAMS

by

Andreas W. Obst

Rakesh K. Kapania

(Department of Aerospace and Ocean Engineering)

(ABSTRACT)

In this study two one-dimensional finite element formulations based on higher-order displacement models have been developed. Both theories account for geometric nonlinearities, a parabolic shear strain distribution through the thickness, and satisfy the shear stress free boundary conditions at the upper and lower surfaces of the beam. The theories also account for the bend-stretch, shear-stretch, and bend-twist couplings inherent to generally laminated composite beams. Further, a coupling between the shear deformation and the twisting is introduced. The lateral strains are assumed nonzero and retained in the formulation.

The first model termed SVHSDT also accounts for the continuity of the inter-laminar shear stresses at the layer interfaces, while keeping the number of degrees of freedom independent of the number of layers. This theory though is restricted

to the analysis of symmetrically laminated cross-ply beams. The formulation has been applied to the linear static and free vibration analysis.

The second model termed RHSDT is valid for generally laminated beams. This model has been applied to the nonlinear static and transient analysis of generally laminated beams, free vibration analysis, and impact analysis. The effect of axial stresses on the nonlinear transient response has also been investigated using this theory.

For generally laminated beams the lateral strains and the shear-twist coupling were found to have a significant effect on the vibrations frequencies. Also, as expected, initial stresses, boundary conditions and the lamination scheme were found to have a significant effect on the nonlinear responses.

Acknowledgements

The author wishes to thank his committee, Dr. E. R. Johnson, Dr. E. Nikolaidis, Dr. J. N. Reddy, and especially his advisor, Dr. R. K. Kapania, for their encouragement and suggestions. The financial support from the Department of Aerospace and Ocean Engineering at Virginia Polytechnic Institute and State University throughout this work is greatly appreciated.

Table of Contents

List of Figures

List of Tables

1. Introduction

Laminated composite materials are used increasingly in aerospace, automotive and naval structures. With their high specific modulus, high specific strength, and their capability of being tailored for specific applications, these materials offer significant advantages compared to traditionally used materials. One important class of structural components made of composite materials are composite beams. Among those symmetrically laminated beams are the most commonly used. However, for some applications like jet turbine fan blades, plate stiffeners, and rotor blades with self adjusting angle of attack the use of asymmetric laminates is considered. Further, asymmetric laminates may result from delaminations and surface damages in composite structures. To best tailor the composite material for a specific application usually requires the use of angle-ply laminates. Thus, composite structures tailored to best serve an application may experience bend-stretch, shear-stretch and bend-twist couplings. These couplings may alter the response of composite structures significantly and thus have to be considered in the analysis of composite structures. A detailed description of the couplings can be found in the work by Raciti and Kapania [1], who developed a finite element based on the first order shear deformation theory that accounts for all the above couplings.

Another important aspect in the analysis of composite structures is the shear deformation. The classical lamination theory, which assumes that normals to the midplane before deformation remain straight and normal to the plane after deformation and thus neglects transverse shear deformation (equivalent to assuming

infinite rigidity in transverse shear), underpredicts deflections and overpredicts natural frequencies. The elasticity solution of Pagano [2] for cylindrical bending of composite beams reveals that the assumptions of the normals remaining normal and straight does not hold for short and moderately short beams. Commonly the first order shear deformation theory is used to account for the shear deformation in structures. However, this theory assumes a constant distribution of the transverse shear through the thickness. This requires a shear correction factor to account for the deviation from the actual parabolic shear strain distribution. But this shear correction factor depends on the geometry of the beam and vibration frequencies and thus can not be uniquely determined. An overview of other theories accounting for shear effects is given by Kapania and Raciti [3].

The current study extends the work by Raciti and Kapania [1] to account for the transverse shear by using higher order shear deformation theories. The advantage of higher order shear deformation theories is that the parabolic distribution of the transverse shear strain through the thickness is accounted for and thus the need of the spurious shear correction factor is eliminated. Also, the stress free boundary conditions at the upper and lower surface of the beam are satisfied directly. Further, a coupling between shear deformation and twisting is introduced which will be shown to be important in the analysis of angle-ply beams.

Higher order shear deformation theories have first been used in the analysis of laminated plates. In 1984 Reddy [4] derived a variationally consistent higher order theory based on a cubic expansion of the inplane displacements . In a recent paper

Reddy [5] reviewed all two-dimensional third-order theories and established their equivalence. He showed that all third order theories published in the last decade are based on the same displacement field and thus are a special case of the theory derived by Reddy in 1984. Bhaskar and Varadan [6] and Savithri and Varadan [7] extended the third order theory of Reddy [4] to account for the continuity of the transverse shear stresses at the layer interfaces. Their theory also accounts for the characteristic slope discontinuities of the inplane displacements at the layer interfaces. The theories derived in the present study are based on the displacement fields proposed by Reddy [4] and Savithri and Varadan [7].

Two approaches to reduce two-dimensional theories to one-dimensional theories are commonly used. In the first approach the lateral displacement components are simply neglected. This results in zero lateral strains and curvatures. Thus, the shear-stretch and bend-twist coupling are not accounted for and the theory is restricted to the analysis of cross-ply beams. This approach was used by Heyliger and Reddy [8] for isotropic beams, by Ghazavi and Gordaninejad [9] and Gordaninejad and Ghazavi [10] for cross-ply beams, and by Kant and Manjunatha [11] and Kant and Patil [12] for asymmetrically laminated cross-ply beams. Chandrashekhara et al. [13] also used this approach for the free vibration of angle-ply beams, but as will be shown subsequently the predicted frequencies using this type of theory may be erroneous.

The second approach to reduce a two-dimensional theory to a one-dimensional one is to derive the equations for the laminate resultant forces from a two-

dimensional displacement field and then to equate the lateral resultant forces to zero. Thus, the lateral strains and curvatures can be expressed in terms of the axial and transverse strains and curvatures and the characteristic couplings are not lost. This approach is used in the present study. It also was used by Chen and Yang [14] for symmetric laminates and by Raciti and Kapania [1] for generally laminated beams. However, these studies used the first order shear deformation theory. In a very recent paper Singh et al. [15] used a similar approach as taken in the present study for their study of the nonlinear free vibration of asymmetric composite beams. However, they did not include the shear deflection in the nonlinear strain terms and did not account for initial stresses in their formulation.

Only few authors studied the nonlinear response of composite beams. Among those Raciti and Kapania [1] and Singh et al. [15] investigated the nonlinear free vibration of asymmetric beams. Ghazavi and Gordaninejad [9] and Sun and Chin [16] studied the nonlinear bending of cross-ply beams and Sensmeier et al. [17] studied the axial impact of beams. The nonlinear transient response of composite plates has been studied by Reddy [18] using the first order shear deformation theory, but no references were found on the nonlinear transient response of asymmetric composite beams including the impact response.

The free vibration of composite beams and the impact of composite beams have been studied extensively by a number of authors. Reference to a number of these investigators is given when the results are discussed in Chapter 5. Also, Kapania and Raciti [19] give a thorough review of free vibration studies and Abrate [20] gives

a review of recent developments in the impact analysis of beams and plates. These papers should be consulted for further references on theses subjects.

The higher order theories derived in this study can be summarized as follows:

1. A consistent strain higher order theory based on the displacement field proposed by Reddy [4] that accounts for nonzero lateral strains and retains all of the characteristic couplings experienced by laminated beams, subsequently called *RHSDT*.
2. A transverse shear stress continuity theory based on a displacement field proposed by Savithri and Varadan [7] that accounts for nonzero lateral strains, but is restricted to the analysis of symmetric beams, subsequently called *SVHSDT*.

Both theories account for geometric nonlinearities by using the von Kármán strains in the derivation.

In Chapter 2, a general derivation of the finite element equations is given and the solution procedures for the different problem statements are discussed. In Chapter 3, the consistent strain third-order theory (RHSDT) is adapted for beams, and in Chapter 4 the same is done for the SVHSDT. Results for the different problem are presented in Chapter 5. First in Section 5.1 results for the linear and nonlinear static problems are presented, then in Section 5.2 the free vibration results are discussed, and then in Section 5.3 the results for the linear and nonlinear transient analysis and the impact analysis are given. Finally, in Chapter 6 conclusions are drawn and recommendations for future work are made.

2. General Derivation of the Finite Element Equations

In this chapter the general derivation of the finite element equations is presented independent of the beam theories. In Section 2.1 the equations for the linear problem are derived. The equations for the nonlinear static and dynamic problem are summarized in Section 2.2, and in Section 2.3 the initial stress matrix is derived. In Sections 2.4, 2.5, and 2.6 the solution procedures for the linear, the nonlinear, and the impact problem, respectively, are presented. Finally, in Section 2.7 a postprocessor to calculate the interlaminar shear stresses is described.

The dimensions of the beam and the coordinate system are shown in Figure 2.1. The coordinates x, y, and z are the axial, the lateral, and the transverse coordinate, respectively. The beam is of length L, height h, and width b. The orientation θ of the individual layers is measured from the x-axis as indicated in Figure 2.1. The lamination scheme for a typical laminate is shown in Figure 2.2. The laminate consists of N layers of orthotropic material. Material properties, orientation and thickness of the individual layers may be different. The element coordinates for a typical element are defined in Figure 2.3. The nodes and elements are numbered consecutively beginning with "1" at $x = 0$. A typical mesh consists of n elements and $n + 1$ nodes. The length l_e of the individual elements may be different.

2.1. Equations of Motion for the Linear Problem

To derive the equations of motion for each of the beam theories an appropriate displacement field of the form

$$\{u(x,y,z,t)\}^T = \{u_1(x,y,z,t), u_2(x,y,z,t), u_3(x,y,z,t)\} \tag{2.1}$$

is assumed, where u_1, u_2, and u_3 denote the displacements in the x, y, and z-direction, respectively. The linear stress-strain relations are

$$\begin{aligned}
\epsilon_1 &= \frac{\partial u_1}{\partial x} \\
\epsilon_2 &= \frac{\partial u_2}{\partial y} \\
\epsilon_3 &= \frac{\partial u_3}{\partial z} \\
\epsilon_4 &= \frac{\partial u_3}{\partial y} + \frac{\partial u_2}{\partial z} \\
\epsilon_5 &= \frac{\partial u_3}{\partial x} + \frac{\partial u_1}{\partial z} \\
\epsilon_6 &= \frac{\partial u_1}{\partial y} + \frac{\partial u_2}{\partial x}.
\end{aligned} \tag{2.2}$$

The general form of the constitutive equations is

$$\{\sigma\} = [C]\{\epsilon\} \tag{2.3}$$

where $[C]$ is the matrix of the transformed laminae stiffnesses and $\{\sigma\}$ and $\{\epsilon\}$ are the transformed stresses and strains, respectively.

To derive the equations of motion, the Hamilton variational principle is used. For the discretized structure this principle can be written as

$$\sum_{e=1}^{n} \int_{t_1}^{t_2} \delta(\Pi^{(e)} - T^{(e)})\, dt = 0 \tag{2.4}$$

where $\Pi^{(e)}$ is the total potential energy and $T^{(e)}$ is the kinetic energy of element e. The total potential energy for an element is

$$\Pi^{(e)} = U^{(e)} - W^{(e)} = \frac{1}{2} \int_v \{\epsilon\}^T \{\sigma\}\, dv - \int_\Omega \{u\}^T \{P\}\, dA \tag{2.5}$$

where U is the strain energy, W represents the work done by the externally applied forces, and $\{P\}$ is the force vector corresponding to the directions x, y, and z, and v is the volume of the element. The kinetic energy for an element can be written as

$$T^{(e)} = \frac{1}{2} \int_v \rho\, \{\dot{u}\}^T \{\dot{u}\}\, dv \tag{2.6}$$

where ρ is the density of the material and $\dot{(\ )} = d(\ )/dt$. Assume that the displacement field in equation (2.1) is given as an explicit expansion in the transverse and lateral coordinates. Then, carrying out the integrations through the thickness and over the lateral coordinate in equations (2.5) and (2.6) the total potential energy $\Pi^{(e)}$ and the kinetic energy $T^{(e)}$ become

$$\begin{aligned} \Pi^{(e)} &= \frac{b}{2} \int_{\ell_e} \{\hat{\epsilon}\}^T \{N\}\, dx - b \int_{\ell_e} \{q\}^T \{\hat{F}\}\, dx \\ T^{(e)} &= \frac{b}{2} \int_{\ell_e} \{\dot{q}\}^T [m] \{\dot{q}\}\, dx \end{aligned} \tag{2.7}$$

where $\{q\}$ and $\{\hat{\epsilon}\}$ denote the generalized displacements and strains, respectively; $\{N\}$ and $\{\hat{F}\}$ are the resultant forces corresponding to $\{\hat{\epsilon}\}$ and the externally applied forces corresponding to $\{q\}$, respectively; and $[m]$ denotes the inertia matrix. The resultant forces $\{N\}$ are related to the generalized strains $\{\hat{\epsilon}\}$ through the laminate stiffness matrix $[D]$, i.e.,

$$\{N\} = [D]\{\hat{\epsilon}\}. \tag{2.8}$$

Introducing the linear operator $[L]$ the generalized strains can be related to the generalized displacements as

$$\{\hat{\epsilon}\} = [L]\{q\}. \tag{2.9}$$

The continuous generalized displacements are discretized as

$$\{q\} = [H]\{a\} \tag{2.10}$$

where $\{a\}$ is the vector of the nodal displacements and $[H]$ is the shape function matrix. Substituting equation (2.10) into equation (2.9) , the generalized strains become

$$\begin{aligned} \{\hat{\epsilon}\} &= [L][H]\{a\} \\ &= [B]\{a\} \end{aligned} \tag{2.11}$$

where $[B]$ is the strain displacement matrix. After substitution of equations (2.11) , (2.8) , and (2.7) into equation (2.5) the equation for Hamilton's principle can

be written as

$$0 = b\int_{t_1}^{t_2}\delta\Big(\frac{1}{2}\int_{\ell_e}\{a\}^T[B]^T[D][B]\{a\}\,dx - \int_{\ell_e}\{a\}^T[H]^T\{\hat{F}\}\,dx - \frac{1}{2}\int_{\ell_e}\{\dot{a}\}^T[H]^T[m][H]\{\dot{a}\}\,dx\Big)\,dt. \tag{2.12}$$

Carrying out the variational operation and noting that the nodal displacements $\{a\}$ are independent of the x-coordinate, equation (2.12) becomes

$$0 = b\int_{t_1}^{t_2}\Big(\{\delta a\}^T\int_{\ell_e}[B]^T[D][B]\,dx\,\{a\} - \{\delta a\}^T\int_{\ell_e}[H]^T\{\hat{F}\}\,dx - \{\delta\dot{a}\}^T\int_{\ell_e}[H]^T[m][H]\,dx\,\{\dot{a}\}\Big)\,dt. \tag{2.13}$$

Integration by parts with respect to time of the last term in equation (2.13) results in

$$0 = b\int_{t_1}^{t_2}\{\delta a\}^T\Big(\int_{\ell_e}[B]^T[D][B]\,dx\,\{a\} - \int_{\ell_e}[H]^T\{\hat{F}\}\,dx + \int_{\ell_e}[H]^T[m][H]\,dx\,\{\ddot{a}\}\Big)\,dt. \tag{2.14}$$

Equation (2.14) has to be valid for all times t and for every virtual displacement $\{\delta a\}$. Thus, the element equations of motion can be obtained from equation (2.14) as

$$[K^e]\{a^e\} + [M^e]\{\ddot{a}^e\} = \{F^e\} \tag{2.15}$$

where

$$[K^e] = b\int_{\ell_e} [B]^T[D][B]\,dx \qquad \text{is the element stiffness matrix,}$$

$$[M^e] = b\int_{\ell_e} [H]^T[m][H]\,dx \qquad \text{is the consistent element mass matrix, and} \tag{2.16}$$

$$\{F^e\} = b\int_{\ell_e} [H]^T\{\hat{F}\}\,dx \qquad \text{is the external element force vector.}$$

The global system of algebraic equations, after assembling the element matrices, is

$$[K]\{a\} + [M]\{\ddot{a}\} = \{F\} \tag{2.17}$$

where the global matrices can be written as a summation of the element matrices as

$$[K] = \sum_{e=1}^{n} [K^e]$$

$$[M] = \sum_{e=1}^{n} [M^e] \tag{2.18}$$

$$\{F\} = \sum_{e=1}^{n} \{F^e\}.$$

This completes the derivation of the general form of the finite element equations for the linear problem.

2.2. Nonlinear Finite Element Equations

In the derivation of the nonlinear finite element equations the same basic steps as for the linear equations are involved. To avoid repeating all of the steps of

the previous section, this section only points out the differences arising from the nonlinear formulation. To account for geometric nonlinearities the stress-strain relations in equation (2.2) are replaced by the von Kármán strains. These are defined as

$$\begin{aligned}
\epsilon_1 &= \frac{\partial u_1}{\partial x} + \frac{1}{2}\left(\frac{\partial u_3}{\partial x}\right)^2 \\
\epsilon_2 &= \frac{\partial u_2}{\partial y} + \frac{1}{2}\left(\frac{\partial u_3}{\partial y}\right)^2 \\
\epsilon_3 &= 0 \\
\epsilon_4 &= \frac{\partial u_3}{\partial y} + \frac{\partial u_2}{\partial z} \\
\epsilon_5 &= \frac{\partial u_3}{\partial x} + \frac{\partial u_1}{\partial z} \\
\epsilon_6 &= \frac{\partial u_1}{\partial y} + \frac{\partial u_2}{\partial x} + \frac{\partial u_3}{\partial x}\frac{\partial u_3}{\partial y}.
\end{aligned} \tag{2.19}$$

Now the relation between the generalized strain vector and the vector of the nodal displacements becomes

$$\{\hat{\epsilon}\} = [B]\{a\} = \left[[B_L] + [B_{NL}(a)]\right]\{a\} \tag{2.20}$$

and the relation between the variation of the strains and the variation of the nodal displacements becomes

$$\{\delta\hat{\epsilon}\} = [B^*]\{\delta a\} = \left[[B_L] + 2\,[B_{NL}(a)]\right]\{\delta a\}. \tag{2.21}$$

Here $[B_L]$ is the same matrix as $[B]$ in equation (2.11) and $[B_{NL}]$ is obtained from the nonlinear parts of equation (2.19) . Note that for the linear case $[B] = [B_L] =$

$[B^*]$. Because for the nonlinear case $[B] \neq [B^*]$ equation (2.14) has to be changed to

$$0 = b \int_{t_1}^{t_2} \{\delta a\}^T \Big(\int_{\ell_e} [B^*]^T [D][B]\, dx\, \{a\} - \int_{\ell_e} [H]^T \{\hat{F}\}\, dx + \int_{\ell_e} [H]^T [m][H]\, dx\, \{\ddot{a}\} \Big)\, dt. \tag{2.22}$$

Thus, the expression for the element stiffness matrix becomes

$$[K^e] = b \int_{\ell_e} [B^*(a)]^T [D][B(a)] dx \tag{2.23}$$

while the expressions for the element mass matrix and the element force vector remain the same as in equation (2.16). The global equations of motion now take the form

$$[K(a)]\{a\} + [M]\{\ddot{a}\} = \{F\}. \tag{2.24}$$

2.3. Initial Stress Matrix

The initial stress matrix due to a distributed axial force has to be considered in a number of problems such as buckling of beams, analysis of initially stressed beams, and beams under selfweight. The work done by a distributed axial force $p(x)$ due to the bending of the beam is given by

$$W_n = \frac{bh}{2} \int_{\ell_e} p(x) \left(\frac{\partial u_3}{\partial x} \right)^2 dx. \tag{2.25}$$

Note that here W_n is assumed to be dependent on the transverse deflection only. The axial force $p(x)$ is positive in tension and negative in compression. Going

through the same procedure as described in Section 2.1 for the stiffness and mass matrix, i.e., taking the variation and discretizing the displacements, the elements of the initial stress matrix corresponding to the transverse displacements can be obtained as

$$K_{ij}^{s} = bh \int_{\ell_e} p(x) \frac{dH_i}{dx} \frac{dH_j}{dx} dx. \tag{2.26}$$

For the analysis of initially stressed beams or beams under selfweight the terms in the initial stress matrix can simply be added to the corresponding terms of the element stiffness matrix. No changes in the solution procedures are necessary.

2.4. Solution of the Linear Problem

1. *Linear Static Problem*

For the linear problem equation (2.17) reduces to

$$[K]\{a\} = \{F\}. \tag{2.27}$$

This system of linear algebraic equations can be solved using any available linear equation solver. In this study the element stiffness matrices are assembled so that $[K]$ is a symmetric banded matrix and a subroutine as given by Reddy [21] is used to solve the equations.

2. *Free Vibration Analysis*

If no forcing term exists equation (2.17) reduces to

$$[M]\{\ddot{a}\} + [K]\{a\} = 0. \tag{2.28}$$

This equation is solved as outlined by Zienkiewicz [22]. The general solution of equation (2.28) is of the form

$$\{a\} = \{\bar{a}\}e^{i\omega t}. \tag{2.29}$$

Upon substitution of equation (2.29) into equation (2.28) the familiar eigenvalue problem

$$\left([K] - \omega^2[M]\right)\{\bar{a}\} = \{0\} \tag{2.30}$$

is obtained. The solution of this problem yields n characteristic values of ω^2 and the corresponding eigenvectors $[\bar{a}]$, where n is the dimension of the matrices $[K]$ and $[M]$. The characteristic values ω are the natural frequencies of the system and the eigenvectors are the corresponding natural modes. Equation (2.30) is solved using the *IMSL* [23] routine *DGVLRG*. This routine returns the eigenvectors in a normalized form so that

$$\{\bar{a}\}^T[M]\{\bar{a}\} = 1 \tag{2.31}$$

for each eigenvector.

3. *Linear Dynamic Problem*

The governing equation for the linear dynamic problem is

$$[M]\{\ddot{a}(t)\} + [K]\{a(t)\} = \{F(t)\}. \tag{2.32}$$

The Newmark-Direct Integration method as described by Reddy [21] is used to solve this equation. If the displacement $\{u\}_s$, the velocity $\{\dot{u}\}_s$, and the acceleration $\{\ddot{u}\}_s$

at time t_s are known the displacement at time t_{s+1} can be approximated as

$$\begin{aligned}
\{u\}_{s+1} &= \{u\}_s + \Delta t\,\{\dot{u}\}_s + \frac{(\Delta t)^2}{2}\{\ddot{u}\}_{s+\gamma} \\
\{\dot{u}\}_{s+1} &= \{\dot{u}\}_s + \Delta t\,\{\ddot{u}\}_{s+\alpha} \\
\{\ddot{u}\}_{s+\theta} &= (1-\theta)\{\ddot{u}\}_s + \theta\,\{\ddot{u}\}_{s+1}.
\end{aligned} \tag{2.33}$$

Appropriate selection of the coefficients α and γ yields several well known time integration schemes:

$$\begin{aligned}
&\alpha = \frac{1}{2}, \gamma = \frac{1}{2} && \text{constant-average acceleration method (stable)} \\
&\alpha = \frac{1}{2}, \gamma = \frac{1}{3} && \text{linear acceleration method (conditionally stable)} \\
&\alpha = \frac{1}{2}, \gamma = 0 && \text{central difference method (conditionally stable).}
\end{aligned} \tag{2.34}$$

The critical timestep for the conditionally stable schemes is

$$\Delta t_{cr} = (\frac{1}{2}\omega_{max}^2[\alpha - \gamma])^{-\frac{1}{2}} \qquad \alpha \geq \frac{1}{2}, \quad \gamma \leq \alpha \tag{2.35}$$

where ω_{max} is the maximum natural frequency of the discretized system. Substitution of equation (2.33) into equation (2.32) results in the following time marching scheme:

$$[\hat{K}]_{s+1}\{u\}_{s+1} = \{\hat{F}\}_{s+1} \tag{2.36}$$

where

$$\begin{aligned}
[\hat{K}]_{s+1} &= [K]_{s+1} + a_3[M]_{s+1} \\
\{\hat{F}\}_{s+1} &= \{F\}_{s+1} + [M]_{s+1}\,(a_3\{u\}_s + a_4\{\dot{u}\}_s + a_5\{\ddot{u}\}_s)
\end{aligned} \tag{2.37}$$

and

$$a_3 = \frac{2}{\gamma(\Delta t)^2} \qquad a_4 = \Delta t\, a_3 \qquad a_5 = \frac{\gamma - 1}{\gamma}. \tag{2.38}$$

Note that the operations in equation (2.37) should be carried out at the element level. Equation (2.36) can be solved for the displacements at time t_{s+1} and then the velocity and acceleration at t_{s+1} can be calculated as

$$\begin{aligned} \{\ddot{u}\}_{s+1} &= a_3\left(\{u\}_{s+1} - \{u\}_s\right) - a_4\{\dot{u}\}_s - a_5\{\ddot{u}\}_s \\ \{\dot{u}\}_{s+1} &= \{\dot{u}\}_s + a_2\{\ddot{u}\}_s + a_1\{\ddot{u}\}_{s+1} \\ a_1 &= \alpha\,\Delta t \qquad a_2 = (1-\alpha)\Delta t. \end{aligned} \tag{2.39}$$

For the first time step the initial conditions $\{u\}_0$, $\{\dot{u}\}_0$, and $\{\ddot{u}\}_0$ need to be known. If either the displacement or the forcing term are nonzero at t_0 the initial acceleration can be obtained as

$$\{\ddot{u}\}_0 = [M]^{-1}\left(\{F(0)\} - [K]\{u\}_0\right). \tag{2.40}$$

2.5. Solution of the Nonlinear Problem

1. *Nonlinear Static Solution*

The general equation for the nonlinear static problem is

$$\left[K\left(\{a\}\right)\right]\{a\} = \{F\}. \tag{2.41}$$

The Newton-Raphson method as described by Reddy [21] is used to solve this system of equations. Equation (2.41) can be rewritten as

$$\left\{R\left(\{a\}\right)\right\} = \left[K\left(\{a\}\right)\right]\{a\} - \{F\} = 0 \tag{2.42}$$

where $\{R(\{a\})\}$ is the residual vector.

Suppose that the solution is known at the r-th iteration and we seek the solution at the $(r+1)$ st iteration. To find this solution $\{R(\{a\})\}$ is expanded into a Taylor series about the known solution $\{a\}^r$. If the higher order terms are neglected this series can be written as

$$\left\{R(\{a\}^{r+1})\right\} = \left\{R(\{a\}^r)\right\} + \left(\frac{\partial\{R\}}{\partial\{a\}}\right)\Big|_{\{a\}^r} \delta\{a\} = 0$$

or (2.43)

$$\left\{R(\{a\}^{r+1})\right\} = \left\{R(\{a\}^r)\right\} + \left[K^{Tan}(\{a\}^r)\right]\delta\{a\} = 0$$

where $\left[K^{Tan}(\{a\}^r)\right]$ is the tangential stiffness matrix. Equation (2.43) can be solved for the increment $\delta\{a\}$

$$\delta\{a\} = -\left[K^{Tan}(\{a\}^r)\right]^{-1}\left\{R(\{a\}^r)\right\} \tag{2.44}$$

and then the solution at the $(r+1)$ st iteration can be obtained as

$$\{a\}^{r+1} = \{a\}^r + \delta\{a\}. \tag{2.45}$$

The iteration is continued until the convergence criterion

$$\sqrt{\frac{\sum(a_i^{r+1} - a_i^r)^2}{\sum(a_i^{r+1})^2}} < \epsilon \tag{2.46}$$

is satisfied.

2. *Nonlinear Dynamic Solution*

The governing equation for the nonlinear dynamic problem is of the form

$$[M]\{\ddot{a}\} + [K(a)]\{a\} = \{F(t)\}. \tag{2.47}$$

To solve this equation the time-approximation scheme from Section 2.4.3. and the Newton-Raphson method are combined as described by Reddy [21]. Suppose that the converged solution at time t_s, i.e., $\{a\}_s$, and the solution of the r-th iteration at time t_{s+1}, i.e., $\{a\}^r_{s+1}$, are known. Then equation (2.47) becomes, after applying the time approximation scheme

$$\left[\hat{K}\left(\{a\}^r_{s+1}\right)\right]\{a\}^r_{s+1} = \{\hat{F}\}_{s+1} \tag{2.48}$$

where

$$\begin{aligned} \left[\hat{K}\left(\{a\}^r_{s+1}\right)\right] &= \left[K\left(\{a\}^r_{s+1}\right)\right] + a_3[M] \\ \{\hat{F}\} &= \{F\}_{s+1} + [M]\left(a_3\{a\}_s + a_4\{\dot{a}\}_s + \{\ddot{a}\}_s\right). \end{aligned} \tag{2.49}$$

Note that $\{\hat{F}\}$ is calculated using the converged solution at time t_s. To find the solution at the $(r+1)$st iteration the Newton-Raphson procedure is applied to equation (2.48) . The residual is

$$\{R\}^r_{s+1} = \left[\hat{K}\left(\{a\}^r_{s+1}\right)\right]\{a\}^r_{s+1} - \{\hat{F}\} = 0 \tag{2.50}$$

and the tangent stiffness matrix is

$$\left[\hat{K}^{Tan}\left(\{a\}^r_{s+1}\right)\right] = \left(\frac{\partial\{R\}}{\partial\{a\}}\right)^r_{s+1}. \tag{2.51}$$

Then the equation

$$[\hat{K}^{Tan}(\{a\}_{s+1}^{r})]\delta\{a\}_{s+1}^{r} = -\{R\}_{s+1}^{r} \tag{2.52}$$

can be solved for the increment $\delta\{a\}_{s+1}^{r}$ and the solution at the $(r+1)$ st iteration becomes

$$\{a\}_{s+1}^{r+1} = \{a\}_{s+1}^{r} + \delta\{a\}_{s+1}^{r}. \tag{2.53}$$

The iteration is continued until the convergence criterion in equation (2.46) is satisfied. Once the converged solution is obtained the iteration for the next timestep can be started.

2.6. Impact Analysis

In this study the impact analysis of isotropic and composite beams is considered. When a beam is impacted by a mass, the beam receives an impulsive force which is the contact force between the mass and the beam. This contact force is the primary unknown in the impact problem. The impact response of the beam depends on a good estimate of the contact force throughout the impact duration. The contact force in turn depends on the indentation of the beam which depends on the deflection. The indentation $\alpha(t)$ can be expressed in terms of the displacement of the mass $v(t)$ and the displacement of the beam at the impact point $w(x_0, t)$, as

$$\alpha(t) = v(t) - w(x_0, t). \tag{2.54}$$

An algorithm similar to the one discussed by Sun and Huang [24] has been implemented to calculate the contact force history and the beam response throughout

the impact duration. In general the contact force is a function of indentation, i.e.,

$$ContactForce = F\big(\alpha(t)\big). \tag{2.55}$$

The equation of motion governing the impacting mass is given by

$$m_s\ddot{v} = -F\big(\alpha(t)\big). \tag{2.56}$$

Assume that at time t_s the deflection, velocity, and acceleration of the mass, i.e., v_s, $\dot{v}_s$, and $\ddot{v}_s$, and the beam, i.e., $w_s(x_0)$, $\dot{w}_s(x_0)$, and $\ddot{w}_s(x_0)$, are known. Then the deflection of the mass and the beam at time t_{s+1} can be approximated by

$$v_{s+1} = v_s + \Delta t\dot{v}_s + \frac{1}{2}\Delta t^2\ddot{v}_s$$

and (2.57)

$$w_{s+1}(x_0) = w_s(x_0) + \Delta t\dot{w}_s(x_0) + \frac{1}{2}\Delta t^2\ddot{w}_s(x_0)$$

respectively. Thus the indentation α at time t_{s+1} is estimated by

$$\alpha_{s+1} = v_{s+1} - w_{s+1}(x_0). \tag{2.58}$$

The contact force at time t_{s+1} can now be approximate as

$$F_{s+1} = F(\alpha_{s+1}). \tag{2.59}$$

Using the first approximation to the contact force, more accurate values for the deflection of the mass and the contact force can be obtained by an iterative procedure. This iteration is carried out for fixed displacement, velocity, and acceleration

of the beam. Sun and Huang [24] also iterate on the displacement, velocity, and acceleration of the beam. This requires solving the finite element equations at each iteration, which is computationally inefficient. The difference in the results using both procedures is negligible. Substituting the estimated contact force F_{s+1} in the equation of motion for the mass (2.56) a refined value for the acceleration of the mass can be obtained as

$$\ddot{v}_{s+1} = -\frac{F_{s+1}}{m_s}. \tag{2.60}$$

Then a new approximation for the deflection of the mass can be obtained as

$$v_{s+1} = v_s + \Delta t \dot{v}_s + \frac{1}{6}\Delta t^2(2\ddot{w}_s + \ddot{w}_{s+1}). \tag{2.61}$$

Using this refined approximation a new value for the indentation α_{s+1} in equation (2.58) and then a new estimate of the contact force can be obtained. This iteration is continued until a convergence criterion is met.

In general the force-indentation laws for composite beams have to be determined experimentally. For isotropic beams two laws that have been often used are the Hertzian contact law for elastic impact and a dynamic plastic force-indentation law for impact with permanent indentation.

The Hertzian law for the contact between a sphere and a beam is given by

$$F = k_2 \alpha^{3/2} \tag{2.62}$$

where the contact point spring constant k_2 is given by

$$k_2 = \frac{4}{3} \frac{R_s^{1/2}}{(1-\nu_s^2)/E_s + (1-\nu_b^2)/E_b}. \tag{2.63}$$

Here R_s is the radius of the sphere, ν_s, E_s and ν_b, E_b are the Poisson's ratios and the Young's moduli of the sphere and the beam, respectively.

The dynamic plastic force-indentation law was proposed by Barnhart and Goldsmith [25]. Upon loading, the contact force between the impactor and the beam is determined by the Hertzian contact law in equation (2.62) . Upon unloading, the contact force will be determined from the relation

$$F = F_m \left(\frac{\alpha - \alpha_0}{\alpha_m - \alpha_0} \right)^{3/2} \tag{2.64}$$

where F_m is the maximum impact force just before unloading, α_m is the indentation corresponding to F_m, and α_0 is the permanent indentation. The permanent indentation in general has to be determined experimentally.

Abrate [20] discusses various contact laws for composite laminates used by different authors in his review paper on the impact on composite materials. Specific impact laws used in this study will be given when the example problems are discussed.

2.7. Postprocessor

The postprocessor is used to calculate the inplane stresses and transverse shear stresses. The inplane stresses in a layer can be obtained directly from the constitutive equations for that layer

$$\{\sigma\}^{(k)} = [C]^{(k)} \{\epsilon\}^{(k)} \tag{2.65}$$

where the superscript k refers to the kth lamina. The interlaminar shear stresses have to be calculated by integrating the equilibrium equations of elasticity. The derivation of the interlaminar stress equations for symmetric laminates is given by Bonanni et al. [26]. This derivation has been modified by Byun and Kapania [27] to account for asymmetric laminates. In the following the formulation of Byun and Kapania for the interlaminar shear stresses is summarized. The equilibrium equations for a typical lamina k in the laminate (see Fig. 2.2) are

$$\begin{aligned} \sigma^k_{x,x} + \tau^k_{xy,y} + \tau^k_{xz,z} &= 0 \\ \tau^k_{xy,x} + \sigma^k_{y,y} + \tau^k_{yz,z} &= 0 \end{aligned} \tag{2.66}$$

in which the body forces are neglected. Equations (2.65) are integrated through the thickness from z_k to z_{k+1} to yield

$$\begin{aligned} N^k_{x,x} + N^k_{xy,y} + t^k_2 - t^k_1 &= 0 \\ N^k_{xy,x} + N^k_{y,y} + s^k_2 - s^k_1 &= 0 \end{aligned} \tag{2.67}$$

where the laminate stress resultants are defined as

$$(N_x, N_y, N_{xy})^k = \int_{z_k}^{z_{k+1}} (\sigma_x, \sigma_y, \tau_{xy})^k dz \tag{2.68}$$

and the surface tractions t^k and s^k are defined by

$$\begin{aligned} (t_2, s_2)^k &= (\tau_{xz}, \tau_{yz})^k \qquad \text{at } z = z_{k+1} \\ (t_1, s_1)^k &= (\tau_{xz}, \tau_{yz})^k \qquad \text{at } z = z_k. \end{aligned} \tag{2.69}$$

The continuity equations of the interlaminar stresses for a perfectly bonded laminate are

$$t_2^k = t_1^{k+1} \quad \text{and} \quad s_2^k = s_2^{k+1} \qquad k = 1, 2, \ldots, N-1. \tag{2.70}$$

Using the continuity equations and summing equations (2.67) from the first to the kth lamina of the laminate, expressions for the interlaminar shear stresses at the $(k+1)$st interface are obtained in terms of the derivatives of the inplane lamina resultants. These equations are

$$\begin{aligned} t_2^k &= t_1^k - \Big(\sum_{l=1}^{k} N_{x,y}^l + \sum_{l=1}^{k} N_{xy,y}^l\Big) \\ s_2^k &= s_1^k - \Big(\sum_{l=1}^{k} N_{xy,x}^l + \sum_{l=1}^{k} N_{y,y}^l\Big). \end{aligned} \tag{2.71}$$

The inplane laminate resultants can be obtained from equations (2.8) . But note that the interlaminar shear stresses depend on the derivatives of the laminate resultants and thus on second-order derivatives of the inplane displacements and on third-order derivatives of the transverse displacements. However, these higher order derivatives of the displacements can not directly be obtained from the finite element formulation. To obtain a good approximation of the higher order derivatives the displacement data over the entire domain of the beam is approximated by orthogonal polynomials. The coefficients of the approximation are obtained using a least-squares technique. Details of this derivation are given by Byun and Kapania [27] and are omitted here.

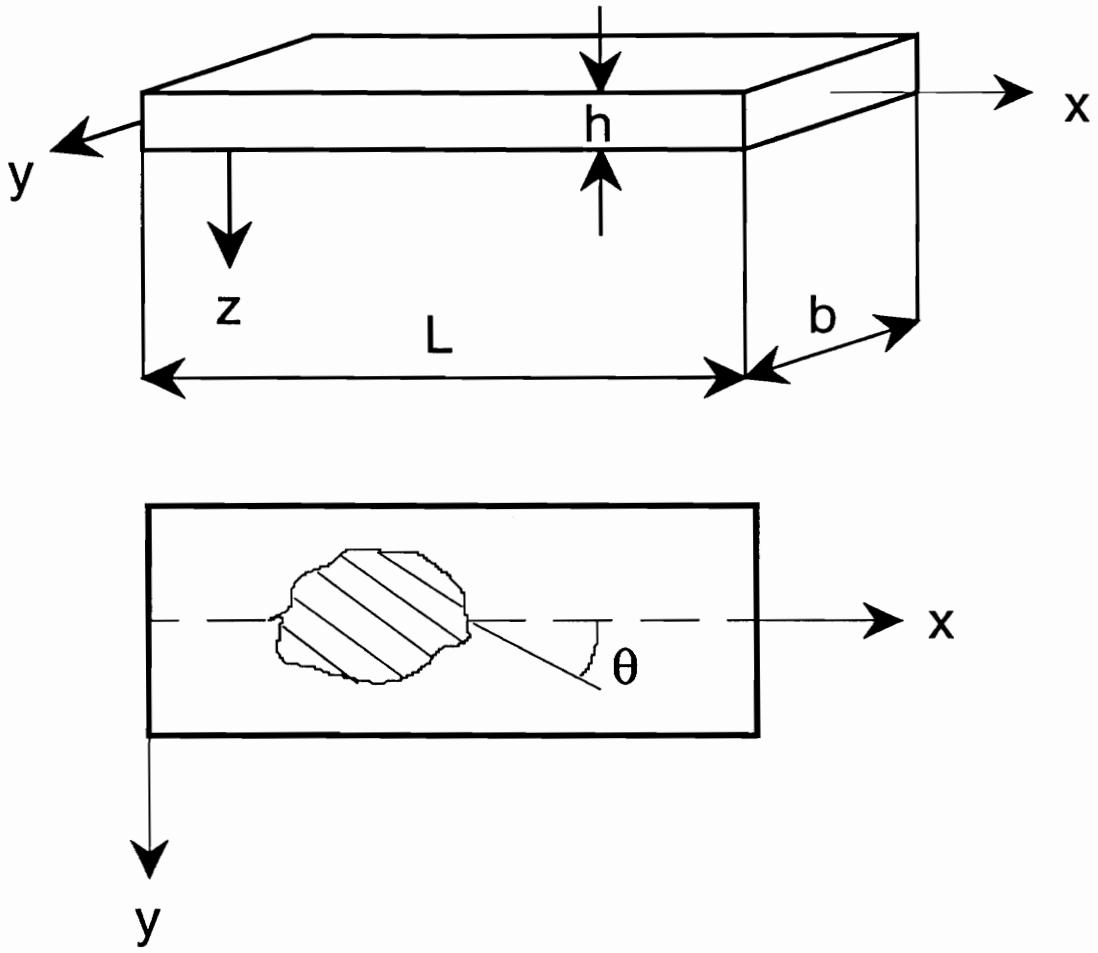

Figure 2.1: *The Coordinate System and Dimensions of the Beam.*

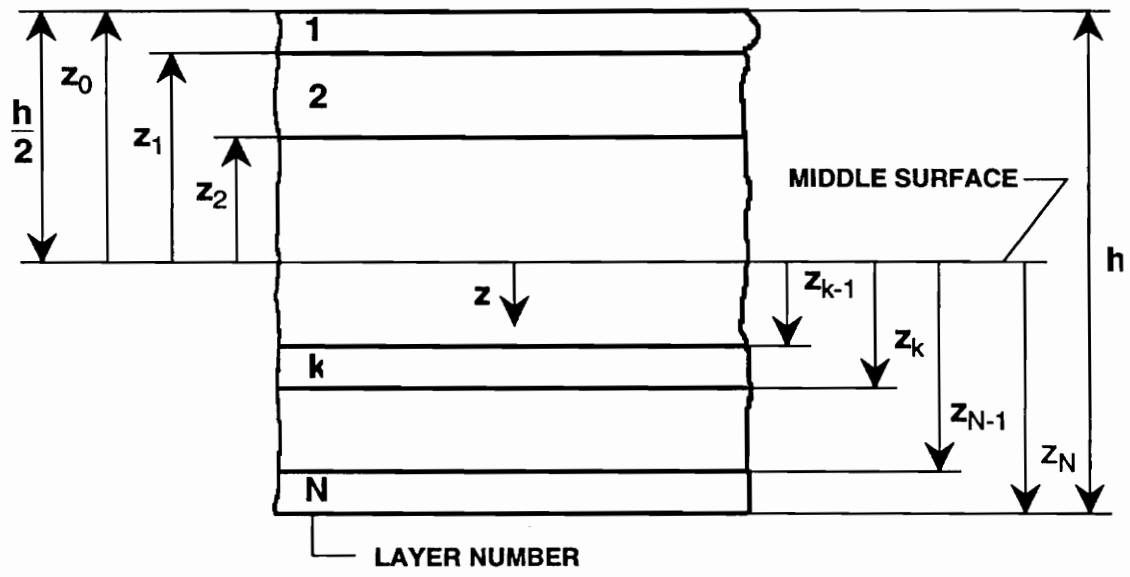

Figure 2.2: *Geometry of a Typical Laminate (from Ref. [28]).*

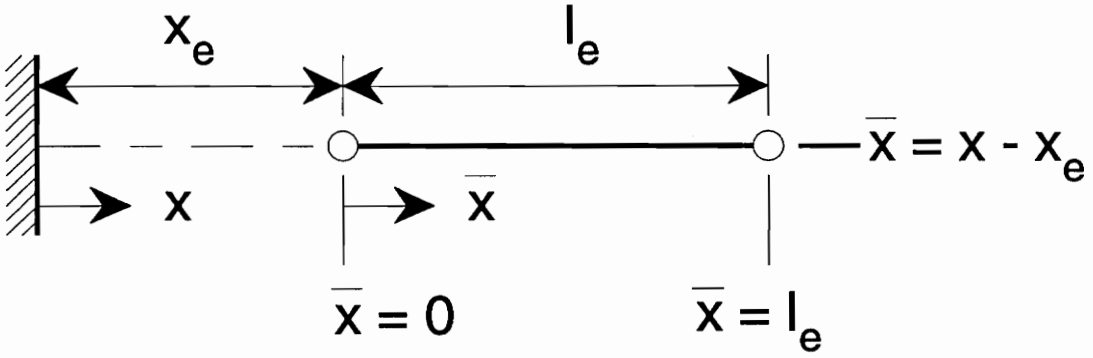

Figure 2.3: *Coordinates of a Typical Element.*

3. Consistent Strain Third Order Theory

As described in the introduction, generally laminated structures may experience bend-stretch coupling, shear-stretch coupling, and bend-twist coupling. Also Poisson-effects may have to be considered to obtain accurate results. In this chapter a general consistent strain third-order theory is derived, which accounts for all of the coupling effects, the Poisson effects and also takes into account the geometric nonlinearities. The equations for the classical lamination theory (CLT) and the first order shear deformation theory (FSDT) can be obtained as special cases of the general theory.

Kinematics

The theory developed in this section is based on a two-dimensional displacement field similar to the one proposed by Reddy [4] for laminated plates. The theory accounts for a parabolic distribution of the shear strains through the thickness and satisfies the condition that the transverse shear stresses vanish at the surfaces of the beam. This requires that the inplane displacements u and v are expanded as cubic functions of the thickness coordinate and the transverse deflection w is constant through the thickness. The assumption of constant w through the thickness can be justified because the transverse normal stress is of the order $(h/L)^2$ times the inplane normal stress. Because of the parabolic variation of the transverse shear strains through the thickness, there is no need to introduce a shear correction coefficient to compute the transverse shear stresses. The displacement field proposed by Reddy

is

$$
\begin{aligned}
u_1 &= u + z\left[\psi_x - \frac{4}{3}\left(\frac{z}{h}\right)^2 \left(\psi_x + \frac{\partial w}{\partial x}\right)\right] \\
u_2 &= v + z\left[\psi_y - \frac{4}{3}\left(\frac{z}{h}\right)^2 \left(\psi_y + \frac{\partial w}{\partial y}\right)\right] \\
u_3 &= w
\end{aligned}
\tag{3.1}
$$

where u and v are the inplane displacements, w is the transverse displacement, and ψ_x and ψ_y are the rotations of the normals to the cross-section. A different form of this displacement can be obtained by using the transformations

$$
w = w_b + w_s, \qquad \psi_x = -\frac{\partial w_b}{\partial x}, \qquad \text{and} \qquad \psi_y = -\frac{\partial w_b}{\partial y} \tag{3.2}
$$

as suggested by Chow [29]. With these transformations the displacement field takes the form

$$
\begin{aligned}
u_1 &= u - z\frac{\partial w_b}{\partial x} - \frac{4z^3}{3h^2}\frac{\partial w_s}{\partial x} \\
u_2 &= v - z\frac{\partial w_b}{\partial y} - \frac{4z^3}{3h^2}\frac{\partial w_s}{\partial y} \\
u_3 &= w_b + w_s
\end{aligned}
\tag{3.3}
$$

where w_b denotes the deflection due bending and w_s denotes the deflection due shear. Note that all displacements can be functions of time t. The von Kármán strains associated with the displacement field in equation (3.3) can be obtained

from equation (2.19) as

$$\begin{aligned}
\epsilon_1 &= \epsilon_1^0 + z\epsilon_1^1 + \frac{4z^3}{3h^2}\epsilon_1^2 \\
\epsilon_2 &= \epsilon_2^0 + z\epsilon_2^1 + \frac{4z^3}{3h^2}\epsilon_2^2 \\
\epsilon_6 &= \epsilon_6^0 + z\epsilon_6^1 + \frac{4z^3}{3h^2}\epsilon_6^2 \\
\epsilon_4 &= \left(1 - \frac{4z^2}{h^2}\right)\epsilon_4^0 \\
\epsilon_5 &= \left(1 - \frac{4z^2}{h^2}\right)\epsilon_5^0
\end{aligned} \tag{3.4}$$

where

$$\begin{aligned}
&\epsilon_1^0 = \frac{\partial u_0}{\partial x} + \frac{1}{2}\left(\frac{\partial u_3}{\partial x}\right)^2 \qquad \epsilon_1^1 = -\frac{\partial^2 w_b}{\partial x^2} \qquad \epsilon_1^2 = -\frac{\partial^2 w_s}{\partial x^2} \\
&\epsilon_2^0 = \frac{\partial v_0}{\partial y} + \frac{1}{2}\left(\frac{\partial u_3}{\partial y}\right)^2 \qquad \epsilon_2^1 = -\frac{\partial^2 w_b}{\partial y^2} \qquad \epsilon_2^2 = -\frac{\partial^2 w_s}{\partial y^2} \\
&\epsilon_6^0 = \frac{\partial u_0}{\partial y} + \frac{\partial v_0}{\partial x} + \frac{\partial u_3}{\partial x}\frac{\partial u_3}{\partial y} \qquad \epsilon_6^1 = -2\frac{\partial^2 w_b}{\partial x \partial y} \qquad \epsilon_6^2 = -2\frac{\partial^2 w_s}{\partial x \partial y} \\
&\epsilon_4^0 = \frac{\partial w_s}{\partial y} \qquad \epsilon_5^0 = \frac{\partial w_s}{\partial x}.
\end{aligned} \tag{3.5}$$

are the generalized strains.

Constitutive Equations

For a laminate of constant thickness h composed of thin layers of orthotropic material, the constitutive equations can be derived as discussed by Vinson and Sierakowsky [30]. Following this derivation, the constitutive equations for a layer

in material coordinates of the layer may be written as

$$\begin{Bmatrix} \sigma_1 \\ \sigma_2 \\ \sigma_6 \end{Bmatrix} = \begin{bmatrix} Q_{11} & Q_{12} & Q_{16} \\ Q_{12} & Q_{22} & 0 \\ 0 & 0 & Q_{66} \end{bmatrix} \begin{Bmatrix} \epsilon_1 \\ \epsilon_2 \\ \epsilon_6 \end{Bmatrix}$$

$$\begin{Bmatrix} \sigma_4 \\ \sigma_5 \end{Bmatrix} = \begin{bmatrix} Q_{44} & 0 \\ 0 & Q_{55} \end{bmatrix} \begin{Bmatrix} \epsilon_4 \\ \epsilon_5 \end{Bmatrix} \tag{3.6}$$

where Q_{ij} are the reduced elastic constants in the material axes of the lamina. Upon transformation, the lamina constitutive equations can be expressed in terms of the stresses and strains in the laminate coordinates as

$$\begin{Bmatrix} \bar{\sigma}_1 \\ \bar{\sigma}_2 \\ \bar{\sigma}_6 \end{Bmatrix} = \begin{bmatrix} \bar{Q}_{11} & \bar{Q}_{12} & \bar{Q}_{16} \\ \bar{Q}_{12} & \bar{Q}_{22} & \bar{Q}_{26} \\ \bar{Q}_{16} & \bar{Q}_{26} & \bar{Q}_{66} \end{bmatrix} \begin{Bmatrix} \bar{\epsilon}_1 \\ \bar{\epsilon}_2 \\ \bar{\epsilon}_6 \end{Bmatrix}$$

$$\begin{Bmatrix} \bar{\sigma}_4 \\ \bar{\sigma}_5 \end{Bmatrix} = \begin{bmatrix} \bar{Q}_{44} & \bar{Q}_{45} \\ \bar{Q}_{45} & \bar{Q}_{55} \end{bmatrix} \begin{Bmatrix} \bar{\epsilon}_4 \\ \bar{\epsilon}_5 \end{Bmatrix} \tag{3.7}$$

where $\bar{Q}_{ij}$ are the transformed reduced material constants.

Resultant Forces and Laminate Stiffnesses

The Hamilton variational principle as discussed in Chapter 2 is used to derive the finite element equations. Substituting the strains from equation (3.4) and the stresses from equation (3.7) into equation (2.5) and integrating through the

thickness the following expressions for the resultant forces can be defined:

$$
\begin{aligned}
(N_x, M_x, P_x) &= \int_h \bar{\sigma}_1 \big(1, z, \frac{4z^3}{3h^2}\big)\, dz \\
(N_y, M_y, P_y) &= \int_h \bar{\sigma}_2 \big(1, z, \frac{4z^3}{3h^2}\big)\, dz \\
(N_{xy}, M_{xy}, P_{xy}) &= \int_h \bar{\sigma}_6 \big(1, z, \frac{4z^3}{3h^2}\big)\, dz \\
Q_y &= \int_h \bar{\sigma}_4 \big(1 - \frac{4z^2}{h^2}\big)\, dz \\
Q_x &= \int_h \bar{\sigma}_5 \big(1 - \frac{4z^2}{h^2}\big)\, dz.
\end{aligned}
\tag{3.8}
$$

The resultant forces can be related to the generalized strains in the usual way by introducing the laminate stiffnesses A_{ij}, B_{ij}, D_{ij}, E_{ij}, F_{ij}, and H_{ij}. This relation can be written in matrix form as

$$
\begin{Bmatrix} N_x \\ N_y \\ N_{xy} \\ M_x \\ M_y \\ M_{xy} \\ P_x \\ P_y \\ P_{xy} \end{Bmatrix} =
\begin{bmatrix}
A_{11} & A_{12} & A_{16} & B_{11} & B_{12} & B_{16} & E_{11} & E_{12} & E_{16} \\
A_{12} & A_{22} & A_{26} & B_{12} & B_{22} & B_{26} & E_{12} & E_{22} & E_{26} \\
A_{16} & A_{26} & A_{66} & B_{16} & B_{26} & B_{66} & E_{16} & E_{26} & E_{66} \\
B_{11} & B_{12} & B_{16} & D_{11} & D_{12} & D_{16} & F_{11} & F_{12} & F_{16} \\
B_{12} & B_{22} & B_{26} & D_{12} & D_{22} & D_{26} & F_{12} & F_{22} & F_{26} \\
B_{16} & B_{26} & B_{66} & D_{16} & D_{26} & D_{66} & F_{16} & F_{26} & F_{66} \\
E_{11} & E_{12} & E_{16} & F_{11} & F_{12} & F_{16} & H_{11} & H_{12} & H_{16} \\
E_{12} & E_{22} & E_{26} & F_{12} & F_{22} & F_{26} & H_{12} & H_{22} & H_{26} \\
E_{16} & E_{26} & E_{66} & F_{16} & F_{26} & F_{66} & H_{16} & H_{26} & H_{66}
\end{bmatrix}
\begin{Bmatrix} \epsilon_1^0 \\ \epsilon_2^0 \\ \epsilon_6^0 \\ \epsilon_1^1 \\ \epsilon_2^1 \\ \epsilon_6^1 \\ \epsilon_1^2 \\ \epsilon_2^2 \\ \epsilon_6^2 \end{Bmatrix}
$$

$$
\begin{Bmatrix} Q_y \\ Q_x \end{Bmatrix} =
\begin{bmatrix} D_{44} & D_{45} \\ D_{45} & D_{55} \end{bmatrix}
\begin{Bmatrix} \epsilon_4^0 \\ \epsilon_5^0 \end{Bmatrix}.
\tag{3.9}
$$

The laminate stiffnesses in equation (3.9) are defined as

$$(A_{ij}, B_{ij}, D_{ij}, E_{ij}, F_{ij}, H_{ij}) = \int_h \bar{Q}_{ij}(1, z, z^2, \frac{4z^3}{3h^2}, \frac{4z^4}{3h^2}, \frac{16z^6}{9h^4})\, dz \qquad i,j = 1,2,6$$

$$D_{ij} = \int_h \bar{Q}_{ij}(1 - \frac{4z^2}{h^2})^2\, dz \qquad i,j = 4,5. \tag{3.10}$$

For a beam it can be assumed that the lateral strains or resultant forces are negligible. This can be done by imposing either

$$\epsilon_2^0 = 0 \qquad \epsilon_2^1 = 0 \qquad \epsilon_2^2 = 0$$

or (3.11)

$$N_y = 0 \qquad M_y = 0 \qquad P_y = 0.$$

The first assumption is generally used for stiffened thin-walled beams, while the second assumption is valid for beams with solid cross-sections. Wu and Sun [31] have used a weighted average of the two conditions in their study of thin-walled beams and have shown that for solid cross-section beams the assumption of zero resultant forces is more accurate. Because in the present study only beams with solid cross-section are considered the resultant forces are assumed to be zero here. This approach is similar to the ones used by Chen and Yang [14] and Raciti and Kapania [1] in their studies of laminated beams using the FSDT. To equate the lateral resultant forces to zero it is convenient to partition equation (3.9) as

$$\begin{Bmatrix} \{N^x\} \\ \{N^y\} \end{Bmatrix} = \begin{bmatrix} [D^{xx}] & [D^{xy}] \\ [D^{yx}] & [D^{yy}] \end{bmatrix} \begin{Bmatrix} \{\epsilon^x\} \\ \{\epsilon^y\} \end{Bmatrix} \tag{3.12}$$

where

$$\begin{aligned}
\{N^x\}^T &= \{N_x, N_{xy}, M_x, M_{xy}, P_x, P_{xy}\} \\
\{\epsilon^x\}^T &= \{\epsilon_1^0, \epsilon_6^0, \epsilon_1^1, \epsilon_6^1, \epsilon_1^2, \epsilon_6^2\} \\
\{N^y\}^T &= \{N_y, M_y, P_y\} \\
\{\epsilon^y\}^T &= \{\epsilon_2^0, \epsilon_2^1, \epsilon_2^2\}
\end{aligned} \tag{3.13}$$

and

$$[D^{xx}] = \begin{bmatrix} A_{11} & A_{16} & B_{11} & B_{16} & E_{11} & E_{16} \\ A_{16} & A_{66} & B_{16} & B_{66} & E_{61} & E_{66} \\ B_{11} & B_{16} & D_{11} & D_{16} & F_{11} & F_{16} \\ B_{16} & B_{66} & D_{16} & D_{66} & F_{61} & F_{66} \\ E_{11} & E_{61} & F_{11} & F_{61} & H_{11} & H_{16} \\ E_{16} & E_{66} & F_{16} & F_{66} & H_{16} & H_{66} \end{bmatrix} \quad [D^{xy}] = \begin{bmatrix} A_{12} & B_{12} & E_{12} \\ A_{26} & B_{26} & E_{62} \\ B_{12} & D_{12} & F_{12} \\ B_{26} & D_{26} & F_{62} \\ E_{21} & F_{21} & H_{12} \\ E_{26} & F_{26} & H_{26} \end{bmatrix}$$

$$[D^{yx}] = \begin{bmatrix} A_{12} & A_{26} & B_{12} & B_{26} & E_{21} & E_{26} \\ B_{12} & B_{26} & D_{12} & D_{26} & F_{21} & F_{26} \\ E_{12} & E_{62} & F_{12} & F_{62} & H_{12} & H_{26} \end{bmatrix} \quad [D^{yy}] = \begin{bmatrix} A_{22} & B_{22} & E_{22} \\ B_{22} & D_{22} & F_{22} \\ E_{22} & F_{22} & H_{22} \end{bmatrix}. \tag{3.14}$$

Now equating $\{N^y\}$ to zero in equation (3.12) yields

$$\{N^y\} = \{0\} = [D^{yx}]\{\epsilon^x\} + [D^{xy}]\{\epsilon^y\} \tag{3.15}$$

and thus

$$\{\epsilon^y\} = -[D^{yy}]^{-1}[D^{yx}]\{\epsilon^x\}. \tag{3.16}$$

After substitution of equation (3.16) into equation (3.12) the resultant vector $\{N^x\}$ can be written as

$$\begin{aligned}
\{N^x\} &= \left[[D^{xx}] - [D^{xy}][D^{yy}]^{-1}[D^{yx}]\right]\{\epsilon^x\} \\
&= [\bar{D}]\{\epsilon^x\}.
\end{aligned} \tag{3.17}$$

The transverse resultant forces Q_x and Q_y can be reduced by equating Q_y to zero. Thus Q_x can be written as

$$\begin{aligned} Q_x &= \Big(D_{55} - \frac{D_{45}^2}{D_{44}}\Big)\epsilon_5^0 \\ &= D_{55}^* \epsilon_5^0. \end{aligned} \tag{3.18}$$

The final form of the relation between the resultant forces and the generalized displacements, corresponding to equation (2.8) is

$$\{N\} = [D]\{\hat{\epsilon}\} \tag{3.19}$$

where

$$\{N\}^T = \{\{N^x\}^T, Q_x\}, \qquad \{\hat{\epsilon}\}^T = \{\{\epsilon^x\}^T, \epsilon_5^0\}, \quad \text{and} \quad [D] = \begin{bmatrix} [\bar{D}] & \{0\} \\ \{0\}^T & D_{55}^* \end{bmatrix}.$$

Approximation to the Displacements

The generalized strains $\{\epsilon^x\}$ in equation (3.13) are assumed to be only functions of the axial coordinate. To retain the twist and the inplane shear as degrees of freedom the following generalized displacements are introduced :

$$\begin{aligned} \beta(x) &= \frac{\partial u_0}{\partial y} + \frac{\partial v_0}{\partial x} && \text{inplane shear rotation} \\ \mathcal{T}_b(x) &= \frac{\partial w_b}{\partial y} && \text{bend} - \text{twist term} \\ \mathcal{T}_s(x) &= \frac{\partial w_s}{\partial y} && \text{shear} - \text{twist term} \end{aligned} \tag{3.20}$$

With these definitions the terms in the generalized strain vector $\{\epsilon^x\}$ become

$$\begin{aligned} \epsilon_1^0 &= \frac{\partial u_0}{\partial x} + \frac{1}{2}\left(\frac{\partial w_0}{\partial x}\right)^2 \qquad \epsilon_1^1 = -\frac{\partial^2 w_b}{\partial x^2} \qquad \epsilon_1^2 = -\frac{\partial^2 w_s}{\partial x^2} \\ \epsilon_6^0 &= \beta + \frac{\partial w_0}{\partial x}\mathcal{T}_0 \qquad\qquad \epsilon_6^1 = -2\frac{\partial \mathcal{T}_b}{\partial x} \qquad \epsilon_6^2 = -2\frac{\partial \mathcal{T}_s}{\partial x} \end{aligned} \tag{3.21}$$

where $w_0 = w_b + w_s$ and $\mathcal{T}_0 = \mathcal{T}_b + \mathcal{T}_s$.

Discretization

It can be shown that the minimum interpolation requirement for u_0, β, $\mathcal{T}_b$, and $\mathcal{T}_s$ are Lagrangian interpolation polynomials, and for w_b and w_s are Hermitian interpolation polynomials. In this study for simplicity all displacements are discretized using Hermitian interpolation polynomials. Thus each of the generalized displacements is interpolated spatially over an element by an expression of the form

$$U = \sum_{i=1}^{4} U_i(t) H_i(x) \tag{3.22}$$

where $U_i(t)$ are the generalized nodal displacements, and $H_i(x)$ are the Hermitian interpolation polynomials. The Hermitian polynomials in element coordinates, as

defined in Figure 2.3, are given by Reddy [32] as

$$
\begin{aligned}
H_1^{(e)} &= 1 - 3\left(\frac{\bar{x}}{l_e}\right)^2 + 2\left(\frac{\bar{x}}{l_e}\right)^3 \\
H_2^{(e)} &= \bar{x}\left(1 - \frac{\bar{x}}{l_e}\right)^2 \\
H_3^{(e)} &= 3\left(\frac{\bar{x}}{l_e}\right)^2 - 2\left(\frac{\bar{x}}{l_e}\right)^3 \\
H_4^{(e)} &= \bar{x}\left[\left(\frac{\bar{x}}{l_e}\right)^2 - \frac{\bar{x}}{l_e}\right].
\end{aligned}
\tag{3.23}
$$

Thus the explicit form of the strain-displacement relation in equation (2.20) can be written as

$$
\begin{Bmatrix} \epsilon_1^0 \\ \epsilon_6^0 \\ \epsilon_1^1 \\ \epsilon_6^1 \\ \epsilon_1^2 \\ \epsilon_6^2 \\ \epsilon_5^0 \end{Bmatrix} =
\left[
\begin{bmatrix}
H_{i,x} & 0 & 0 & 0 & 0 & 0 \\
0 & H_i & 0 & 0 & 0 & 0 \\
0 & 0 & -H_{i,xx} & 0 & 0 & 0 \\
0 & 0 & 0 & 0 & -2H_{i,x} & 0 \\
0 & 0 & 0 & -H_{i,xx} & 0 & 0 \\
0 & 0 & 0 & 0 & 0 & -2H_{i,x} \\
0 & 0 & 0 & H_{i,x} & 0 & 0
\end{bmatrix} +
\frac{1}{2}
\begin{bmatrix}
0 & 0 & w_{0,x}H_{i,x} & w_{0,x}H_{i,x} & 0 & 0 \\
0 & 0 & \mathcal{T}_0 H_{i,x} & \mathcal{T}_0 H_{i,x} & w_{0,x}H_i & w_{0,x}H_i \\
0 & 0 & 0 & 0 & 0 & 0 \\
0 & 0 & 0 & 0 & 0 & 0 \\
0 & 0 & 0 & 0 & 0 & 0 \\
0 & 0 & 0 & 0 & 0 & 0 \\
0 & 0 & 0 & 0 & 0 & 0
\end{bmatrix}
\right]
\begin{Bmatrix} u_{0i} \\ \beta_i \\ w_{bi} \\ w_{si} \\ \mathcal{T}_{bi} \\ \mathcal{T}_{si} \end{Bmatrix}
\tag{3.24}
$$

$$
= \left[[B_L] + [B_{NL}(a)]\right]\{a\}
$$

where $\{a\}$ is the vector of the nodal displacements.

Element Stiffness Matrix and Force Vector

The element stiffness matrix can now be obtained by calculating $[B^*]$ from equation (2.21) and then substituting it along with $[B] = [B_L] + [B_{NL}]$ and the reduced laminate stiffness matrix $[D]$ into equation (2.23). The element force vector can be obtained by substituting the Hermitian polynomials into equation (2.16). With the nodal displacement vector $\{a\}$ defined as $\{a\}^T = \{\{u\}, \{\beta\}, \{w_b\}, \{w_s\}, \{\mathcal{T}_b\}, \{\mathcal{T}_s\}\}$ the explicit form of the finite element equations for the static problem becomes

$$\begin{bmatrix} [K^{11}] & [K^{12}] & [K^{13}] & [K^{14}] & [K^{15}] & [K^{16}] \\ [K^{21}] & [K^{22}] & [K^{23}] & [K^{24}] & [K^{25}] & [K^{26}] \\ [K^{31}] & [K^{32}] & [K^{33}] & [K^{34}] & [K^{35}] & [K^{36}] \\ [K^{41}] & [K^{42}] & [K^{43}] & [K^{44}] & [K^{45}] & [K^{46}] \\ [K^{51}] & [K^{52}] & [K^{53}] & [K^{54}] & [K^{55}] & [K^{56}] \\ [K^{61}] & [K^{62}] & [K^{63}] & [K^{64}] & [K^{65}] & [K^{66}] \end{bmatrix} \begin{Bmatrix} \{u\} \\ \{\beta\} \\ \{w_b\} \\ \{w_s\} \\ \{\mathcal{T}_b\} \\ \{\mathcal{T}_s\} \end{Bmatrix} = \begin{Bmatrix} \{F^1\} \\ \{F^2\} \\ \{F^3\} \\ \{F^4\} \\ \{F^5\} \\ \{F^6\} \end{Bmatrix} \tag{3.25}$$

Because the geometric nonlinearities are included in this derivation the stiffness matrix is not symmetric.

Tangential Stiffness Matrix

To calculate the tangential stiffness matrix equation (2.50) for the residual vector is rewritten as

$$R_i^\alpha = \sum_{\beta=1}^{6} \sum_{j=1}^{4} K_{ij}^{\alpha\beta} a_j^\beta - F_i^\alpha \qquad \alpha = 1, \ldots, 6 \qquad i = \ldots, 4. \tag{3.26}$$

Here a_j^β is the j-th entry of the β-th subvector of the nodal displacement vector $\{a\}$. Now the submatrices $\left(K_{ij}^{\alpha\beta}\right)^{Tan}$ for the tangential stiffness matrix corresponding to

the submatrices $K_{ij}^{\alpha\beta}$ in equation (3.25) can be obtained from the equation

$$\left(K_{ij}^{\alpha\beta}\right)^{Tan} = \frac{\partial R_i^\alpha}{\partial a_j^\beta} \tag{3.27}$$

Note that the tangent stiffness matrix is symmetric.

Initial Stress Matrix

The initial stress matrix $[K_s]$ can be obtained by substituting $u_3 = w_b + w_s$ into equation (2.24). The explicit expressions for the submatrices of $[K_s]$ thus become

$$(K_{ij}^{\alpha\beta})_s = \int_{\ell_e} p(x) \frac{dH_i}{dx} \frac{dH_j}{dx}\, dx \qquad \alpha, \beta = 3, 4 \tag{3.28}$$

All other submatrices are zero.

Mass Matrix

Neglecting inplane inertia and using the displacement approximations from equation (3.20) the velocity vector in the kinetic energy expression in equation (2.6) becomes

$$\{\dot{u}\} = \begin{Bmatrix} -z\dot{w}_{b,x} - (4z^3/3h^2)\dot{w}_{s,x} \\ -z\dot{T}_{b,x} - (4z^3/3h^2)\dot{T}_{s,x} \\ \dot{w}_b + \dot{w}_s \end{Bmatrix} \tag{3.29}$$

Carrying out the calculations described in Section 2.1, the explicit expressions for the mass matrix, can be obtained.

The explicit form of the most general set of finite element equations and the expressions for all element matrices are given in the appendix.

4. Shear Stress Continuity Theory

Examining the elasticity solution for beams in cylindrical bending of Pagano [2] shows that at the layer interfaces the transverse shear stresses are continuous and the inplane displacements experience a sudden change in their slope. The change in slope of the inplane displacements is most pronounced for relatively short beams ($L/h < 10$). Thus, to accurately model a composite beam, the theory should include both, the continuity of the transverse shear stresses and the sudden change of slopes of the inplane displacements at the layer interfaces. In this chapter such a theory is introduced. The theory is based on a displacement field proposed by Savithri and Varadan [7] for the analysis of orthotropic plates. The shear stress continuity is enforced while keeping the number of degrees of freedom independent of the number of layers. The theory is restricted to the analysis of symmetrically laminated cross-ply beams.

Kinematics

As for the consistent strain theory the inplane displacements u and v are expanded as cubic functions of the thickness coordinate z and the transverse deflection w is assumed to be constant through the thickness. The displacement field is chosen as:

$$\begin{aligned} u_1 &= u^* - z\,\frac{\partial w_b}{\partial x} - J_{a1}(z)\,\frac{\partial w_s}{\partial x} \\ u_2 &= v^* - z\,\frac{\partial w_b}{\partial y} - J_{b1}(z)\,\frac{\partial w_s}{\partial y} \\ u_3 &= w_b + w_s \end{aligned} \tag{4.1}$$

where

$$J_{a1}(z) = \frac{4z^3}{3h^2} - \sum_{i=1}^{N-1} \big(p(z) - p(z_i)\big) a_i H(z - z_i)$$
$$J_{b1}(z) = \frac{4z^3}{3h^2} - \sum_{i=1}^{N-1} \big(p(z) - p(z_i)\big) b_i H(z - z_i). \tag{4.2}$$

Here $p(z) = z\,(1 - 4z^2/3h^2)$ and $H(z - z_i)$ is the Heaviside unit step function, z_i being the z-coordinate of the i-th interface as defined in Fig. 2.2 . The coefficients a_i and b_i are determined from the condition of continuous transverse shear stresses at the layer interfaces

$$\sigma_{yz}^{(k)}(z_k) = \sigma_{yz}^{(k+1)}(z_k)$$
$$\sigma_{xz}^{(k)}(z_k) = \sigma_{xz}^{(k+1)}(z_k) \tag{4.3}$$

as

$$a_1 = \frac{Q_{55}^{(1)}}{Q_{55}^{(2)}} - 1 \qquad a_k = \Big(\frac{Q_{55}^{(k)}}{Q_{55}^{(k+1)}} - 1\Big)\Big(1 + \sum_{s=1}^{k-1} a_s\Big) \qquad \text{for } k > 1$$
$$b_1 = \frac{Q_{44}^{(1)}}{Q_{44}^{(2)}} - 1 \qquad b_k = \Big(\frac{Q_{44}^{(k)}}{Q_{44}^{(k+1)}} - 1\Big)\Big(1 + \sum_{s=1}^{k-1} b_s\Big) \qquad \text{for } k > 1. \tag{4.4}$$

The inplane displacements u^* and v^* are defined as

$$u^* = u^{**} + u_0$$
$$v^* = v^{**} + v_0 \tag{4.5}$$

where u_0 and v_0 denote the midplane displacements in the x- and y-direction, respectively. u^{**} and v^{**} are some axial displacements introduced by the functions

$J_{a1}(z)$ and $J_{b1}(z)$ because in general $J_{a1}(0) \neq 0$ and $J_{a1}(0) \neq 0$. The displacements u^{**} and v^{**} can be expressed in terms of $\partial w_s/\partial x$ and $\partial w_s/\partial y$ as suggested by Varadan [33].

Because of the assumption of constant transverse deflection through the thickness the inplane displacements at the middle surface $z = 0$ are zero for symmetric laminates , i.e., $u\,(z = 0) = 0$, $v\,(z = 0) = 0$, $u_0 = 0$, and $v_0 = 0$. Thus the first two equations in Eqs. (4.1) become

$$\begin{aligned} u_1(z = 0) &= u^{**} - J_{a1}(0)\,\frac{\partial w_s}{\partial x} = 0 \\ u_2(z = 0) &= v^{**} - J_{b1}(0)\,\frac{\partial w_s}{\partial y} = 0 \end{aligned} \tag{4.6}$$

and can be solved for u^{**} and v^{**}. Thus,

$$\begin{aligned} u^{**} &= J_{a1}(0)\,\frac{\partial w_s}{\partial x} \\ v^{**} &= J_{b1}(0)\,\frac{\partial w_s}{\partial y} \end{aligned} \tag{4.7}$$

Finally, upon substitution of equation (4.7) into equation (4.1) the displacement field can be written as:

$$\begin{aligned} u_1 &= u_0 - z\,\frac{\partial w_b}{\partial x} - J_a(z)\,\frac{\partial w_s}{\partial x} \\ u_2 &= v_0 - z\,\frac{\partial w_b}{\partial y} - J_b(z)\,\frac{\partial w_s}{\partial y} \\ u_3 &= w_b + w_s \end{aligned} \tag{4.8}$$

where $J_a(z) = J_{a1}(z) - J_{a1}(0)$ and $J_b(z) = J_{b1}(z) - J_{b1}(0)$.

The von Kármán strains associated with the displacement field in equation (4.8) can be obtained from equation (2.19) as

$$\begin{aligned}
\epsilon_1 &= \epsilon_1^0 + z\epsilon_1^1 + J_a(z)\epsilon_1^2 \\
\epsilon_2 &= \epsilon_2^0 + z\epsilon_2^1 + J_b(z)\epsilon_2^2 \\
\epsilon_6 &= \epsilon_6^0 + z\epsilon_6^1 + \frac{1}{2}\big(J_a(z) + J_b(z)\big)\,\epsilon_6^2 \\
\epsilon_4 &= J_b^*(z)\epsilon_4^0 \\
\epsilon_5 &= J_a^*(z)\epsilon_5^0
\end{aligned} \tag{4.9}$$

where with $w_0 = w_b + w_s$

$$\begin{aligned}
&\epsilon_1^0 = \frac{\partial u_0}{\partial x} + \frac{1}{2}\left(\frac{\partial w_0}{\partial x}\right)^2 \qquad \epsilon_1^1 = -\frac{\partial^2 w_b}{\partial x^2} \qquad \epsilon_1^2 = -\frac{\partial^2 w_s}{\partial x^2} \\
&\epsilon_2^0 = \frac{\partial v_0}{\partial y} + \frac{1}{2}\left(\frac{\partial w_0}{\partial y}\right)^2 \qquad \epsilon_1^1 = -\frac{\partial^2 w_b}{\partial y^2} \qquad \epsilon_2^2 = -\frac{\partial^2 w_s}{\partial y^2} \\
&\epsilon_6^0 = \frac{\partial u_0}{\partial y} + \frac{\partial v_0}{\partial x} + \frac{\partial w_0}{\partial x}\frac{\partial w_0}{\partial y} \qquad \epsilon_6^1 = -2\frac{\partial^2 w_b}{\partial x \partial y} \qquad \epsilon_6^2 = -2\frac{\partial^2 w_s}{\partial x \partial y} \\
&\epsilon_4^0 = \frac{\partial w_s}{\partial y} \qquad \epsilon_5^0 = \frac{\partial w_s}{\partial x}
\end{aligned} \tag{4.10}$$

and

$$\begin{aligned}
J_a^*(z) &= \left(1 - \frac{4z^2}{h^2}\right)\left(1 + \sum_{i=1}^{N-1} a_i H(z - z_i)\right) \\
J_b^*(z) &= \left(1 - \frac{4z^2}{h^2}\right)\left(1 + \sum_{i=1}^{N-1} b_i H(z - z_i)\right)
\end{aligned} \tag{4.11}$$

Constitutive Equations

The constitutive equations for this theory simplify because for orthotropic cross-ply laminates the laminae stiffnesses $\bar{Q}_{16}$ and $\bar{Q}_{26}$ are always zero. Hence the equations for the transformed laminae stiffnesses become

$$\begin{Bmatrix} \bar{\sigma}_1 \\ \bar{\sigma}_2 \\ \bar{\sigma}_6 \end{Bmatrix} = \begin{bmatrix} \bar{Q}_{11} & \bar{Q}_{12} & 0 \\ \bar{Q}_{12} & \bar{Q}_{22} & 0 \\ 0 & 0 & \bar{Q}_{66} \end{bmatrix} \begin{Bmatrix} \bar{\epsilon}_1 \\ \bar{\epsilon}_2 \\ \bar{\epsilon}_6 \end{Bmatrix}$$

$$\begin{Bmatrix} \bar{\sigma}_4 \\ \bar{\sigma}_5 \end{Bmatrix} = \begin{bmatrix} \bar{Q}_{44} & 0 \\ 0 & \bar{Q}_{55} \end{bmatrix} \begin{Bmatrix} \bar{\epsilon}_4 \\ \bar{\epsilon}_5 \end{Bmatrix} \tag{4.12}$$

where $\bar{Q}_{ij}$ are the transformed reduced material constants.

Laminate Stiffnesses and Resultant Forces

Substituting the strains from equation (4.9) and the stresses from equation (4.12) and integrating through the thickness the following resultant forces can be defined:

$$\begin{aligned}
(N_x, M_x, P_x) &= \int_h \bar{\sigma}_1 \big(1, z, J_a(z)\big)\, dz \\
(N_y, M_y, P_y) &= \int_h \bar{\sigma}_2 \big(1, z, J_b(z)\big)\, dz \\
(N_{xy}, M_{xy}, P_{xy}) &= \int_h \bar{\sigma}_6 \Big(1, z, \frac{1}{2}\big(J_a(z) + J_b(a)\big)\Big)\, dz \\
Q_y &= \int_h \bar{\sigma}_4 J_b^*(z)\, dz \\
Q_x &= \int_h \bar{\sigma}_5 J_a^*(z)\, dz
\end{aligned} \tag{4.13}$$

The matrix equation for the resultant forces is of the same form as given in equation (3.9) for the RHSDT. However, the expressions for the laminate stiffnesse are different. For the SVHSDT the laminate stiffnesses are defined as

$$
\begin{aligned}
&(B_{ij}, E_{ij}) = 0 && i,j = 1,2,6 \\
&(A_{ij}, D_{ij}, F_{ij}, H_{ij}) = 0, && ij = 16,26,61,62 \\
&(A_{ij}, D_{ij}) = \int_h \bar{Q}_{ij}\left(1, z^2\right) dz && ij = 11,12,21,22,66 \\
&F_{11} = \int_h \bar{Q}_{11} J_a(z)\, z\, dz && F_{12} = \int_h \bar{Q}_{12} J_b(z)\, z\, dz \\
&F_{21} = \int_h \bar{Q}_{12} J_a(z)\, z\, dz && F_{22} = \int_h \bar{Q}_{22} J_b(z)\, z\, dz \\
&F_{66} = \int_h \bar{Q}_{66} \frac{1}{2}\left(J_a(z) + J_b(z)\right) z\, dz
\end{aligned}
\tag{4.15}
$$

$$
\begin{aligned}
&H_{11} = \int_h \bar{Q}_{11} J_a^2(z)\, dz && H_{12} = \int_h \bar{Q}_{12} J_a(z) J_b(z)\, dz \\
&H_{22} = \int_h \bar{Q}_{22} J_b^2(z)\, dz && H_{66} = \int_h \bar{Q}_{66} \frac{1}{4}\left(J_a(z) + J_b(z)\right)^2 dz \\
&D_{44} = \int_h \bar{Q}_{44}\left(J_b^*(z)\right)^2 dz && D_{55} = \int_h \bar{Q}_{55}\left(J_a^*(z)\right)^2 dz.
\end{aligned}
$$

The further derivation is the same as for the theory described in Chapter 3 and is omitted here. The expressions for the element matrices are the same as those given in Chapter 3 and their explicit forms are given in the appendix. The only difference between the element stiffness matrix for the RHSDT and the SVHSDT is in the different laminate matrix $[D]$.

5. Results

The theories derived in the previous chapters are evaluated by solving a number of example problems. Whenever possible results are compared with existing solutions in literature. In the presentation of the results the following notation is used to denote the different theories:

CLT	Classical Lamination Theory
FSDT	First Order Shear Deformation Theory
RHSDT	Consistent Strain Higher Order Theory (Chapter 3)
SVHSDT	Higher Order Theory with transverse shear stress continuity (Chapter 4).

First results for the static analysis are presented in Section 5.1, then results for the eigenvalue analysis are shown in Section 5.2, and finally results for the transient problem are discussed in Section 5.3.

5.1. Static Analysis

5.1.1. Linear Analysis

In this section the theories are evaluated by solving some examples available in literature. It will be shown that the SVHSDT is superior to the other theories in the analysis of symmetrically laminated cross-ply beams. First results for symmetrically and asymmetrically laminated cross-ply beams are shown and compared to Pagano's elasticity solution [2]. Then results for symmetrically laminated anisotropic beams are presented and compared to solutions obtained with a theory presented by Chen

and Yang [14]. In all of the examples in this section the following material properties were used unless otherwise noted

$$E_L = 25 \times 10^6 \text{psi} \qquad E_T = 1 \times 10^6 \text{psi}$$

$$G_{LT} = .5 \times 10^6 \text{psi} \qquad G_{TT} = .2 \times 10^6 \text{psi} \tag{5.1}$$

$$\nu_{LT} = \nu_{TT} = 0.25.$$

The results obtained for the cross-ply beams are nondimensionalized as

$$\bar{\sigma}_x = \frac{\sigma_x\left(\frac{l}{2}, z\right)}{q_0} \qquad \bar{\tau}_{xz} = \frac{\tau_{xz}\left(0, z\right)}{q_0} \qquad \bar{u} = \frac{E_T u(0,z)}{h q_0} \qquad \bar{w} = \frac{100 E_T h^3 w\left(\frac{l}{2}, z\right)}{q_0 l^4} \tag{5.2}$$

where q_0 is the magnitude of a distributed load.

Simply-Supported Beam [0°/90°/0°] under Sinusoidal Load

First the convergence of the finite element solution for the higher order theories was studied. As can be seen in Table 5.1 the deflections converge if the full beam is modeled with four elements and the stresses converge if the full beam is modeled with eight elements. Therefore in the investigations eight elements were used to model the full beam.

Table 5.1: *Convergence of the Maximum Transverse Deflection, the Maximum Normal Stress, and the Maximum Transverse Shear Stress for the RHSDT and the SVHSDT for a Simply-Supported Beam* ($[0°/90°/0°]$, $L/h = 4$).

No. of	$\bar{w}$		$\bar{\sigma}_x$		$\bar{\tau}_{xz}$	
Elements	RHSDT	SVHSDT	RHSDT	SVHSDT	RHSDT	SVHSDT
2	2.711	2.813	19.596	22.920		
4	2.701	2.801	17.808	20.764	2.211	2.291
8	2.700	2.801	17.205	20.056	1.563	1.619
16	2.700	2.801	17.044	19.869	1.561	1.617

The maximum deflections for the CLT, the FSDT, the RHSDT, the SVHSDT, and Pagano's elasticity solution [2] are compared in Figure 5.1. As expected, the CLT underpredicts the deflection for $L/h \leq 40$. For moderately thick beams ($20 \leq L/h \leq 40$) all shear deformation theories give excellent results compared to the exact solution, while for thick beams ($L/h \leq 20$) higher order theories have to be used to obtain good results. In Tables 5.2 and 5.3 results for the maximum deflection $\bar{w}$, the maximum normal stress $\bar{\sigma}_x$, the maximum transverse shear stress $\bar{\tau}_{xz}$, and the interfacial transverse shear stress $\tau_{xz,interfacial}$ obtained with the RHSDT and the SVHSDT are compared to the exact solution [2]. Note that in this comparison the values for the maximum transverse shear stress for the RHSDT and the SVHSDT are taken at the locations of maximum shear stress as calculated from the elasticity solution, i.e., for $L/h = 4$ at $z/h = 0.25$ and for $L/h = 10$ at $z/h = 0$. As can be seen, results predicted by the SVHSDT for the transverse deflection and shear stresses for $L/h = 10$ are essentially the same as those predicted by the

Table 5.2: *Comparison of the Maximum Deflection and the Maximum Normal Stress for the RHSDT, the SVHSDT, and the Exact Solution.*

	$\bar{w}$			$\bar{\sigma}_x$		
L/h	RHSDT	SVHSDT	Pagano	RHSDT	SVHSDT	Pagano
4	2.7001	2.8006	2.8872	17.205	20.056	18.808
10	0.8750	0.9323	0.9320	71.040	75.197	73.7

Table 5.3: *Comparison of the Maximum Transverse Shear Stress and the Interfacial Transverse Shear Stress.*

	$\bar{\tau}_{max}$			$\tau_{xz,interfacial}$		
L/h	RHSDT	SVHSDT	Pagano	RHSDT	SVHSDT	Pagano
4	1.5052	1.6190	1.5827	1.5630	1.3565	1.4270
10	4.3497	4.2378	4.24	4.3314	4.2281	4.22

exact solution, whereas the RHSDT slightly underpredicts the deflection and slightly overpredicts the transverse shear stresses.

For $L/h = 4$ results from the SVHSDT are closer to the exact solution than results from the RHSDT. Note that in this case the RHSDT fails to predict the location for the maximum shear stresses. To show this, the distribution of the transverse shear stress through the thickness is plotted in Figure 5.2 for the RHSDT, the SVHSDT, and for the exact solution. An interesting aspect of the deformation of laminated beams is shown in Figures 5.3 (a) and 5.3 (b) , in which the distribution of the axial displacement $\bar{u}$ through the thickness of the laminate for two different aspect ratios ($L/h = 4$ and $L/h = 10$) is shown. The exact solution of Pagano shows that the Kirchhoff assumption that normals to the midplane remain straight after deformation does not hold for short beam ($L/h = 4$). But with increasing

aspect ratio the normals get closer to straight lines. Figure 5.3 (a) also shows that only the SVHSDT has the same characteristic sudden change in slope of the inplane displacement at the layer interfaces as the exact solution. For $L/h = 10$ the solution from the RHSDT and the SVHSDT are both close to the exact solution. Finally, in Tables 5.4 and 5.5 the results obtained with the SVHSDT are compared to results reported by Yuan and Miller [34], who used a layerwise theory and integration of the equilibrium equations of elasticity to obtain the interlaminar shear stresses. The material properties for this example are:

$$E_L = 172.0\text{GPa} \qquad E_T = 6.9\text{GPa}$$

$$G_{LT} = 3.4\text{GPa} \qquad G_{TT} = 1.4\text{GPa}$$

$$\nu_{LT} = \nu_{TT} = 0.25$$

For $L/h = 4$ the layerwise theory is closer to the exact solution than the SVHSDT, but for $L/h = 10$, both theories predict the results equally well. The major disadvantage of the layerwise theory is that it is computationally inefficient for laminates with a larger number of layers. The number of degrees of freedom for the layerwise theory per element is $7 + 9n$, where n is the number of layers. In comparison the number of degrees of freedom required by the SVHSDT is independent of the number of layers (24 degrees of freedom per element).

In conclusion it can be said that a new theory for the analysis of symmetrically laminated cross-ply beams has been developed, which is better than the RHSDT for low L/h ratios, and is far superior to both the FSDT and the CLT. For moderate

L/h ratios, both, the RHSDT and the SVHSDT, are superior to the FSDT and the CLT. The drawback of the SVHSDT is that it is valid only for symmetric beams. In the next example the performance of the RHSDT for the analysis of asymmetrically laminated cross-ply beams is investigated.

Table 5.4: *Comparison of the Maximum Deflection and the Maximum Normal Stress for the SVHSDT, a Layerwise Theory [34], and the Exact Solution [2].*

	$\bar{w}$			$\bar{\sigma}_x$		
L/h	SVHSDT	Ref. [34]	Pagano [2]	SVHSDT	Ref. [34]	Pagano [2]
4	2.7982	2.9065	2.9127	19.946	18.640	18.808
10	0.9312	0.9310	0.9316	75.025	74.657	73.670

Table 5.5: *Comparison of the Maximum Transverse Shear Stress and the Interfacial Transverse Shear Stress.*

	$\bar{\tau}_{max}$			$\tau_{xz,interfacial}$		
L/h	SVHSDT	Ref. [34]	Pagano [2]	SVHSDT	Ref. [34]	Pagano [2]
4	1.6137	1.5849	1.5776	1.3635	1.4292	1.4270
10	4.2420	4.2374	4.2393	4.2320	4.2169	4.2200

Simply-Supported Beam $[0°/90°]_T$ under Sinusoidal Load

In this example the bending of an asymmetrically laminated beam is analyzed. Results from the RHSDT and the elasticity solution of Pagano [2] are compared for two different aspect ratios ($L/h = 4$ and $L/h = 10$). The material properties given in equation (5.1) are used. In Table 5.6 the results for the nondimensionalized

Table 5.6: *Nondimensionalized Deflection and Normal Stresses of Simply-Supported Asymmetric Cross-Ply Beams Under Sinusoidal Load.*

	$\bar{w}$		$\bar{\sigma}_x$ (upper surface)		$\bar{\sigma}_x$ (lower surface)	
L/h	RHSDT	Pagano [2]	RHSDT	Pagano	RHSDT	Pagano
4	4.4469	4.6953	34.049	30.029	3.123	3.836
10	2.9185	2.9538	182.623	176.53	19.196	19.829

deflection $\bar{w}$ and normal stresses $\bar{\sigma}_x$ at the upper and lower surface of the beam are compared. Agreement for $L/h = 10$ is good and agreement for $L/h = 4$ is fair.

In Figures 5.4 (a) and 5.4 (b) the distribution of the transverse shear stress $\bar{\tau}_{xz}$ through the thickness from the RHSDT and Pagano's solution are compared. Agreement between the numerical results and the exact solution is excellent for $L/h = 10$ and is good for $L/h = 4$.

Anisotropic $[45°/-45°]_S$ Cantilever Beams Under End Load

In this example the deflection and twisting angle of an anisotropic cantilever beam under an end load were investigated. Chen and Yang [14] have previously shown some results for this problem. Because the theory of Chen and Yang is a special case of the FSDT, results obtained using their theory were exactly the same as those of the FSDT and therefore are not shown here. In Table 5.7 the maximum deflection and twisting angle are compared for the FSDT and the RHSDT. For both aspect ratios ($L/h = 10$ and $L/h = 50$) the results are not in good agreement. It is surprising that the differences do not vanish for larger aspect ratios.

A comparison shows that the ratios of the maximum deflections and the ratios

Table 5.7: *Maximum Deflection and Twisting Angle of an Anisotropic Cantilever Beam Under End Load.*

	w_{max}		$\mathcal{T}_{max}$	
L/h	FSDT	RHSDT	FSDT	RHSDT
10	2.323×10^{-3}	2.755×10^{-3}	$-.306 \times 10^{-4}$	-5.904×10^{-4}
50	0.286	0.340	-0.766×10^{-3}	-0.147×10^{-1}

of the maximum twisting angles remain almost the same for both aspect ratios

$$\text{for } L/h = 10: \quad \frac{w_{max,RHSDT}}{w_{max,FSDT}} = 1.19 \qquad \frac{\mathcal{T}_{max,RHSDT}}{\mathcal{T}_{max,FSDT}} = 19.29$$

$$\text{for } L/h = 50: \quad \frac{w_{max,RHSDT}}{w_{max,FSDT}} = 1.19 \qquad \frac{\mathcal{T}_{max,RHSDT}}{\mathcal{T}_{max,FSDT}} = 19.19$$

The difference between the results for the FSDT and the RHSDT can be attributed to the fact that the FSDT does not account for the shear twisting term. A testcase in which the RHSDT had been used, but all shear twist degrees of freedom were restrained, supports this, because in that case the results were close to the results obtained using the FSDT.

Although the twisting angle predicted by the RHSDT is almost 20 times the one predicted by the FSDT, it is physically still small. For the case of a beam of 50 *in* length and 1 *in* thickness the maximum deflection obtained is $w_{max} = 0.340$ *in* and the maximum twisting angle is $\mathcal{T}_{max} = 0.842°$. Both results are small compared to the dimensions of the beam and hence physically possible. It would be interesting to obtain experimental results for the twisting angle for a comparison.

5.1.2. Nonlinear Analysis

In this section the nonlinear static response of uniformly loaded beams is studied. The effects of boundary conditions and lamination scheme on the displacement and the inplane resultant force are studied. All results were obtained using the RHSDT. The boundary conditions used in the following examples are depicted in Figure 5.5.

Pinned-pinned Cross-Ply Beam

In this example numerical results for the nonlinear bending of a pinned-pinned $[0°/90°]_T$ beam under uniformly distributed load are compared to an analytical solution by Sun and Chin [16]. Sun and Chin investigated the problem for an aspect ratio of $L/h = 225$ using the CLT. Because of this high aspect ratio, the transverse shear effects are negligible. Therefore, results obtained using the RHSDT are expected to be close to the CLT. The material properties used by Sun and Chin were $E_1 = 20\ msi, E_2 = 1.4\ msi, \nu_{12} = 0.3$, and $G_{12} = G_{13} = G_{23} = 0.7\ msi$. The laminate dimensions were taken as $L = 9\ in., b = 1.5\ in.$, and $h = 0.04\ in.$ Figures 5.6 (a) and 5.6 (b) show the results for the maximum deflection and the inplane force resultants at the center of the beam for different load magnitudes. Note, that the deflection and the force resultant are different for positive and negative loads. The agreement between the analytical and the numerical solution is excellent.

In the next examples the effect of aspect ratios, boundary conditions, and lamination schemes on the nonlinear static response is studied. For these examples the material properties given in equation (5.1) were used.

Effect of Aspect Ratio L/h

A $[0°/90°]_T$ pinned-pinned cross-ply beam under uniformly distributed load was analyzed to study the effect of the aspect ratio. The aspect ratios considered were $L/h = 10$, $L/h = 20$, $L/h = 50$, and $L/h = 100$. In Figure 5.7 (a) the ratios of the linear to the nonlinear deflection at the center of the beam are plotted against the load-parameter α, and in Figure 5.7 (b) the nondimensionalized inplane resultant forces $\bar{N}_x$ at the center of the beam are plotted against α. $\bar{N}_x$ and α are defined as

$$\alpha = \frac{q_0}{E_2}\left(\frac{L}{h}\right)^4$$

$$\bar{N}_x = \frac{N_x}{E_2 h}\left(\frac{L}{h}\right)^2.$$

As can be seen, this ratio only has a small effect on the nonlinear response. For small aspect ratios the ratios of the linear to the nonlinear center deflections are slightly higher than the ones for larger ratios. For the ratios $L/h = 50$ and $L/h = 100$ almost no difference can be seen. The effect of the L/h ratios on the nondimensionalized inplane resultant forces is negligible. In all cases the softening effect due to the initially compressive inplane resultant force resultants for positive loads can be observed.

Effect of Boundary Conditions on the Nonlinearity

To study the effect of the boundary conditions on the nonlinearity a $[0°/90°]_T$ cross-ply beam with an aspect ratio of $L/h = 10$ under uniformly distibuted load

was analyzed. All boundary conditions shown in Figure 5.5 were considered. In Figure 5.8 (a) the ratios of the linear to the nonlinear deflection at the center of the beam are plotted against the applied load q_0, and in Figure 5.8 (b) the variations of the inplane resultant force N_x with the applied load q_0 for the different boundary conditions are shown. As can be seen in Figures 5.8 (a) and 5.8 (b) , the magnitude of the inplane force depends on the boundary conditon and the ratio of the the linear displacement w_L to the nonlinear displacement w_{NL} in turn depends on the magnitude of the inplane resultant force. Because the simply-supported beam is free to move in the axial direction almost no inplane resultant force is developed and the linear displacement is the same as the nonlinear displacement. The effect of the nonlinearity on the pinned-pinned beam is the most significant. For this beam the magnitude of the inplane resultant force and the magnitude of the deflection depend on the direction of the transverse load. The inplane force resultant for negative transverse loads is tensile and thus has a stiffening effect. For positive transverse loads the inplane resultant is first compressive due to the extension bending coupling, but then becomes tensile as the transverse load increases. The initial compressive inplane resultant has a softening effect on the beam. This explains why the transverse deflection obtained using the nonlinear theory is initially higher than the transverse deflection obtained from the linear theory. This important effect should be considered in the design of structures. It is interesting to see that for the clamped-clamped boundary conditions the response of the beam does not depend on the direction of the loading. Both, negative and positive transverse

loads, produce a tensile inplane resultant force which has a stiffening effect. The nonlinear deflection is always lower then the linear deflection.

Effect of Lamination Scheme on the Nonlinearity $(L/h = 10)$

Because the nonlinear effects are most significant for the pinned-pinned beam, the effect of the lamination scheme on the nonlinear response is studied for these boundary conditions. The following lamination schemes were studied:

1. a bending stiff $[0°/90°]_T$ laminate,
2. a torsion stiff $[45°/-45°]_T$ laminate, and
3. a quasi-isotropic $[0°/45°/-45°/90°]_T$ laminate.

The $[0°/45°/-45°/90°]_T$ beam shows the same characteristic nonlinear effects as discussed before for the pinned-pinned $[0°/90°]_T$ beam. The direction of the transverse load has, as expected, no effect on the inplane resultant force and the deflection of the torsion stiff $[45°/-45°]_T$ beam. But it is interesting to note that for this beam the nonlinear effect on the center deflection of the beam is the most significant. This shows that the stiffening effect of the tensile inplane resultant force is highest for the torsion stiff beam.

5.2. Free Vibration Analysis

In this section free vibration results for symmetrically and asymmetrically laminated beams are presented. Again the superiority of the higher order theory (RHSDT) over the FSDT and CLT is demonstrated. Further it is shown that for angle-ply beams it is essential to consider Poisson effects to obtain accurate results.

Homogeneous Graphite-Epoxy and Boron-Epoxy Cantilever Beams

In this example numerical results from the CLT, FSDT, and RHSDT are compared to experimental results obtained by Abarcar and Cunniff [35] for the free vibration of homogeneous 15° and 30° Graphite-Epoxy and Boron-Epoxy beams. The dimensions of the test specimens used in the experiment were $L = 7.5\ in, b = 0.5\ in$, and $h = 0.125\ in$. The material properties are shown in Table 5.8.

Table 5.8: *Elastic Properties for Graphite-Epoxy and Boron-Epoxy.*

Elastic Properties	Graphite-Epoxy	Boron-Epoxy
E_1 [psi]	18.74×10^6	36.6×10^6
E_2 [psi]	1.367×10^6	3.851×10^6
G_{12} [psi]	0.7479×10^6	1.334×10^6
G_{13} [psi]	0.6242×10^6	0.7408×10^6
G_{23} [psi]	0.3686×10^6	3.845×10^6
ν_{12}	0.3	0.267
ρ [lb-s^2-in^{-4}]	0.142×10^{-3}	0.1943×10^{-3}

Note that in Tables 5.9 - 5.12 "T" denotes predominately torsional modes. In Table 5.9 the results obtained from the RHSDT with 2, 4, and 8 elements over the length of a 30° Graphite-Epoxy Beam are shown. As can be seen the results for the natural frequencies converge when the beam is modeled with 8 elements. Hence for all subsequent studies 8 elements were used over the length of the beam.

The numerical results obtained using the CLT, the FSDT, and the RHSDT are compared to the experimental results for the 15° and 30° Graphite-epoxy beams. These results are shown in Tables 5.10 and 5.11, respectively. Because of the large

Table 5.9: *Convergence of Finite Element Results from the RHSDT for the Natural Frequencies (in Hz.) of an 30° Orthotropic Graphite-Epoxy Beam.*

Mode	2 Elements	4 Elements	8 Elements	Experiment [35]
1	53.2	53.2	53.1	52.7
2	335.6	333.0	332.5	331.8
3	1275.1	936.7	927.8	924.7
4				1766.9 T
5	3518.6	1837.6	1810.9	1827.4
6	8513.3	3723.9	2984.5	2984.0
7	8514.1	6134.8	4454.6	4432.4

aspect ratio of $L/h = 60$, the CLT, the FSDT, and the RHSDT all yield accurate results for the lower vibration frequencies. The CLT overpredicts the higher vibration frequencies, while both, the FSDT and the RHSDT, accurately predict these frequencies. This shows that shear deformation becomes more important for higher modes.

In Table 5.12 the numerical results from the RHSDT for the first six vibration modes of a 15° and a 30° Graphite-epoxy beam are compared to the experimental results of Abarcar and Cunniff. Again, the results are in good agreement. The differences for the 15° case can be attributed to the fact that Abarcar and Cunniff did not report a unique value for the shear modulus G_{12}, but rather a range of values, and that the value chosen for this study was closer to the value reported for the 30° beam than to the one for the 15° beam.

Because the present model does not account for torsional deformation, the predominately torsional modes found by Abarcar and Cunniff were not predicted.

Table 5.10: *Comparison of the Vibration Frequencies (in Hz.) of a* 15° *Graphite-Epoxy Beam* $(L/h = 60)$.

Mode	CLT	FSDT	RHSDT	Experiment [35]
1	83.1	83.1	83.0	82.5
2	520.6	517.8	517.8	511.3
3	1457.0	1438.4	1438.4	1423.4
4				1526.9 T
5	2856.2	2790.1	2790.3	2783.6
6	4733.3	4562.2	4562.7	4364.6
7				4731.6 T

Table 5.11: *Comparison of the Vibration Frequencies (in Hz.) of a* 30° *Graphite-Epoxy Beam* $(L/h = 60)$.

Mode	CLT	FSDT	RHSDT	Experiment [35]
1	53.2	53.2	53.1	52.7
2	333.4	332.5	332.5	331.8
3	933.3	927.8	927.8	924.7
4				1766.9 T
5	1830.8	1810.9	1810.9	1827.4
6	3036.7	2984.5	2984.5	2984.0
7	4568.9	4454.3	4454.6	4432.4

Table 5.12: *Comparison of Finite Element Results from the RHSDT and Experimental Results* [35] *for the Natural Frequencies (in Hz.) of Boron-Epoxy Beams.*

	15°		30°	
Mode	RHSDT	Experiment	RHSDT	Experiment
1	96.6	91.0	62.5	62.5
2	601.3	567.5	390.9	391.7
3	1665.6	1575.5	1090.5	1090.5
4		1767.4 T	2127.7	2107.7
5	3217.5	3073.6		2174.3 T
6	5235.2	4926.7	3505.4	3542.4

Simply-Supported Symmetrically Laminated Angle-Ply Beams

This example demonstrates the importance of the Poisson-effects for the analysis of angle-ply beams. Results obtained using the RHSDT with and without Poisson-effects are compared to results reported by Chandrashekhara et al. [13]. In the finite element formulation Poisson-effects can be neglected by equating the generalized strains ϵ_2^0, ϵ_2^1, and ϵ_2^2 in equation (3.9) to zero. Then the laminate matrix $[D]$ in equation (3.14) becomes $[D] = [D^{xx}]$. Bend-twist coupling can be eliminated by restraining the torsional degrees of freedom in the input for the finite element program.

Chandrashekhara et al. presented an analytical solution for the fundamental frequencies of symmetrically laminated angle-ply beams, including shear-effects and rotatory inertia, but neglecting Poisson-effects and bend-twist coupling. In Table 5.13 results for the following cases are shown:

Case 1 RHSDT including Poisson-effects

Case 2 RHSDT neglecting Poisson-effects

Case 3 RHSDT neglecting Poisson-effects and bend-twist coupling

Case 4 Results reported by Chandrashekhara et al.

The material properties used in this example were

$$E_L = 21.0 \times 10^6 \text{psi}, \qquad E_T = 1.4 \times 10^6 \text{psi}, \qquad G_{TT} = 0.5 \times 10^6 \text{psi}$$

$$G_{LT} = 0.6 \times 10^6 \text{psi}, \qquad \nu_{LT} = \nu_{TT} = 0.25, \qquad \rho = 0.13 \times 10^{-3} lbs^2 in^{-4} \tag{5.3}$$

and the fundamental frequency has been nondimensionalized as

$$\bar{\omega} = \omega L^2 \sqrt{\frac{\rho}{E_1 h^2}}. \tag{5.4}$$

The results in Table 5.13 show that it is essential to include Poisson-effects in the analysis of angle-ply beams. Neglecting the Poisson-effects can lead to a serious overprediction of the fundamental frequency. For the $[45/-45]_s$ beam the fundamental frequency predicted by Chandrashekhara is 72.5% too high.

Table 5.13: *Influence of the Poisson Effects on the Nondimensionalized Fundamental Frequencies of Simply Supported Angle-Ply* $[\theta/-\theta/-\theta/\theta]$ *Beams* $(L/h = 15)$.

	θ (deg)						
Case	0	15	30	45	60	75	90
1	2.6510	2.2522	1.4520	0.8909	0.7358	0.7252	0.7301
2	2.6570	2.3440	1.8930	1.4040	0.9729	0.7584	0.7322
3	2.6570	2.5110	2.1041	1.5370	1.0126	0.7613	0.7322
4	2.6560	2.5105	2.1032	1.5308	1.0124	0.7611	0.7320

Free Vibration of Asymmetrically Laminated Cantilevered Composite Panels

This example is used to validate the RHSDT for asymmetrically laminated beams. The fundamental frequencies for a number of cantilevered composite panels are calculated and compared to experimental results by Thornton [36]. All of the panels considered had a bottom layer oriented at 0 degrees and a top layer oriented at 0, 22.5, 45, 67.5, and 90 degrees, respectively, for the different panels. The geometry is shown in Table 5.14 and in Figure 5.10. The material properties used were:

$$E_L = 23.3 \times 10^6 \text{psi}, \qquad E_T = 1.81 \times 10^6 \text{psi}, \qquad G_{LT} = G_{TT} = 0.976 \times 10^6 \text{psi}$$

$$\nu_{LT} = \nu_{TT} = 0.22, \qquad \rho = 0.174 \times 10^{-3} lbs^2 in^{-4} \tag{5.5}$$

Table 5.14: *Characteristics of the Boron-epoxy Panels.*

	θ (deg)		
Panel	Bottom Layer	Top Layer	Panel Thickness [in]
1	0.	0.	0.0452
2	0.	22.5	0.0492
3	0.	45.	0.0460
4	0.	67.5	0.0470
5	0.	90.	0.0442

The results are shown in Table 5.15. Agreement between the experimental and numerical results is good. The discrepancy can be attributed to the modelling of a square plate as a one-dimensional beam.

Table 5.15: *Comparison of the Fundamental Frequencies (in Hz) of Asymmetrically Laminated Composite Panels [θ/0°].*

	θ (deg)				
Method	0	22.5	45	67.5	90
Experiment [36]	41.2	34.3	24.4	21.8	21.4
RHSDT	41.7	31.2	24.3	22.6	22.4

Asymmetrically Laminated Clamped-Clamped Beams

In this example some results for the free vibration of asymmetrically laminated beams are presented. Again the superiority of the RHSDT over the FSDT and the CLT is shown. Three different lamination schemes were chosen to study the effect of the bend-stretch and the bend-twist coupling. The schemes were:

1. a bending stiff $[0°/90°]_T$ laminate,

2. a torsion stiff $[45°/-45°]_T$ laminate, and

3. a quasi-isotropic $[0°/45°/-45°/90°]_T$ laminate.

In Table 5.16 results obtained with the CLT, FSDT, and RHSDT for clamped-clamped beams are compared for two different aspect ratios ($L/h = 10$ and $L/h = 100$). The same material properties and nondimensionalization of the results as given in equations (5.3) and (5.4) , respectively, were used.

Table 5.16: *Comparison of the Nondimensionalized Fundamental Frequencies of Clamped-Clamped Graphite-Epoxy Beams.*

Lay-up	L/h	10	100
$[0°/90°]_T$	CLT	3.065	3.080
	FSDT	2.577	3.074
	RHSDT	2.631	3.075
$[0°/45°/-45°/90°]_T$	CLT	3.037	3.054
	FSDT	2.560	3.047
	RHSDT	2.536	2.957
$[45°/-45°]_T$	CLT	1.950	1.959
	FSDT	1.804	1.958
	RHSDT	1.789	1.935

As expected, the fundamental frequencies for the slender beams ($L/h = 100$) predicted by the three theories were practically the same. For $L/h = 10$ the CLT overpredicted the fundamental frequencies. For all lamination schemes the fundamental mode was a flexural mode. This explains that the fundamental frequencies for the bending stiff beams ($[0°/90°]_T$ and $[0°/45°/-45°/90°]_T$) were much higher than the fundamental frequencies for the torsion stiff beam ($[45°/-45°]_T$).

Clamped-Clamped and Clamped-Free Cross-Ply [0°/90°/90°/0°] Beam.

The last example in this section is used to compare the vibration frequencies predicted by the RHSDT and the SVHSDT for symmetrically laminated cross-ply beams. The same material properties as in equation (5.5) were used. The results are shown in Table 5.17. The vibration frequencies predicted by both theories are in good agreement.

Table 5.17: *Comparison of Finite Element Results from the RHSDT and the SVHSDT for the Vibration Frequencies* ($\bar{\omega} = \omega L^2\sqrt{\rho/(E_1 h^2)}$) *of a Symmetric* [0/90/90/0] *Cross-Ply Beams* ($L/h = 15$).

BC	Clamped-Clamped		Clamped-Free	
Mode	RHSDT	SVHSDT	RHSDT	SVHSDT
1	4.781	4.875	0.927	0.930
2	18.378	18.951	5.045	5.122

5.3. Transient Analysis

5.3.1. Linear Transient Analysis

In this section the finite element model is verified for the linear transient analysis. A simply-supported isotropic beam subjected to a sine pulse given by

$$P = P_0 \, sin\frac{\pi t}{\tau} \qquad \text{for} \quad 0 \leq t \leq \tau$$

$$P = 0 \qquad \text{for} \quad t \geq \tau$$

is considered. The force is located at the center of the beam. The material properties used were

$$E_1 = E_2 = 30 \times 10^6\ psi, \quad G_{12} = G_{13} = G_{23} = 11.538 \times 10^6\ psi,$$
$$\nu = 0.3, \quad \text{and} \quad \rho = 733 \times 10^{-6}\ lb/in^3. \tag{5.6}$$

The dimensions of the beam were $L = 30\ in$ and $h = b = 0.5\ in$, and the numerical values for the sine pulse taken were $P_0 = 1000\ lb$, and $\tau = 20 \times 10^{-6}\ s$. Harris and Crede [37] obtained an analytical solution for the center deflection for this problem using the CLT. In Table 5.18, the numerical results for the center deflection obtained using the RHSDT are compared to the analytical results of Harris and Crede. The agreement between the numerical results and the analytical solution is good. Differences can be attributed to the different theories used. The convergence of the finite element solution to the analytical results for small times ($t < 20\ \mu s$) is fair, but is good for larger times ($t > 20\ \mu s$). In Table 5.18 N denotes the number of elements used in the mesh and Δt denotes the timestep used.

Table 5.18: *Central Deflection [in] of a Beam Subjected to a Sine Pulse at the Center*

$t[\mu s]$	$N = 5$ $\Delta t = 1\ \mu s$	$N = 10$ $\Delta t = 1\ \mu s$	$N = 20$ $\Delta t = 0.1\ \mu s$	$N = 30$ $\Delta t = 0.05\ \mu s$	Ref. [37]
1	1.209E-7	2.406E-7	3.224E-7	4.750E-7	5.328E-7
5	9.945E-6	1.932E-5	3.282E-5	3.915E-5	2.868E-5
10	7.082E-5	1.282E-4	1.723E-4	1.810E-4	1.441E-4
20	3.722E-4	5.325E-4	5.516E-4	5.491E-4	4.984E-4
30	6.787E-4	7.706E-4	7.506E-4	7.528E-4	7.210E-4
40	8.961E-4	9.326E-4	9.121E-4	9.118E-4	8.861E-4
50	1.048E-3	1.047E-3	1.046E-3	1.047E-3	1.024E-3
60	1.174E-3	1.144E-3	1.164E-3	1.166E-3	1.146E-3

5.3.2. Nonlinear Transient Analysis

The nonlinear transient response of $[0°/90°]_T$ and $[90°/0°]_T$ Graphite-Epoxy beams to a suddenly applied concentrated load at the center of the beam is investigated in this section. The effect of the lamination, boundary conditions and axial loads is studied. The material properties used in all cases were $E_1 = 144.8\ GPa$, $E_2 = 9.65\ GPa$, $G_{12} = G_{13} = 4.14\ GPa$, $G_{23} = 3.45\ GPa$, $\nu = 0.3$, and $\rho = 1389.23\ kg/m^3$. The dimensions of the beam were chosen as $L = 0.1\ m$, and $b = h = 0.01\ m$, the timestep used was $\Delta t = 0.1\ \mu s$, and the applied load was $P = 10kN$. No results on the nonlinear transient response of asymmetric composite beams have been found in literature. Thus, it is believed that the results presented here can serve as a benchmark for future investigations.

Effect of Lamination Scheme and Boundary Conditions

The effect of the lamination scheme on the nonlinear transient response was studied for pinned-pinned and clamped-clamped beams. Reversing lamination actually amounts to changing the direction of the transverse load, as was discussed in the examples for the nonlinear static analysis. Considering the results obtained from the nonlinear static response of cross-ply beams, it was expected that the transient response of pinned-pinned beams would be affected by the orientation of the beam (i.e., by the direction of the force), but that the response of the clamped-clamped beam would be independent of the beam orientation. In Figures 5.11 (a) and 5.11 (b) the center deflection and the inplane force resultant for pinned-pinned beams

are compared. As can be seen the response is significantly affected by the orientation of the beam. For the $[0°/90°]_T$ beam the center deflection and the vibration period are higher than for the $[90°/0°]_T$ beam. The same can be observed for the inplane resultant forces N_x. For the clamped-clamped beam the orientation of the beam has no effect on the transient response. As shown in Figures 5.12 (a) and 5.12 (b), the curves for both orientation are almost indistinguishable.

Effect of Axial Stresses

The effect of the axial stresses on the center deflection and inplane resultant forces of pinned-pinned beams has been investigated. The center deflections and inplane resultant forces for the prestressed beam have been compared to the deflections and resultant forces of the unstressed beams for three different magnitudes of tensile and compressive axial stresses. These results are shown in Figures 5.13, 5.14, and 5.15. As expected, tensile axial stresses have a stiffening effect and thus lower the deflection of the beam, and compressive axial stresses have a softening effect and increase the deflection of the beam. For low axial forces the effect is almost negligible, but for higher axial forces the change in the response of the beam is significant. For both, tensile and compressie axial forces the vibration period of the beam is lowered. This might be caused by the high tensile resultant forces induced by the large deflections of the beam.

5.3.3. Impact Analysis

To evaluate the finite element model in the prediction of the impact response a number of problems found in literature were solved.

Goldsmith Problem

If the mass of the impactor is not small compared to the mass of the beam, then multiple collisions may occur. This problem was considered first by Goldsmith [38]. Goldsmith considered the problem of a simply-supported beam subjected to a transverse impact of a 2 cm radius steel ball with initial vlocity of 1 cm/s. The dimensions of the beam were $L = 30.7\ cm$, $b = h = 1\ cm$ and the material properties were $E_1 = E_2 = 31.3 \times 10^6\ psi$, $\nu = 0.289$, and $\rho = 0.00894\ slug/in^3$. Nosier et al. [39] solved this problem analytical and observed a three collions. In Figures 5.16 (a) and 5.16 (b), numerical results obtained using the EBT and the RHSDT are compared to Nosiers analytical results. Agreement between the solutions is excellent.

Impact with Permanent Indentation

The impact response of a simply-supported steel beam is considered here. The beam is impacted by a $1/2\ in$ diameter steel ball at the center of the beam with dimension $L = 30\ in$ and $b = h = 0.5\ in$. The initial velocity of the ball was 150 ft/s and the material properties used were the same as given in equation (5.6) . To solve this problem Sun and Huang [24] used the following force indentation law:

$$F = 1.29 \times 10^6 \alpha^{1.128} \quad 0 \leq \alpha \leq \alpha_m$$

for the loading process and

$$F = F_m \left[\frac{\alpha - \alpha_p}{\alpha_m - \alpha_p} \right]^{3/2} \quad \alpha_m \geq \alpha \geq \alpha_p$$

for the unloading process. Here α_m is the maximum indentation corresponding to the maximum impact force F_m. The permanent indentation was $\alpha_p = 0.0123\ in.$ In Figures 5.17 (a) and 5.17 (b) the impact force history and displacement history obtained using the EBT and the RHSDT are compared to the results by Sun and Huang [24]. Agreement between the EBT and the reference results is excellent. The RHSDT predicts a slightly lower impact force and higher displacements.

Impact of Composite Beams

Sankar and Sun [40] studied the impact response of clamped-clamped composite beams. In their numerical analysis they used a two-dimensional plain strain finite element. The material properties for the Graphite-Epoxy beam were given as $E_1 = 130\ GPa$, $E_2 = 12.9\ GPa$, $G_{12} = G_{13} = G_{23} = 5.17\ GPa$, $\nu = 0.24$, and $\rho = 1490\ kg/m^3$. The dimensions of the beam were $L = 180\ mm$, $b = 25.4\ mm$, and $h = 2.8\ mm$ and the lamination scheme was $[0_2^\circ/90_2^\circ/0_2^\circ/90_2^\circ/0_2^\circ]_s$. The contact law was determined experimentally by Sankar and Sun to be

$$F = 1.293 \times 10^{11}\alpha^2 \quad [N/m^2].$$

The beam was impacted by a 12.7 mm diameter steel ball with a mass of 8.18 $grams$. An impact velocity of 35 m/s was chosen. Results for the time histories of the impact force and the deflection of the beam are shown in Figure 5.18. Agreement between the solutions is good up to a time of 200μs. After that time the agreement is fair. The difference in the results is most likely due to the different theories used. The plain strain finite element allows for deformation of the transverse normal of the

beam. This deformation is not taken into account in the RHSDT and may cause the difference in the results.

The final example shows that it is important to consider geometric nonlinearities in the impact analysis. The same beam as in the previous example was analyzed. In Figure 5.19 the impact force histories obtained using the linear and nonlinear formulations are shown. In the beginning, the differences in the linear and nonlinear results are small. This is because the motion of the beam is not significant during the initial impact. For larger times the stiffening effect due to the geometric nonlinearities becomes more important. The vibration period of the beam is reduced (compared to the linear formulation) and further collisions between the impactor and the beam occur earlier than predicted by the linear formulation.

In Figures 5.20 and 5.21 the impact force histories for unstressed and prestressed beams (tensile and compressive) are compared. The linear response is shown in Figure 5.20 and the nonlinear response is shown in Figure 5.21. It can be seen that in both cases tensile axial stresses have a stiffening effect, and compressive axial stresses have a softening effect. But it also can be seen that the stiffening effect due to the induced resultant axial forces N_x for the nonlinear response are even more significant than the stiffening or softening effects due to the initial stresses.

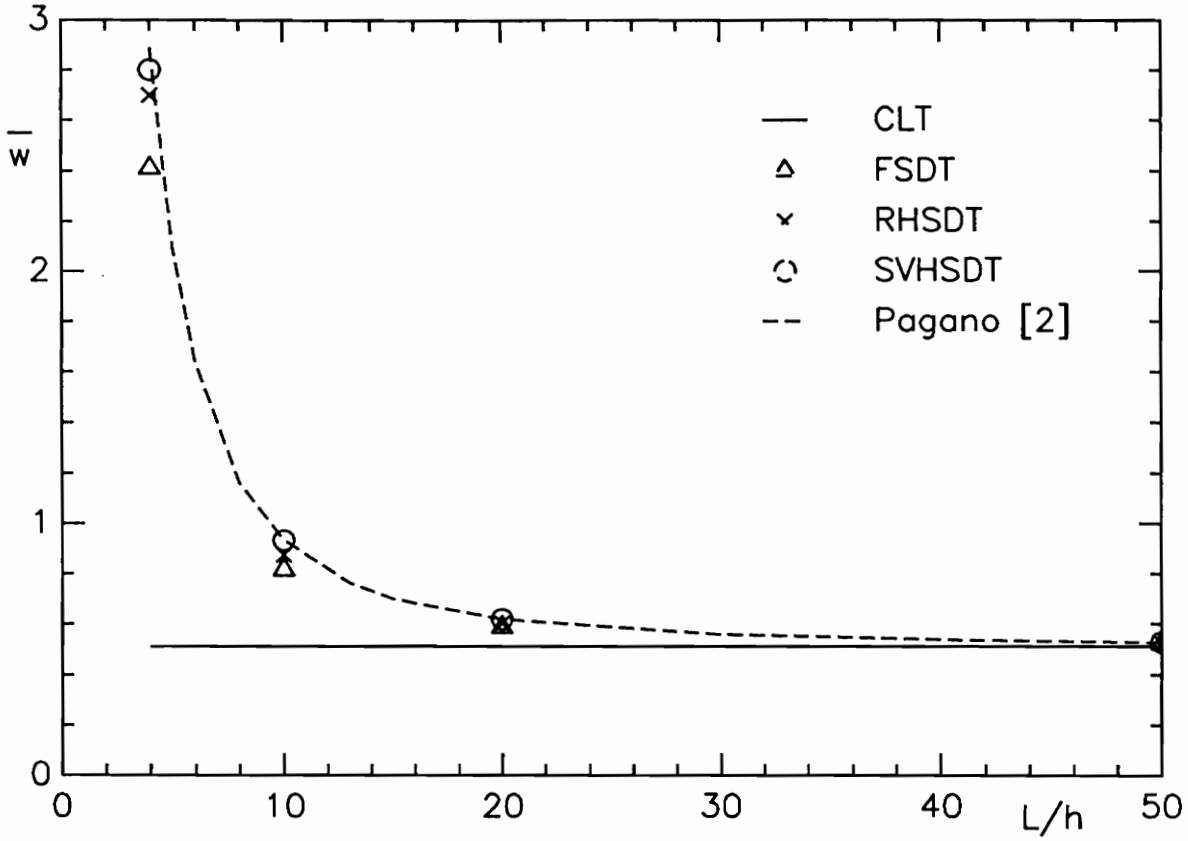

Figure 5.1: *Comparison among the CLT, the FSDT, the RHSDT, the SVHSDT and the Elasticity Theory for the Maximum Deflection.*

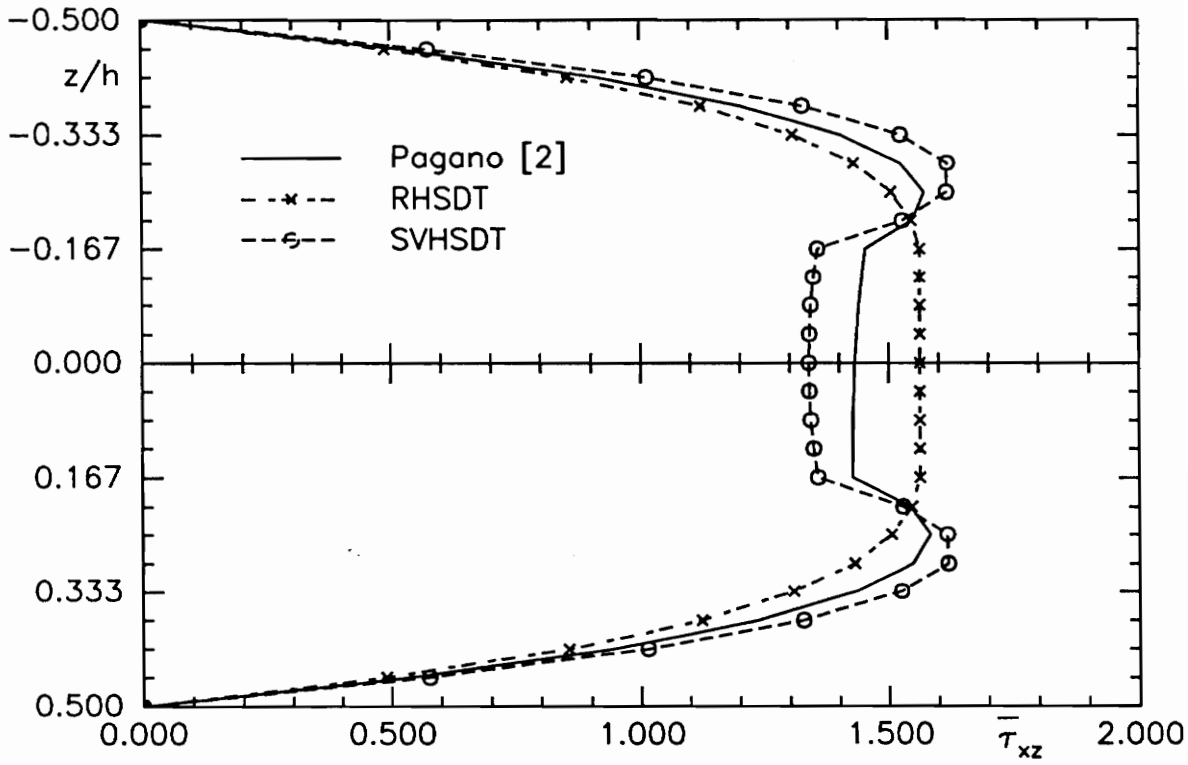

Figure 5.2: *Variation of the Transverse Shear Stresses through the Thickness for the RHSDT, the SVHSDT, and the Exact Solution for a* $[0°/90°/0°]$ *Simply-Supported Beam Under Sinusoidal Load.*

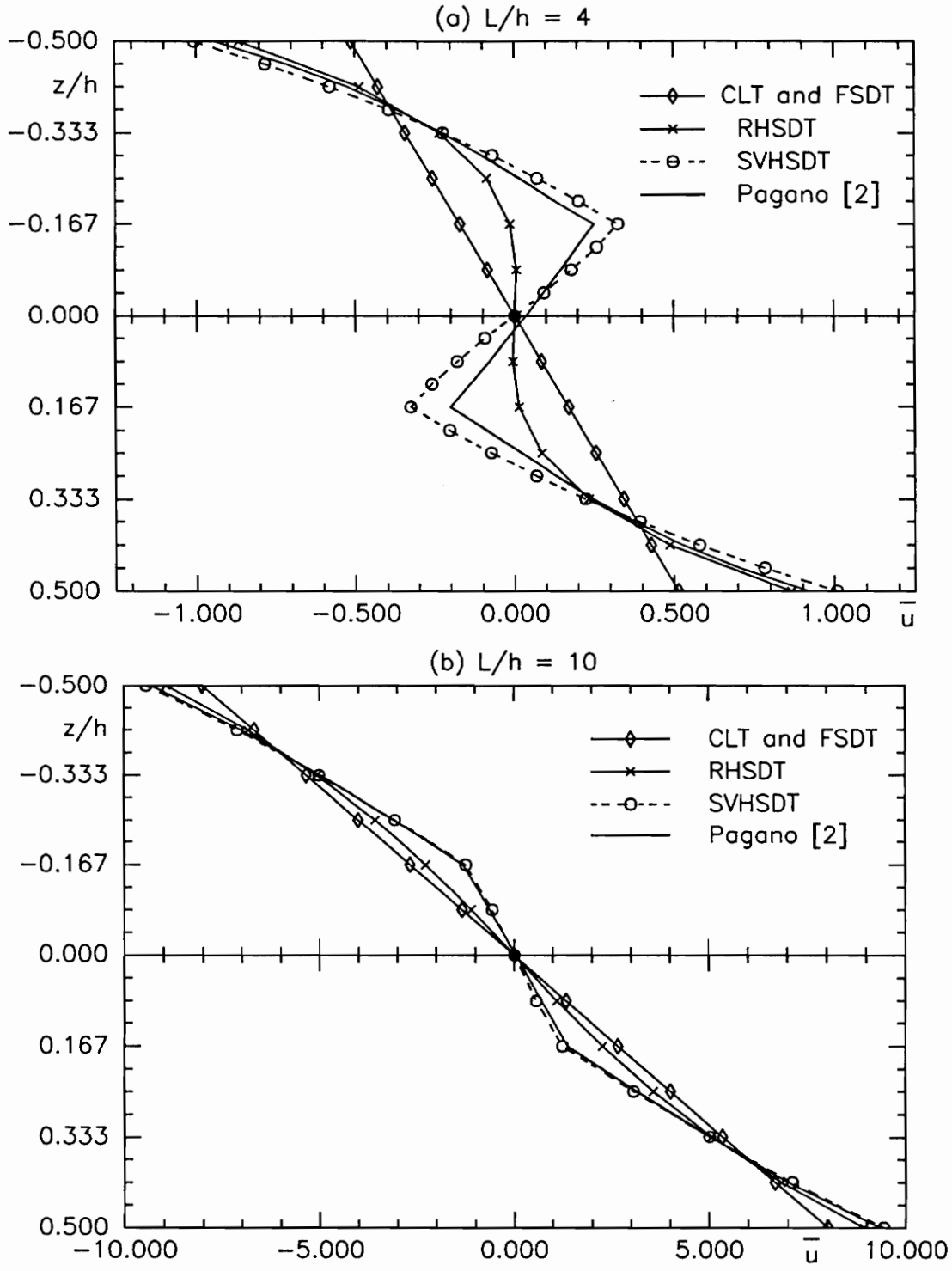

Figure 5.3: *Variation of the Axial Displacement $\bar{u}$ through the Thickness of the Laminate for (a) $L/h = 4$ and (b) $L/h = 10$ for a $[0°/90°/0°]$ Simply-Supported Beam Under Sinusoidal Load.*

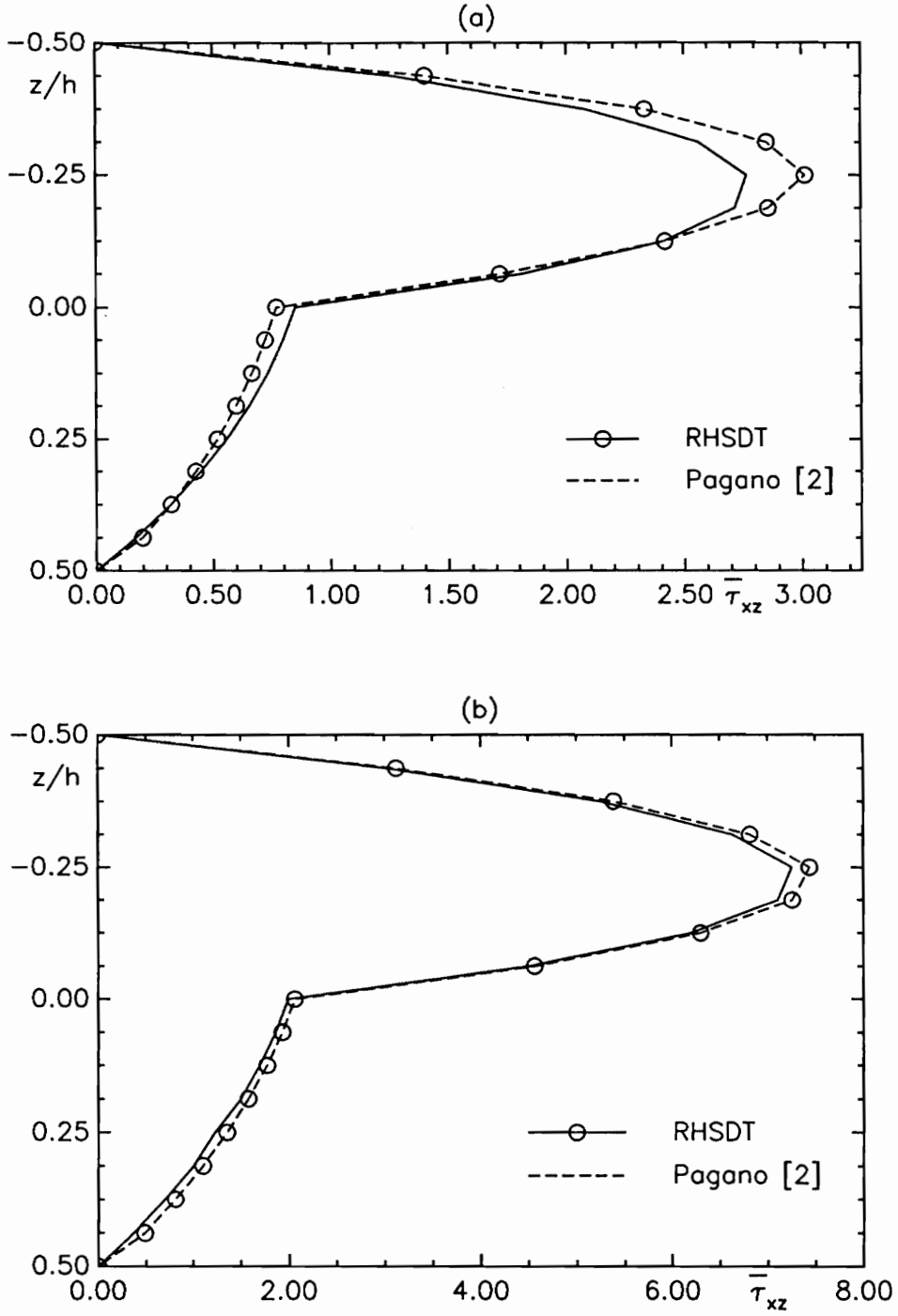

Figure 5.4: *Variation of the Transverse Shear Stresses $\bar{\tau}_{xz}$ through the Thickness of the Laminate for (a) $L/h = 4$ and (b) $L/h = 10$ for a $[0°/90°]_T$ Simply-Supported Beam Under Sinusoidal Load.*

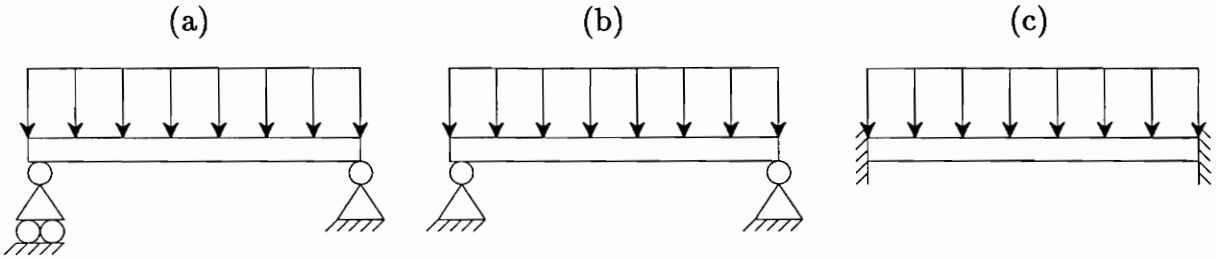

Figure 5.5: *Boundary Conditions : (a) Simply-supported, (b) Pinned-Pinned, and (c) Clamped-Clamped.*

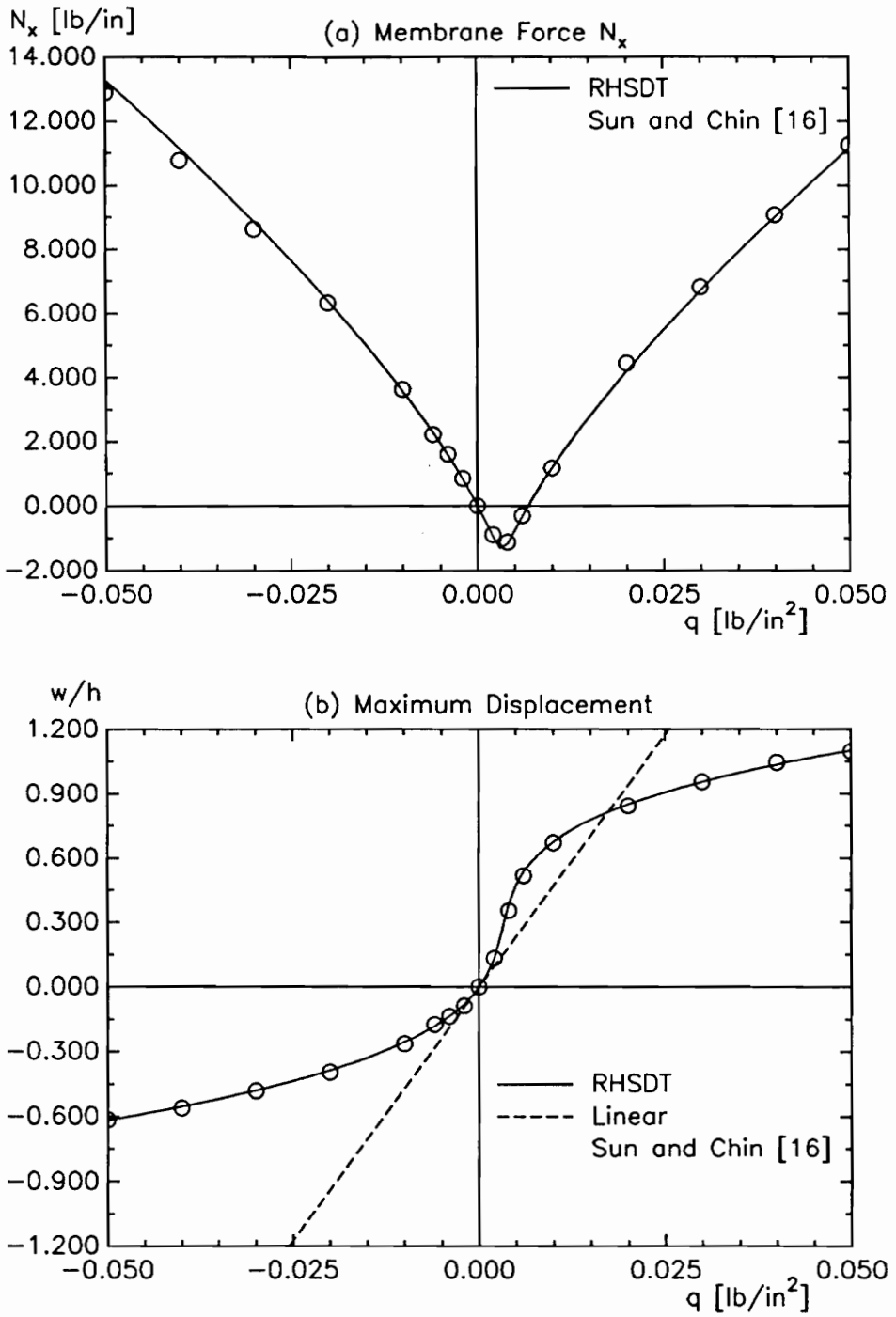

Figure 5.6: *Pinned-Pinned* $[0°/90°]_T$ *Beam* $(L/h = 225)$ *under Uniformly Distributed Load : (a) Membrane Force* N_x*, (b) Maximum Displacement.*

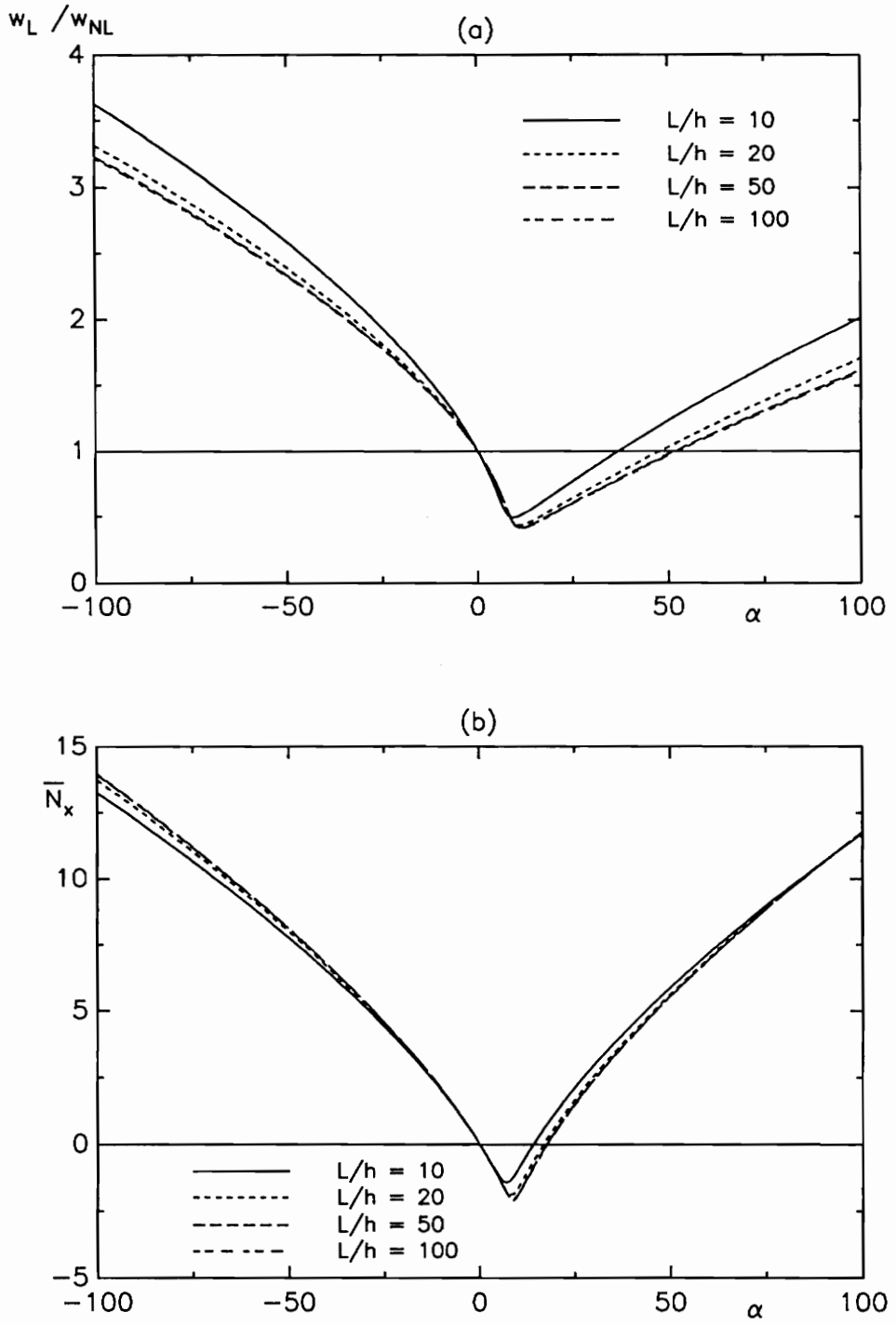

Figure 5.7: *Effect of Aspect Ratios on the Nonlinear Response of Uniformly Loaded* $[0°/90°]_T$ *Beams: (a)* w_L/w_{NL} *versus Load-Parameter* α*, (b) Nondimensionalized Inplane Resultant Force* $\bar{N}_x$ *versus Load-Parameter* α*.*

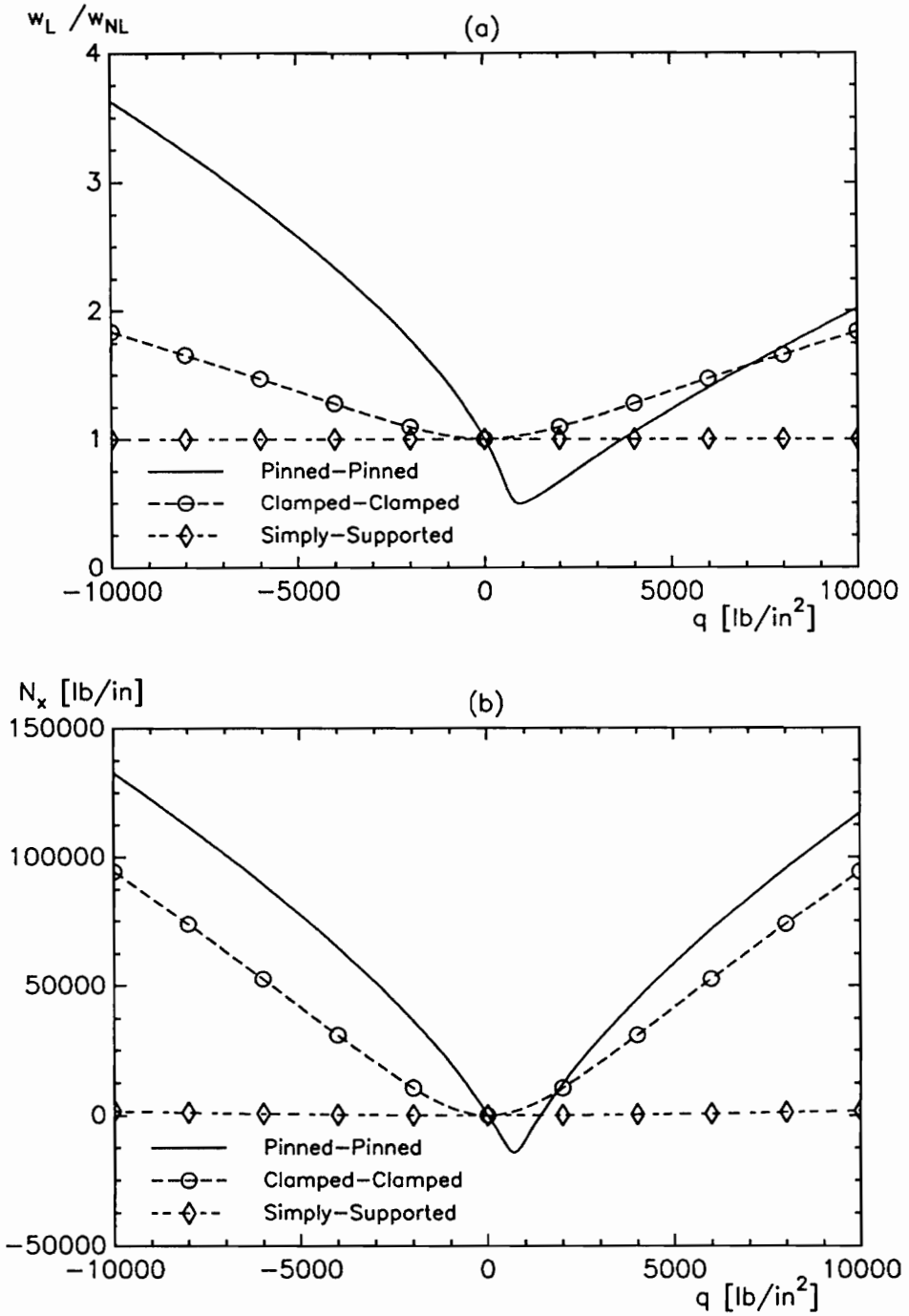

Figure 5.8: *Effect of Boundary Conditions on the Nonlinear Response of Uniformly Loaded* $[0°/90°]_T$ *Beams* $(L/h = 10)$*: (a)* w_L/w_{NL} *versus Load, (b) Inplane Resultant Force versus Load.*

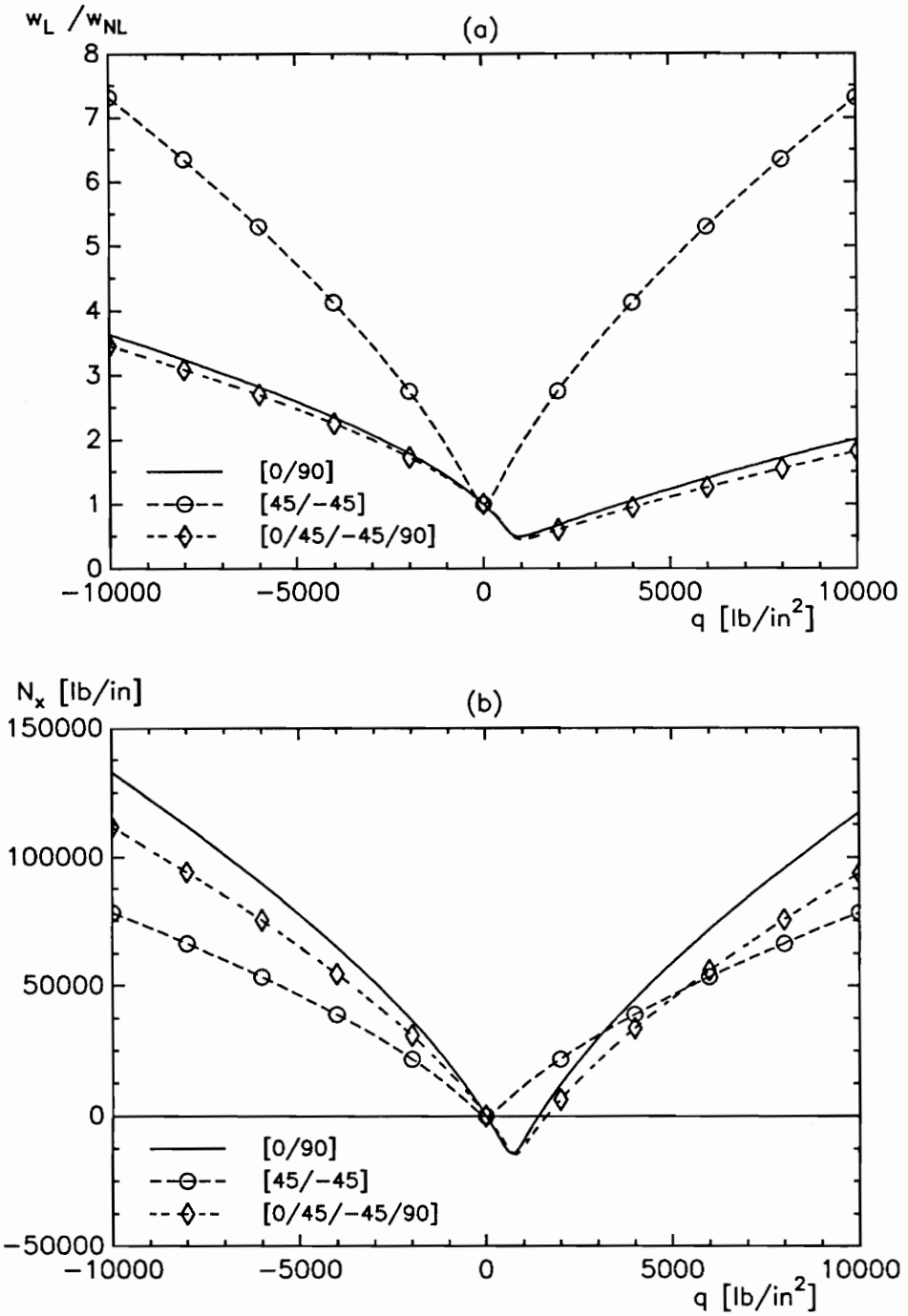

Figure 5.9: *Effect of the Lamination Scheme on the Nonlinear Response of Uniformly Loaded Beams* $(L/h = 10)$*: (a)* w_L/w_{NL} *versus Load, (b) Inplane Resultant Force versus Load.*

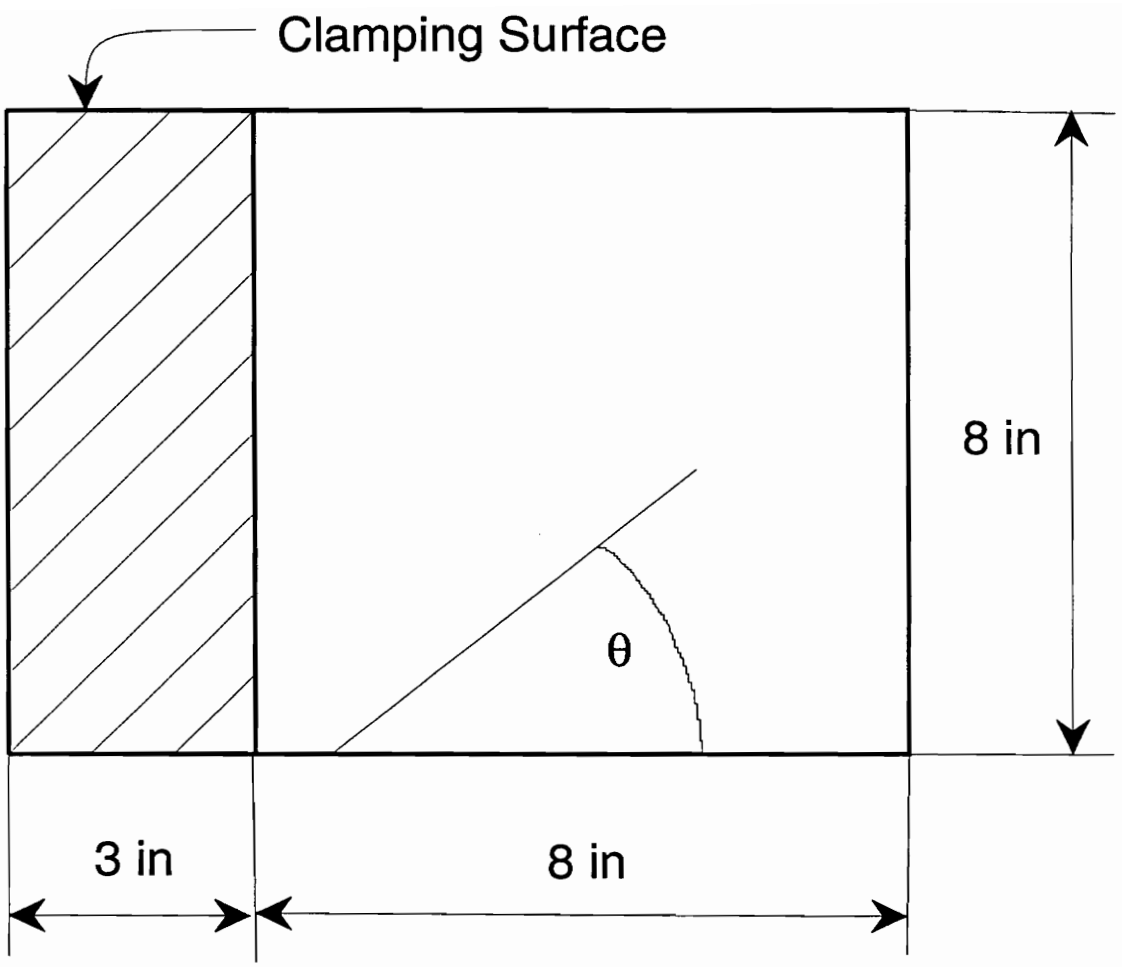

Figure 5.10: *Geometry of the Boron-Epoxy Panels.*

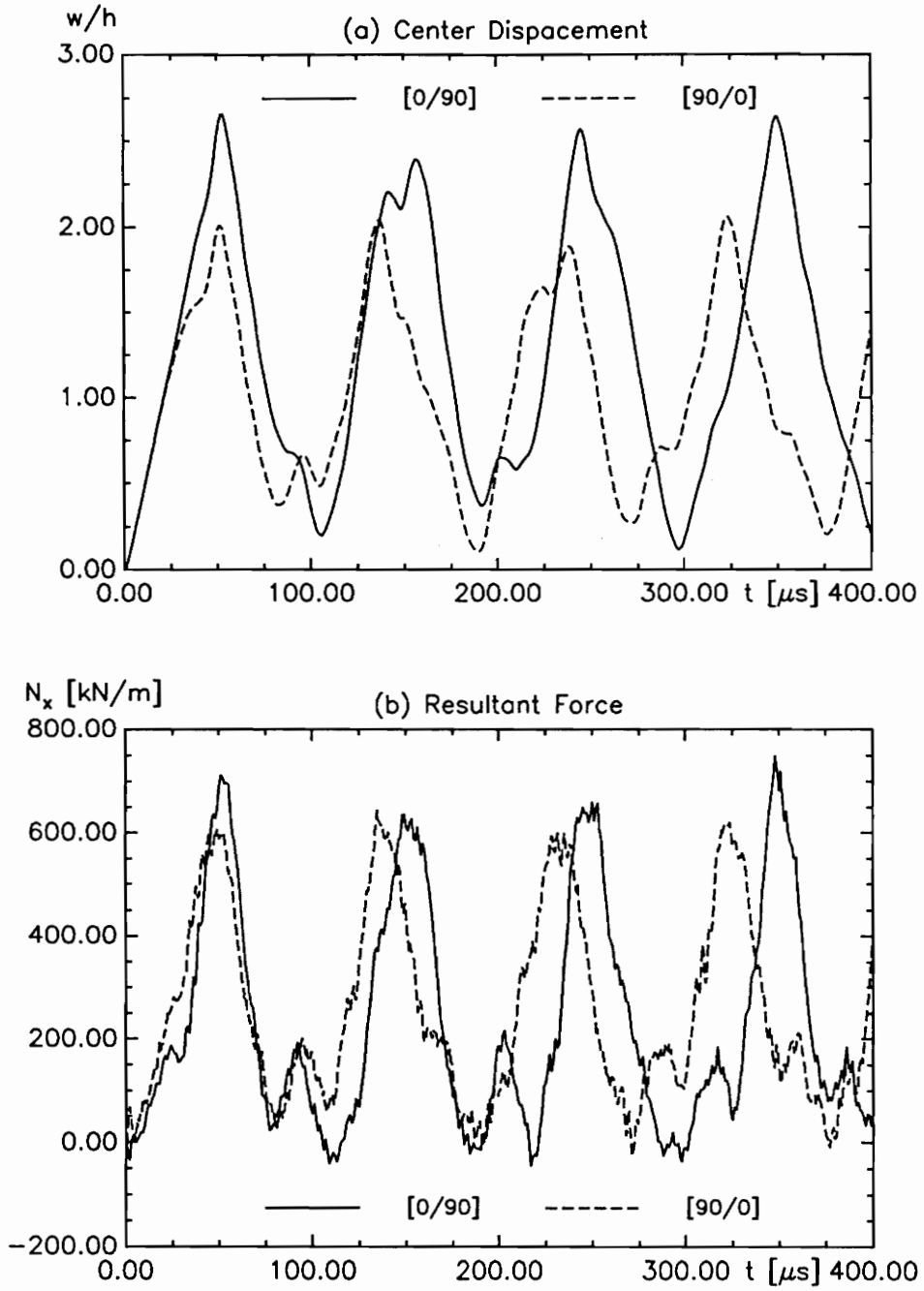

Figure 5.11: *Transient Response of Pinned-Pinned Beams to Suddenly Applied Concentrated Force: (a) Center Deflection , (b) Inplane Resultant Force.*

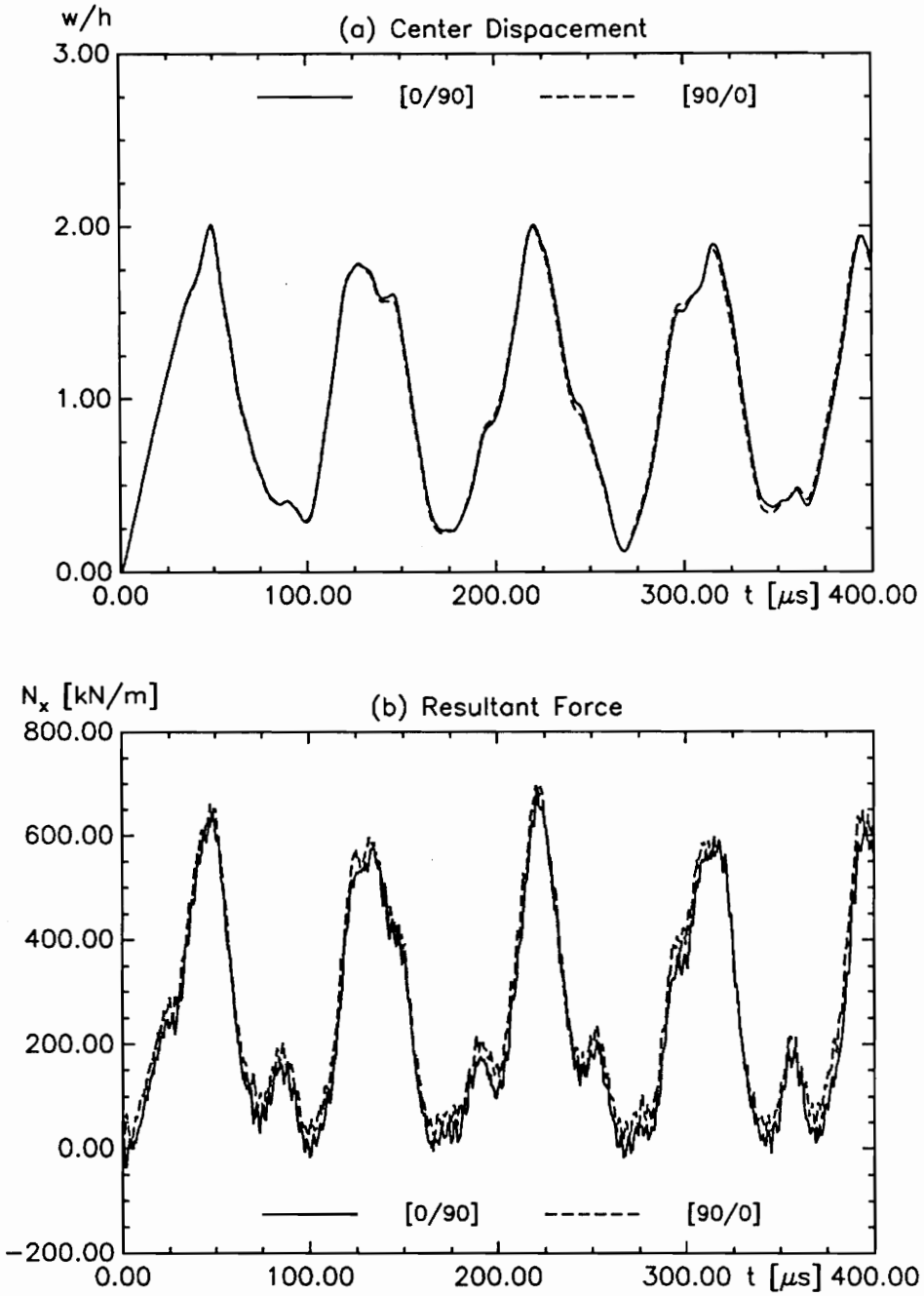

Figure 5.12: *Transient Response of Clamped-Clamped Beams to Suddenly Applied Concentrated Force: (a) Center Deflection , (b) Inplane Resultant Force.*

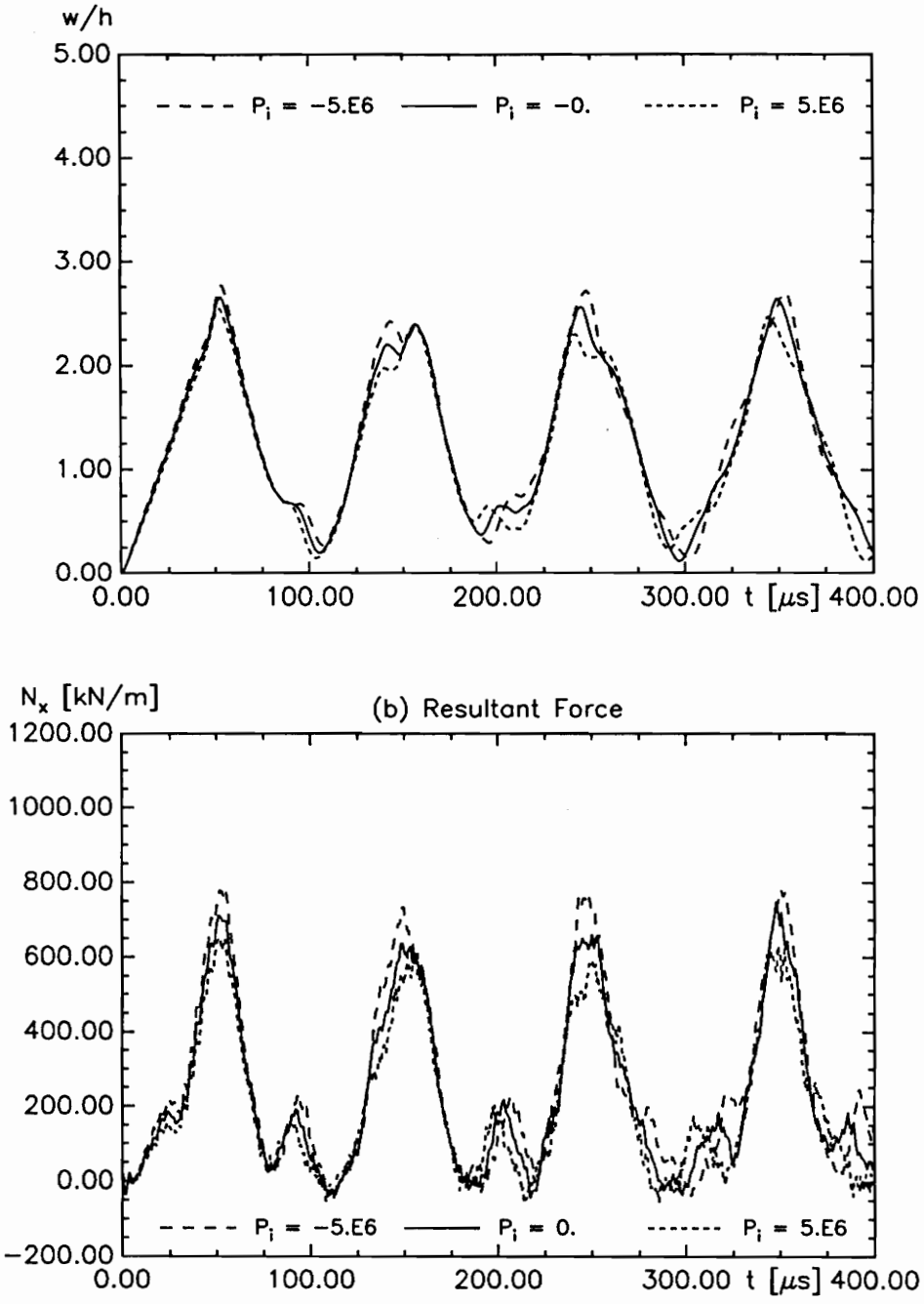

Figure 5.13: *Comparison of the Transient Response of Pinned-Pinned Beams ($P_i = \pm 5.E6\ N/m^2$): (a) Center Deflection, (b) Inplane Force Resultant.*

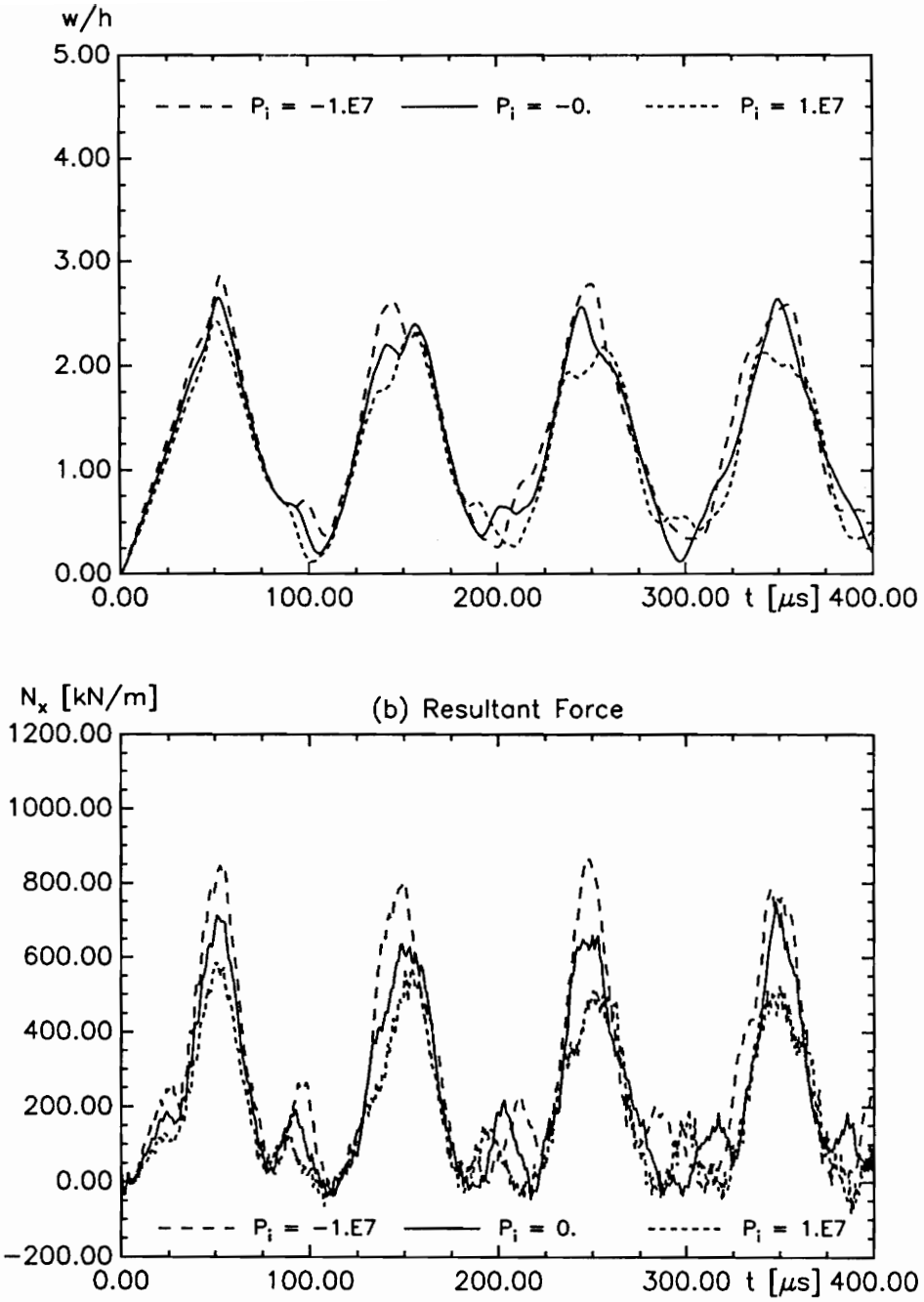

Figure 5.14: *Comparison of the Transient Response of Pinned-Pinned Beams ($P_i = \pm 1.E7\ N/m^2$): (a) Center Deflection, (b) Inplane Force Resultant.*

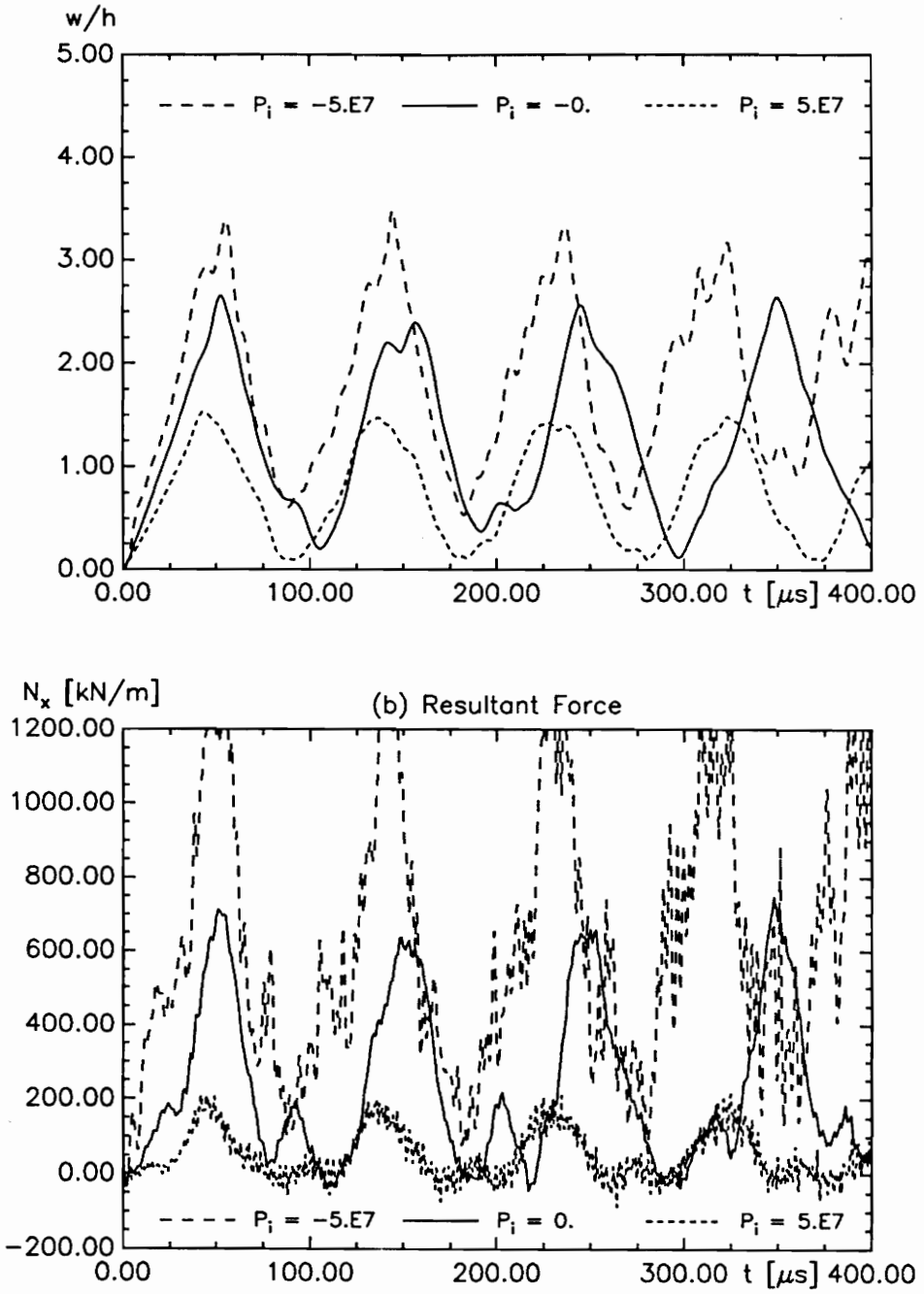

Figure 5.15: *Comparison of the Transient Response of Pinned-Pinned Beams ($P_i = \pm 5.E7\ N/m^2$): (a) Center Deflection, (b) Inplane Force Resultant.*

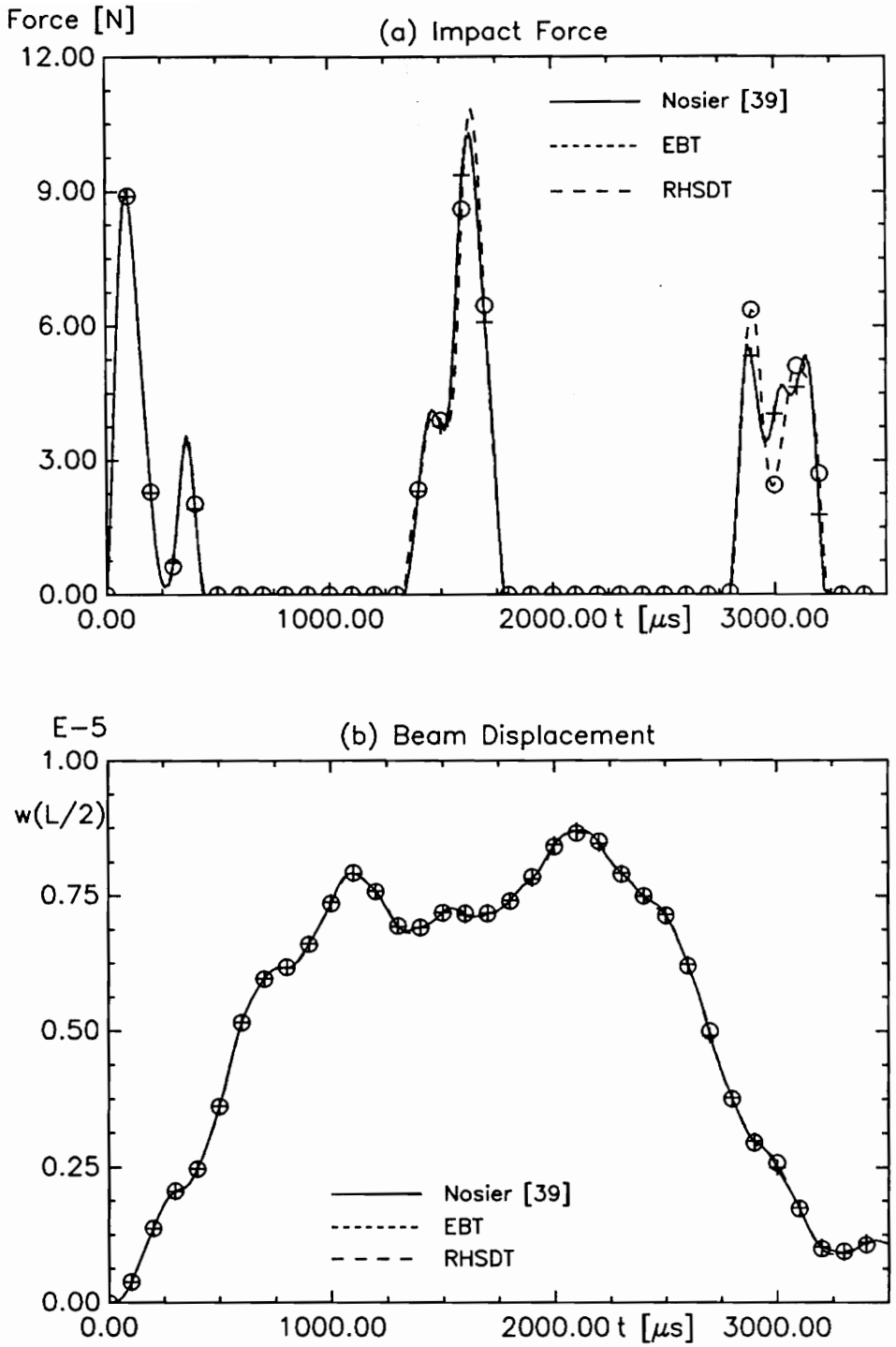

Figure 5.16: *Impact Response of a Simply-Supported Beam: (a) Impact Force, (b) Beam Displacement.*

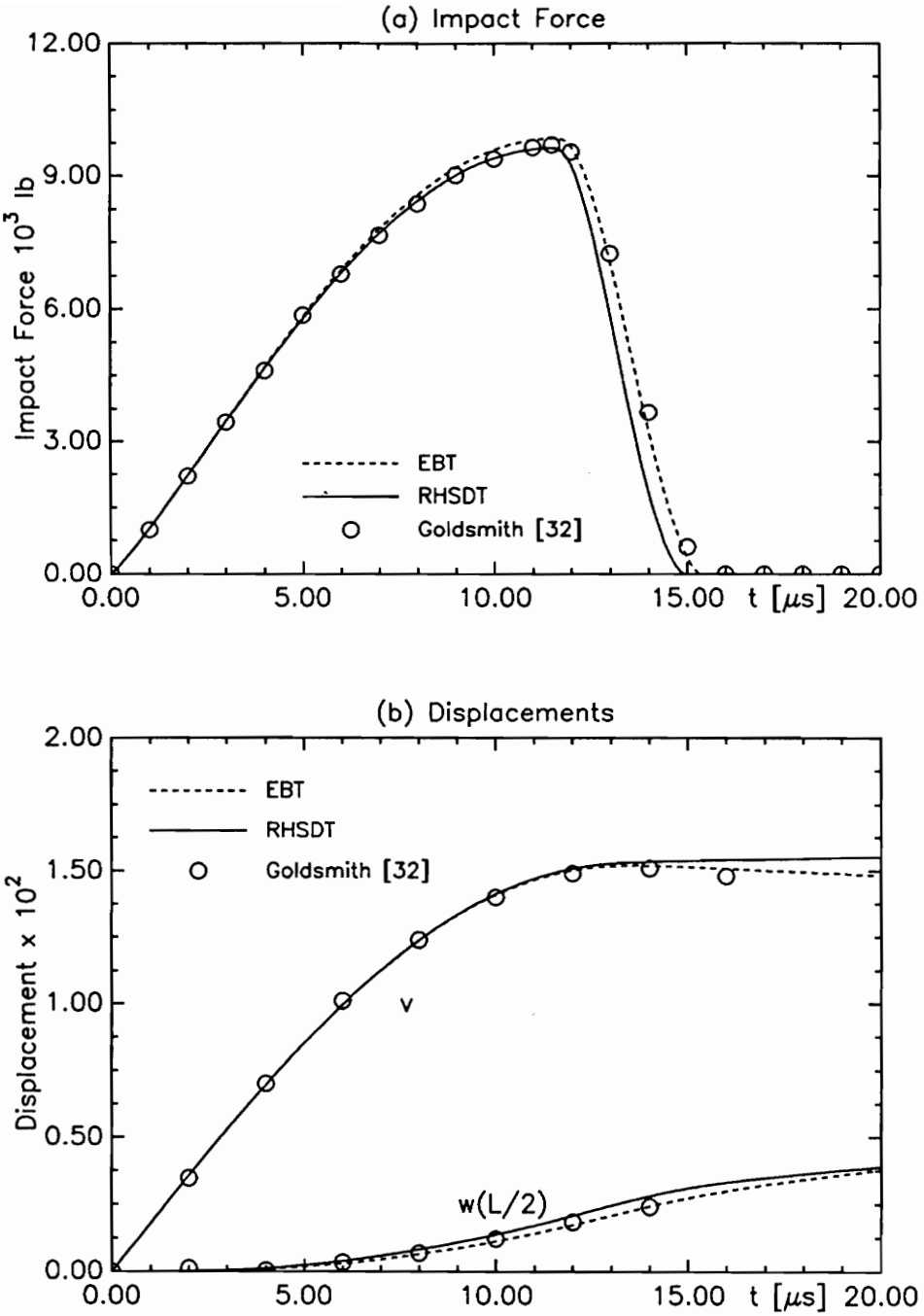

Figure 5.17: *Impact Response of a Simply-Supported Beam: (a) Impact Force, (b) Beam ($w(L/2)$) and Impactor (v) Displacements.*

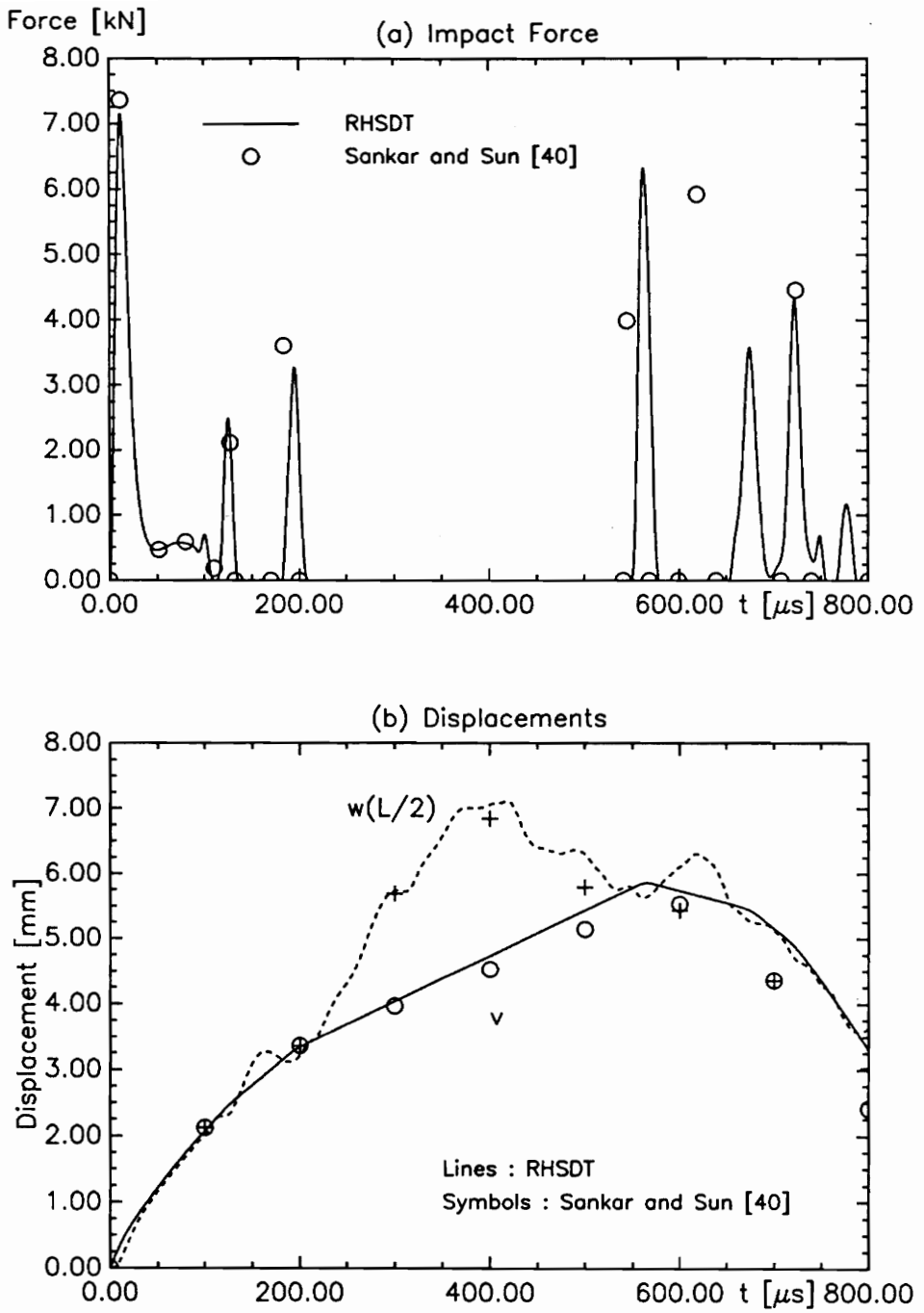

Figure 5.18: *Impact Response of Clamped-Clamped Composite Beams: (a) Impact Force, (b) Beam ($w(L/2)$) and Impactor (v) Displacements.*

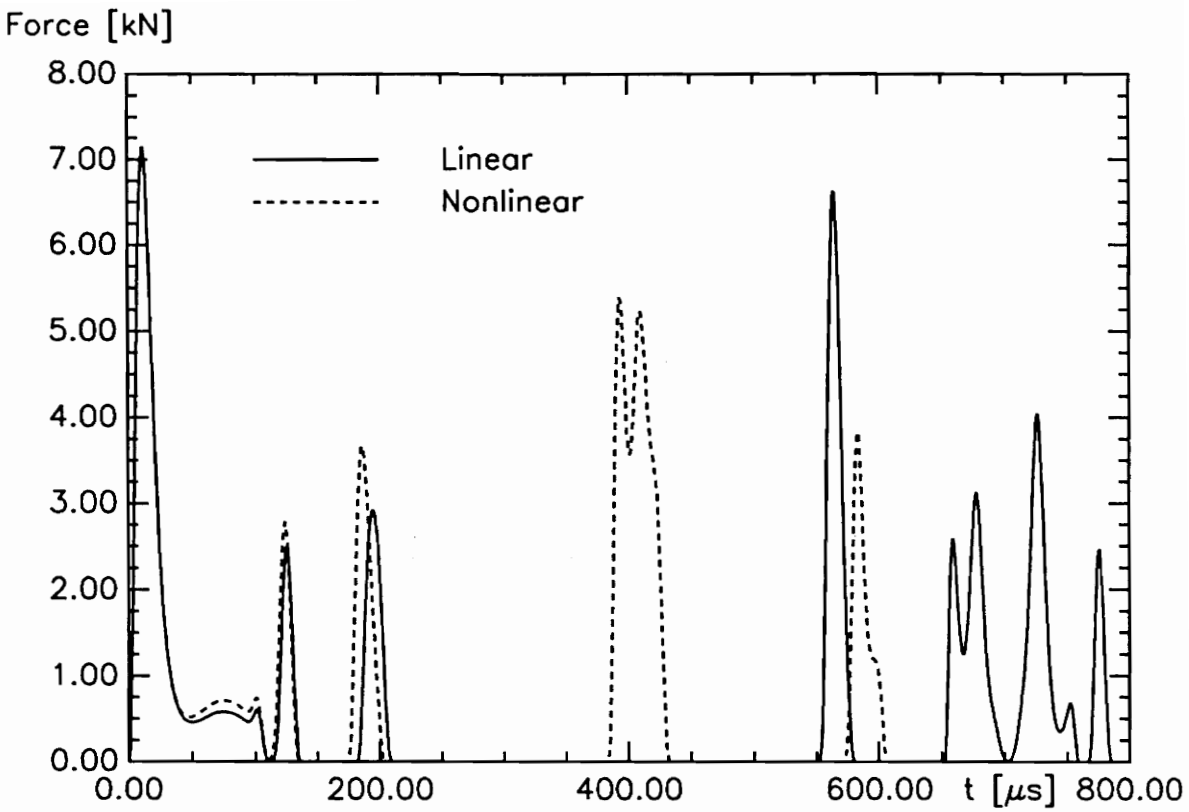

Figure 5.19: *Comparison of the Linear and Nonlinear Impact Response of Clamped-Clamped Composite Beams.*

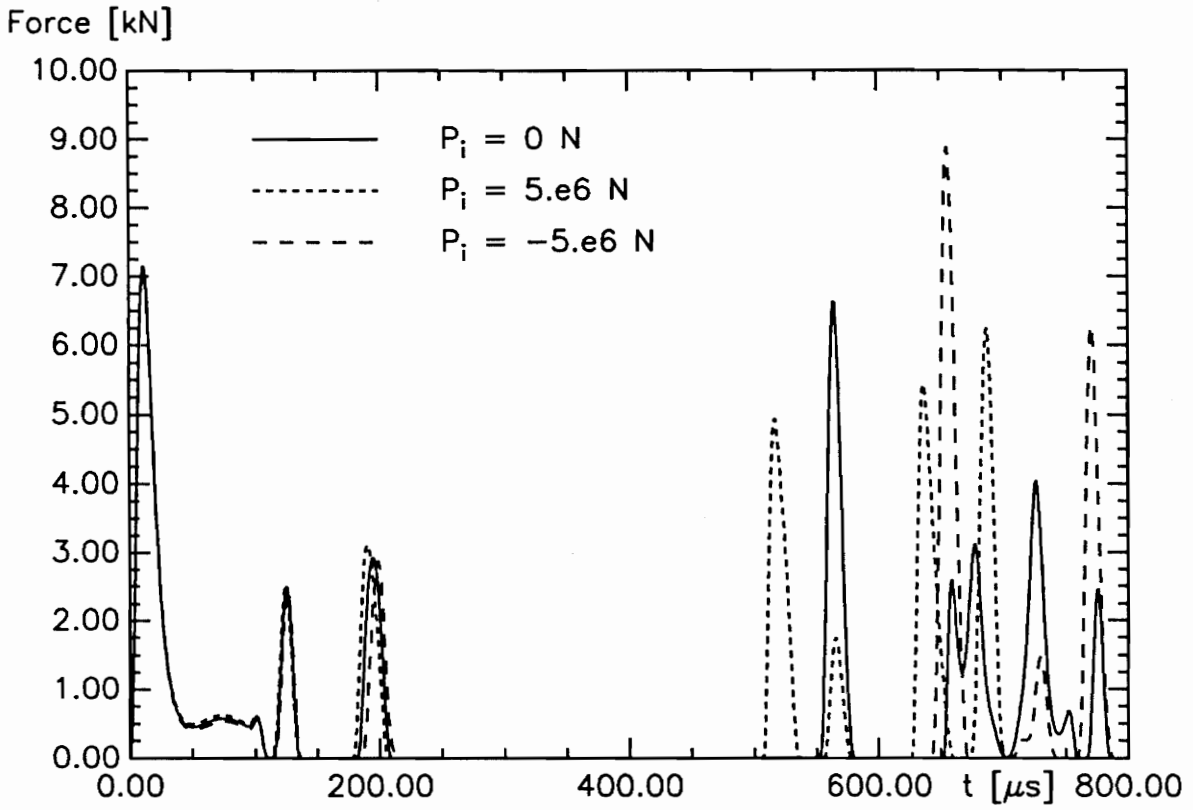

Figure 5.20: *Linear Impact Response of Pre-Stressed Clamped-Clamped Composite Beams.*

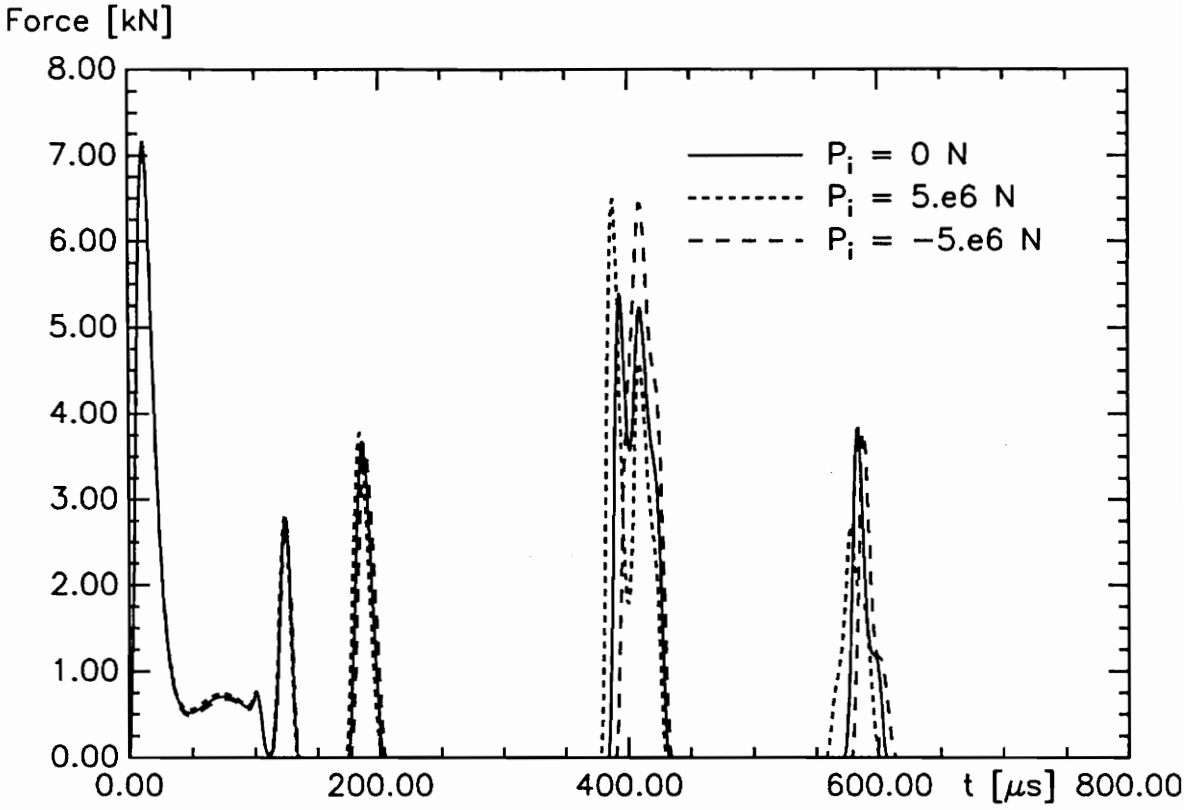

Figure 5.21: *Nonlinear Impact Response of Pre-Stressed Clamped-Clamped Composite Beams.*

6. Conclusions and Future Work

Conclusions

In this study two higher order shear deformation theories for the analysis of laminated composite beams have been developed. The first theory, RHSDT, allows for the analysis of generally laminated beams and accounts for all couplings that characterize generally laminated beams. The second theory, SVHSDT, is restricted to the analysis of symmetrically laminated cross-ply beams. This theory, however, accounts for the continuity of the interlaminar shear stresses at the layer interfaces while keeping the number of degrees of freedom independent of the number of layers.

The SVHSDT has been applied to the linear static analysis and to the free vibration problem. It has been found that this theory performs very well even for short composite beams (Tables 5.2 and 5.3) for which shear deformation is significant. In the cylindrical bending problem for short beams the characteristic discontinuities of the slope of the inplane displacement at the layer interfaces can be observed (Figure 5.3). More important, the magnitude and location of the maximum transverse shear stresses is predicted correctly even for beams with a length to thickness ratio of four (Table 5.5). The CLT, the FSDT, and the RHSDT fail to predict these stresses accurately for beams with $L/h < 10$. Thus, it can be concluded that it is essential to account for the shear stress continuity at the layer interfaces in a theory if short beams are to be analyzed.

The RHSDT has been applied to a series of examples on the linear and nonlinear static response, free vibration, linear and nonlinear transient response, and the

impact response of generally laminated beams. The free vibration results clearly show that even though for beams the resultant laminate forces N_y and Q_y, and moments M_y may be equated to zero, the corresponding strains can not be neglected. Neglecting these strains may lead to a serious overprediction of vibration frequencies (Table 5.13).

The bending-stretching coupling has been found to be essential in the nonlinear analysis of asymmetric beams. The deflection of the beam and the magnitude of the inplane resultant force may depend on the direction of loading of the beam (Figures 5.6- 5.9). The most significant effect of the loading direction on the nonlinear response was observed for pinned-pinned beams, while for clamped-clamped beams the response was independent of the loading direction. For pinned-pinned boundary conditions initially compressive inplane resultant forces may change the nonlinearity from a hardening type to a softening type. Thus, displacements predicted by the nonlinear theory are higher than displacements predicted by the linear theory. This effect should be considered in the design of structures because displacements constraints may be violated. Also, inplane boundary conditions were found to have a significant effect on the nonlinear response.

The same characteristics as discussed for the nonlinear static problem were observed for the nonlinear transient analysis of asymmetric beams. Further, superimposed axial stresses were found to have a significant effect on the transient response of laminated beams. A compressive axial stress causes higher vibration amplitudes and a tensile stress causes lower amplitudes, while both, compressive

and tensile stresses, may reduce the vibration period (Figures 5.13- 5.15). The finite element model has also been validated for impact analysis. Further, it has been shown that geometric nonlinearities have to be concidered to obtain accurate impact results for composite beams (Figures 5.19- 5.21).

Future Work

Some recommendations for future work are:

1. In the present study the buckling of laminated beams has not been investigated. It is straight forward to extend the current formulation to buckling analysis. The problem is interesting because asymmetric beams tend to deflect out-of-plane as soon as inplane loads are applied.
2. The present formulation assumes that initially the beam is perfectly straight. However, for beams with bending-stretching coupling the undeformed beam may not be perfectly straight due to the residual stresses introduced in the curing process. Thus, it would be important to include initial imperfections in the formulation.
3. It has been shown that the continuity of interlaminar shear stresses should be included in the formulation when short beams are analyzed. A theory which accounts for the interlaminar shear stress continuity should be developed that can be applied to asymmetric and angle-ply beams.
4. The higher order shear deformation theory has been shown to yield good results for the impact on isotropic beams. For composite beams the initial response to impact loads was also predicted adequately but some difference could be

observed when multiple collisions occur. Sankar and Sun [40] used a two-dimensional plain strain finite element in their impact analysis and obtained good agreement between experimental and analytical results for composite beams. The plain strain finite element allows for deformation of the transverse normal of the beam. Hence, it is expected that extending the present formulation to allow for the deformation of the transverse normal would also yield results that compare well to experimental results even for multiple impacts. A displacement field suggested by Reddy [5] may be used to derive such a theory. Also, using higher order finite elements that include up to the second derivative of the displacements as degrees of freedom may be used. Sun and Huang [24] showed that the convergence of such elements is much higher than for conventional elements. Such a formulation would also be suited particularly well for the study of wave propagation in composite beams.

References

[1] Raciti, S. and Kapania, R. K., "A Twenty DOF Element for Nonlinear Analysis of Unsymmetrically Laminated Beams," Virginia Polytechnic Institute and State University, CCMS-87-03, 1989.

[2] Pagano, N. J., "Exact Solutions for Composite Laminates in Cylindrical Bending," *Journal of Composite Materials*, 3, pp. 398–411, 1969.

[3] Kapania, R. K. and Raciti, S., "Recent Advances in Analysis of Laminated Beams and Plates, Part I: Shear Effects and Buckling," *AIAA Journal*, 27, no. 7, pp. 923–935, 1989.

[4] Reddy, J. N., "A Simple Higher-Order Theory for Laminated Composite Plates," *Journal of Applied Mechanics*, 51, pp. 745–752, 1984.

[5] Reddy, J. N., "A General Non-Linear Third-Order Theory of Plates with Moderate Thickness," *International Journal of Nonlinear Mechanics*, 25, no. 6, pp. 677 – 686, 1990.

[6] Bhaskar, K. and Varadan, T. K., "Refinement of Higher-Order Laminated Plate Theories," *AIAA Journal*, 27, no. 12, pp. 1830–1831, 1989.

[7] Savithri, S. and Varadan, T. K., "Accurate Bending Analysis of Laminated Orthotropic Plates," *AIAA Journal*, 28, no. 10, pp. 1842–1844, 1990.

[8] Heyliger, P. R. and Reddy, J. N., "A Higher Order Beam Finite Element for Bending and Vibration Problems," *Journal of Sound and Vibration*, 126, no. 2, pp. 309–326, 1988.

[9] Ghazavi, A. and Gordaninejad, F., "Nonlinear Bending of Thick Beams Laminated from Bimodular Composite Materials," *Composite Science and Technology*, 36, pp. 289 – 298, 1989.

[10] Gordaninejad, F. and Ghazavi, A., "Effect of Shear Deformation on Bending of Laminated Composite Beams," *Journal of Pressure Vessel Technology*, 111, pp. 159–164, 1989.

[11] Kant, T. and Manjunatha, B. S., "Higher-Order Theories for Symmetric and Unsymmetric Fiber Reinforced Composite Beams with C^0 Finite Elements," *Finite Elements in Analysis and Design*, 6, pp. 303–320, 1990.

[12] Kant, T. and Patil, H. S., "Buckling Loads of Sandwich Columns with a Higher-Order Theory," *Journal of Reinforced Plastics and Composites*, 10, pp. 102 – 109, 1991.

[13] Chandrashekhara, K., Krishnamurthy, K. and Roy, S., "Free Vibration of Composite Beams Including Rotary Inertia and Shear Deformation," *Composite Structures*, 14, pp. 269 – 279, 1990.

[14] Chen, A. T. and Yang, T. Y., "Static and Dynamic Formulation of a Symmetricaly Laminated Beam Finite Element for a Microcomputer," *Journal of Composite Materials*, 19, pp. 459 – 475, 1985.

[15] Singh, G., Rao, G. V. and Iyengar, N. G. R., "Analysis of the Nonlinear Vibration of Unsymmetrically Laminated Composite Beams.," *AIAA Journal*, 29, no. 10, pp. 1727 – 1735, 1991.

[16] Sun, C. T. and Chin, H., "Analysis of Asymmetric Composite Laminates," *AIAA Journal*, 26, no. 6, pp. 714 –718, 1988.

[17] Sensmeier, M. D., Griffen,Jr., O. H. and Johnson, E. R., "Static and Dynamic Large Deflection Flexural Response of Graphite-Epoxy Beams," Virginia Polytechnic Institute and State University, CCMS-87-07, 1987.

[18] Reddy, J. N., "Geometrically Nonlinear Transient Analysis of Laminated Composite Plates," *AIAA Journal*, 21, no. 4, pp. 621–629, 1983.

[19] Kapania, R. K. and Raciti, S., "Recent Advances in Analysis of Laminated Beams and Plates, Part II: Vibrations and Wave Propagation," *AIAA Journal*, 27, no. 7, pp. 935–946, 1989.

[20] Abrate, S., "Impact on Laminatd Composite Materials," *Applied Mechanics Review*, 44, no. 4, pp. 155–190, April 1991.

[21] Reddy, J. N., "Finite Element Analysis," to be presented at Lecture Notes, 1991.

[22] Zienkiewicz, O. C., *The Finite Element Method.* New York, NY, McGraw-Hill, 1977.

[23] IMSL Math/Library, FORTRAN Subroutines for Mathematical Applications, Version 1.1, Houston, Texas, 1989.

[24] Sun, C. T. and Huang, S. N., "Transverse Impact Problems by Higher Order Beam Finite Element," *Computers & Structures*, 5, pp. 297–303, 1975.

[25] Barnhart, K. E. and Goldsmith, W., "Stresses in Beams During Transverse Impact," *Journal of Applied Mechanics*, 24, pp. 440–446, 1957.

[26] Bonanni, D. L., Johnson, E. R. and Starnes, J. H., "Local Buckling and Crippling of Composite Stiffener Sections," Virginia Polytechnic Institute and State University, CCMS-89-20, 1989.

[27] Byun, C. and Kapania, R. K., "Prediction of Interlaminar Stresses in Laminated Plates Using Global Orthogonal Interpolation Polynomials," to be presented at 13th Winter Annual Meeting, ASME, Atlanta, Georgia , Dec. 2 -5,1991.

[28] Jones, R. M., *Mechanics of Composite Materials.* New York, NY, Hemisphere Publishing Corporation, 1975.

[29] Senthilnathan, N. R., Lim, S. P., Lee, K. H. and Chow, S. T., "Buckling of Shear-Deformable Plates," *AIAA Journal*, 25, no. 9, pp. 1268 – 1271, 1987.

[30] Vinson, J. R. and Sierakowsky, R. L., *The Behaviour of Structures Composed of Composite Materials.* Boston, Martinus Nijhoff Publishers, 1986.

[31] Wu, X. X. and Sun, C. T., "Vibration Analysis of Laminated Composite Thin-Walled Beams Using Finite Elements," *AIAA Journal*, 29, no. 5, pp. 736 – 742, 1991.

[32] Reddy, J. N., *An Introduction to the Finite Element Method.* New York, NY, McGraw-Hill, 1984.

[33] Varadan, T. K., Personal Communications, April 1991.

[34] Yuan, F. G. and Miller, R. E., "A Higher Order Finite Element for Laminated Beams," *Composite Structures*, 14, pp. 125–150, 1990.

[35] Abarcar, R. B. and Cunniff, P. F., "The Vibration of Cantilever Beams of Fiber Reinforced Material," *Journal of Composite Materials*, 6, pp. 504 – 517, 1972.

[36] Thornton, E. A., "Free Vibration of Unsymmetrically Laminated Cantilevered Composite Panels," *Shock Vibr. Bull.* , Pt.2, pp. 79 – 88, 1976.

[37] Harris, C. M. and Crede, C. E., Eds., *Shock and Vibration Handbook*, vol. 1. New York, NY: McGraw-Hill, 1961.

[38] Goldsmith, W., *Impact.* London, Edward Arnold, 1960.

[39] Nosier, A., Kapania, R. K. and Reddy, J. N., "Efficient Impact Analysis of Laminated Structures," Virginia Polytechnic Institute and State University, preprint, 1991 .

[40] Sankar, B. V. and Sun, C. T., "Low-Velocity Impact Response of Laminated Beams Subjected to Initial Stresses," *AIAA Journal*, 23, no. 12, pp. 1962–1969, 1985.

Appendix: Finite Element Equations and Element Matrices

The finite element equations may be written as

$$[M]\{\ddot{a}\} + [K(a)]\{a\} = \{F\}$$

where

$$[K(a)] = [K_L] + [K_{NL}(a)] + [K_s].$$

$[K_L]$ is the linear stiffness matrix,

$[K_{NL}(a)]$ is the nonlinear stiffness matrix, and

$[K_s]$ is the initial stress matrix.

Substituting the nodal displacement vector

$$\{a\}^T = \{\{u\}, \{\beta\}, \{w_b\}, \{w_s\}, \{\mathcal{T}_b\}, \{\mathcal{T}_s\}\}$$

this equation can be rewritten as

$$\begin{bmatrix} [0] & [0] & [0] & [0] & [0] & [0] \\ [0] & [0] & [0] & [0] & [0] & [0] \\ [0] & [0] & [M^{33}] & [M^{34}] & [0] & [0] \\ [0] & [0] & [M^{43}] & [M^{44}] & [0] & [0] \\ [0] & [0] & [0] & [0] & [M^{55}] & [M^{56}] \\ [0] & [0] & [0] & [0] & [M^{65}] & [M^{66}] \end{bmatrix} \begin{Bmatrix} \{\ddot{u}\} \\ \{\ddot{\beta}\} \\ \{\ddot{w}_b\} \\ \{\ddot{w}_s\} \\ \{\ddot{\mathcal{T}}_b\} \\ \{\ddot{\mathcal{T}}_s\} \end{Bmatrix}$$

$$+ \begin{bmatrix} [K^{11}] & [K^{12}] & [K^{13}] & [K^{14}] & [K^{15}] & [K^{16}] \\ [K^{21}] & [K^{22}] & [K^{23}] & [K^{24}] & [K^{25}] & [K^{26}] \\ [K^{31}] & [K^{32}] & [K^{33}] & [K^{34}] & [K^{35}] & [K^{36}] \\ [K^{41}] & [K^{42}] & [K^{43}] & [K^{44}] & [K^{45}] & [K^{46}] \\ [K^{51}] & [K^{52}] & [K^{53}] & [K^{54}] & [K^{55}] & [K^{56}] \\ [K^{61}] & [K^{62}] & [K^{63}] & [K^{64}] & [K^{65}] & [K^{66}] \end{bmatrix} \begin{Bmatrix} \{u\} \\ \{\beta\} \\ \{w_b\} \\ \{w_s\} \\ \{\mathcal{T}_b\} \\ \{\mathcal{T}_s\} \end{Bmatrix} = \begin{Bmatrix} \{F^1\} \\ \{F^2\} \\ \{F^3\} \\ \{F^4\} \\ \{F^5\} \\ \{F^6\} \end{Bmatrix}.$$

The explicit expressions for the element submatrices are given below.

Element Mass Matrix

$$M_{ij}^{33} = \int_{\ell_e} RH_iH_j\,dx + \int_{\ell_e} I\frac{dH_i}{dx}\frac{dH_j}{dx}\,dx$$

$$M_{ij}^{34} = M_{ij}^{43} = \int_{\ell_e} RH_iH_j\,dx + \int_{\ell_e} S\frac{dH_i}{dx}\frac{dH_j}{dx}\,dx$$

$$M_{ij}^{44} = \int_{\ell_e} RH_iH_j\,dx + \int_{\ell_e} T\frac{dH_i}{dx}\frac{dH_j}{dx}\,dx$$

$$M_{ij}^{55} = \int_{\ell_e} RH_iH_j\,dx$$

$$M_{ij}^{56} = M_{ij}^{65} = \int_{\ell_e} SH_iH_j\,dx$$

$$M_{ij}^{66} = \int_{\ell_e} TH_iH_j\,dx$$

where

$$(R, I, S, T) = \int_h \rho\,(1, z^2, \frac{4z^4}{3h^2}, \frac{16z^6}{9h^4})\,dz$$

Linear Element Stiffness Matrix

$$(K_{ij}^{11})_L = \int_{le} D_{11}\frac{dH_i}{dx}\frac{dH_j}{dx}\,dx$$

$$(K_{ij}^{12})_L = (K_{ij}^{21})_L = \int_{le} D_{12}\frac{dH_i}{dx}\frac{dH_j}{dx}\,dx$$

$$(K_{ij}^{13})_L = (K_{ji}^{31})_L = -\int_{le} D_{13}\frac{dH_i}{dx}\frac{d^2H_j}{dx^2}\,dx$$

$$(K_{ij}^{14})_L = (K_{ji}^{41})_L = -\int_{le} D_{15} \frac{dH_i}{dx} \frac{d^2H_j}{dx^2}\, dx$$

$$(K_{ij}^{15})_L = (K_{ji}^{51})_L = -2\int_{le} D_{14} \frac{dH_i}{dx} \frac{dH_j}{dx}\, dx$$

$$(K_{ij}^{16})_L = (K_{ji}^{61})_L = -2\int_{le} D_{16} \frac{dH_i}{dx} \frac{dH_j}{dx}\, dx$$

$$(K_{ij}^{22})_L = \int_{le} D_{22} H_i H_j\, dx$$

$$(K_{ij}^{23})_L = (K_{ji}^{32})_L = -\int_{le} D_{23} H_i \frac{d^2H_j}{dx^2}\, dx$$

$$(K_{ij}^{24})_L = (K_{ji}^{42})_L = -\int_{le} D_{25} H_i \frac{d^2H_j}{dx^2}\, dx$$

$$(K_{ij}^{25})_L = (K_{ji}^{52})_L = -2\int_{le} D_{24} H_i \frac{dH_j}{dx}\, dx$$

$$(K_{ij}^{26})_L = (K_{ji}^{62})_L = -2\int_{le} D_{26} H_i \frac{dH_j}{dx}\, dx$$

$$(K_{ij}^{33})_L = \int_{le} D_{33} \frac{d^2H_i}{dx^2} \frac{d^2H_j}{dx^2}\, dx$$

$$(K_{ij}^{34})_L = (K_{ji}^{43})_L = \int_{le} D_{35} \frac{d^2H_i}{dx^2} \frac{d^2H_j}{dx^2}\, dx$$

$$(K_{ij}^{35})_L = (K_{ji}^{53})_L = 2\int_{le} D_{34} \frac{d^2H_i}{dx^2} \frac{dH_j}{dx}\, dx$$

$$(K_{ij}^{36})_L = (K_{ji}^{63})_L = 2\int_{le} D_{36} \frac{d^2H_i}{dx^2} \frac{dH_j}{dx}\, dx$$

$$(K_{ij}^{44})_L = \int_{le} D_{55} \frac{d^2H_i}{dx^2} \frac{d^2H_j}{dx^2}\, dx + \int_{le} D_{77} \frac{dH_i}{dx} \frac{dH_j}{dx}\, dx$$

$$(K_{ij}^{45})_L = (K_{ji}^{54})_L = 2\int_{le} D_{45} \frac{d^2H_i}{dx^2} \frac{dH_j}{dx}\, dx$$

$$(K_{ij}^{46})_L = (K_{ji}^{64})_L = 2\int_{le} D_{56}\frac{d^2H_i}{dx^2}\frac{dH_j}{dx}\,dx$$

$$(K_{ij}^{55})_L = 4\int_{le} D_{44}\frac{dH_i}{dx}\frac{dH_j}{dx}\,dx$$

$$(K_{ij}^{56})_L = (K_{ji}^{65})_L = 4\int_{le} D_{46}\frac{dH_i}{dx}\frac{dH_j}{dx}\,dx$$

$$(K_{ij}^{66})_L = 4\int_{le} D_{66}\frac{dH_i}{dx}\frac{dH_j}{dx}\,dx$$

Nonlinear Element Stiffness Matrix

$$(K_{ij}^{11})_{NL} = (K_{ij}^{12})_{NL} = (K_{ij}^{21})_{NL} = (K_{ij}^{22})_{NL} = 0$$

$$(K_{ij}^{13})_{NL} = 0.5(K_{ji}^{31})_{NL} = 0.5\int_h (D_{11}\frac{dw_0}{dx} + D_{12}\mathcal{T}_0)\frac{dH_i}{dx}\frac{dH_j}{dx}\,dx$$

$$(K_{ij}^{14})_{NL} = 0.5(K_{ji}^{41})_{NL} = (K_{ij}^{13})_{NL}$$

$$(K_{ij}^{15})_{NL} = 0.5(K_{ji}^{51})_{NL} = 0.5\int_h D_{12}\frac{dw_0}{dx}\frac{dH_i}{dx}H_j\,dx$$

$$(K_{ij}^{16})_{NL} = 0.5(K_{ji}^{61})_{NL} = (K_{ij}^{15})_{NL}$$

$$(K_{ij}^{23})_{NL} = 0.5(K_{ji}^{32})_{NL} = 0.5\int_h (D_{12}\frac{dw_0}{dx} + D_{22}\mathcal{T}_0)H_i\frac{dH_j}{dx}\,dx$$

$$(K_{ij}^{24})_{NL} = 0.5(K_{ji}^{42})_{NL} = (K_{ij}^{23})_{NL}$$

$$(K_{ij}^{25})_{NL} = 0.5(K_{ji}^{52})_{NL} = 0.5\int_h D_{22}\frac{dw_0}{dx}H_iH_j\,dx$$

$$(K_{ij}^{26})_{NL} = 0.5(K_{ji}^{62})_{NL} = (K_{ij}^{25})_{NL}$$

$$(K_{ij}^{33})_{NL} = 0.5 \int_{\ell_e} \left(D_{11}\left(\frac{dw_0}{dx}\right)^2 + 2D_{12}\frac{dw_0}{dx}\mathcal{T}_0 + D_{22}(\mathcal{T}_0)^2\right)\frac{dH_i}{dx}\frac{dH_j}{dx}\,dx -$$

$$0.5 \int_{\ell_e} (D_{13}\frac{dw_0}{dx} + D_{23}\mathcal{T}_0)\,(\frac{d^2H_i}{dx^2}\frac{dH_j}{dx} + 2\frac{dH_i}{dx}\frac{d^2H_j}{dx^2})\,dx$$

$$(K_{ij}^{34})_{NL} = 0.5 \int_{\ell_e} \left(D_{11}\left(\frac{dw_0}{dx}\right)^2 + 2D_{12}\frac{dw_0}{dx}\mathcal{T}_0 + D_{22}(\mathcal{T}_0)^2\right)\frac{dH_i}{dx}\frac{dH_j}{dx}\,dx -$$

$$0.5 \int_{\ell_e} \left((D_{13}\frac{dw_0}{dx} + D_{23}\mathcal{T}_0)\frac{d^2H_i}{dx^2}\frac{dH_j}{dx} + 2(D_{15}\frac{dw_0}{dx} + D_{25}\mathcal{T}_0)\frac{dH_i}{dx}\frac{d^2H_j}{dx^2}\right)dx$$

$$(K_{ij}^{35})_{NL} = 0.5 \int_{\ell_e} \left((D_{12}\frac{dw_0}{dx} + D_{22}\mathcal{T}_0)\frac{dw_0}{dx}\frac{dH_i}{dx}H_j - D_{23}\frac{dw_0}{dx}\frac{d^2H_i}{dx^2}H_j\right)dx -$$

$$2 \int_{\ell_e} (D_{14}\frac{dw_0}{dx} + D_{24}\mathcal{T}_0)\frac{dH_i}{dx}\frac{dH_j}{dx}\,dx$$

$$(K_{ij}^{36})_{NL} = 0.5 \int_{\ell_e} \left((D_{12}\frac{dw_0}{dx} + D_{22}\mathcal{T}_0)\frac{dw_0}{dx}\frac{dH_i}{dx}H_j - D_{23}\frac{dw_0}{dx}\frac{d^2H_i}{dx^2}H_j\right)dx -$$

$$2 \int_{\ell_e} (D_{16}\frac{dw_0}{dx} + D_{26}\mathcal{T}_0)\frac{dH_i}{dx}\frac{dH_j}{dx}\,dx$$

$$(K_{ij}^{43})_{NL} = 0.5 \int_{\ell_e} \left(D_{11}\left(\frac{dw_0}{dx}\right)^2 + 2D_{12}\frac{dw_0}{dx}\mathcal{T}_0 + D_{22}(\mathcal{T}_0)^2\right)\frac{dH_i}{dx}\frac{dH_j}{dx}\,dx -$$

$$0.5 \int_{\ell_e} \left((D_{15}\frac{dw_0}{dx} + D_{25}\mathcal{T}_0)\frac{d^2H_i}{dx^2}\frac{dH_j}{dx} + 2(D_{13}\frac{dw_0}{dx} + D_{23}\mathcal{T}_0)\frac{dH_i}{dx}\frac{d^2H_j}{dx^2}\right)dx$$

$$(K_{ij}^{44})_{NL} = 0.5 \int_{\ell_e} \left(D_{11}\left(\frac{dw_0}{dx}\right)^2 + 2D_{12}\frac{dw_0}{dx}\mathcal{T}_0 + D_{22}(\mathcal{T}_0)^2\right)\frac{dH_i}{dx}\frac{dH_j}{dx}\,dx -$$

$$0.5 \int_{\ell_e} (D_{15}\frac{dw_0}{dx} + D_{25}\mathcal{T}_0)\,(\frac{d^2H_i}{dx^2}\frac{dH_j}{dx} + 2\frac{dH_i}{dx}\frac{d^2H_j}{dx^2})\,dx$$

$$(K_{ij}^{45})_{NL} = 0.5 \int_{\ell_e} \left((D_{12} \frac{dw_0}{dx} + D_{22} \mathcal{T}_0) \frac{dw_0}{dx} \frac{dH_i}{dx} H_j - D_{25} \frac{dw_0}{dx} \frac{d^2 H_i}{dx^2} H_j \right) dx -$$

$$2 \int_{\ell_e} (D_{14} \frac{dw_0}{dx} + D_{24} \mathcal{T}_0) \frac{dH_i}{dx} \frac{dH_j}{dx} \, dx$$

$$(K_{ij}^{46})_{NL} = 0.5 \int_{\ell_e} \left((D_{12} \frac{dw_0}{dx} + D_{22} \mathcal{T}_0) \frac{dw_0}{dx} \frac{dH_i}{dx} H_j - D_{25} \frac{dw_0}{dx} \frac{d^2 H_i}{dx^2} H_j \right) dx -$$

$$2 \int_{\ell_e} (D_{16} \frac{dw_0}{dx} + D_{26} \mathcal{T}_0) \frac{dH_i}{dx} \frac{dH_j}{dx} \, dx$$

$$(K_{ij}^{53})_{NL} = 0.5 \int_{\ell_e} \left((D_{12} \frac{dw_0}{dx} + D_{22} \mathcal{T}_0) \frac{dw_0}{dx} H_i \frac{dH_j}{dx} - 2 D_{23} \frac{dw_0}{dx} H_i \frac{d^2 H_j}{dx^2} \right) dx -$$

$$\int_{\ell_e} (D_{14} \frac{dw_0}{dx} + D_{24} \mathcal{T}_0) \frac{dH_i}{dx} \frac{dH_j}{dx} \, dx$$

$$(K_{ij}^{54})_{NL} = 0.5 \int_{\ell_e} \left((D_{12} \frac{dw_0}{dx} + D_{22} \mathcal{T}_0) \frac{dw_0}{dx} H_i \frac{dH_j}{dx} - 2 D_{25} \frac{dw_0}{dx} H_i \frac{d^2 H_j}{dx^2} \right) dx -$$

$$\int_{\ell_e} (D_{14} \frac{dw_0}{dx} + D_{24} \mathcal{T}_0) \frac{dH_i}{dx} \frac{dH_j}{dx} \, dx$$

$$(K_{ij}^{55})_{NL} = \int_{\ell_e} \left(- D_{24} \frac{dw_0}{dx} \left(\frac{dH_i}{dx} H_j + 2 H_i \frac{dH_j}{dx} \right) + 0.5 D_{22} \left(\frac{dw_0}{dx} \right)^2 H_i H_j \right) dx$$

$$(K_{ij}^{56})_{NL} = - \int_{\ell_e} \left(\frac{dw_0}{dx} \left(D_{24} \frac{dH_i}{dx} H_j + 2 D_{26} H_i \frac{dH_j}{dx} \right) - 0.5 D_{22} \left(\frac{dw_0}{dx} \right)^2 H_i H_j \right) dx$$

$$(K_{ij}^{63})_{NL} = 0.5 \int_{\ell_e} \left((D_{12} \frac{dw_0}{dx} + D_{22} \mathcal{T}_0) \frac{dw_0}{dx} H_i \frac{dH_j}{dx} - 2 D_{23} \frac{dw_0}{dx} H_i \frac{d^2 H_j}{dx^2} \right) dx -$$

$$\int_{\ell_e} (D_{16} \frac{dw_0}{dx} + D_{26} \mathcal{T}_0) \frac{dH_i}{dx} \frac{dH_j}{dx} \, dx$$

$$(K_{ij}^{64})_{NL} = 0.5 \int_{\ell_e} \left((D_{12}\frac{dw_0}{dx} + D_{22}\mathcal{T}_0)\frac{dw_0}{dx} H_i \frac{dH_j}{dx} - 2D_{25}\frac{dw_0}{dx} H_i \frac{d^2H_j}{dx^2} \right) dx -$$

$$\int_{\ell_e} (D_{16}\frac{dw_0}{dx} + D_{26}\mathcal{T}_0)\frac{dH_i}{dx}\frac{dH_j}{dx}\, dx$$

$$(K_{ij}^{65})_{NL} = -\int_{\ell_e} \left(\frac{dw_0}{dx}(D_{26}\frac{dH_i}{dx}H_j + 2D_{24}H_i\frac{dH_j}{dx}) - 0.5D_{22}\left(\frac{dw_0}{dx}\right)^2 H_iH_j \right) dx$$

$$(K_{ij}^{66})_{NL} = \int_{\ell_e} \left(-D_{26}\frac{dw_0}{dx}(\frac{dH_i}{dx}H_j + 2H_i\frac{dH_j}{dx}) + 0.5D_{22}\left(\frac{dw_0}{dx}\right)^2 H_iH_j \right) dx$$

Initial Stress Matrix

$$(K_{ij}^{\alpha\beta})_s = \int_{\ell_e} p(x)\frac{dH_i}{dx}\frac{dH_j}{dx}\, dx \qquad \alpha, \beta = 3, 4$$

All other submatrices are zero.

Tangential Stiffness Matrix

$$(K_{ij}^{11})^{Tan} = (K_{ij}^{11})_L$$

$$(K_{ij}^{12})^{Tan} = (K_{ij}^{12})_L$$

$$(K_{ij}^{13})^{Tan} = (K_{ji}^{31})^{Tan} = (K_{ij}^{13})_L + 2(K_{ij}^{13})_{NL}$$

$$(K_{ij}^{14})^{Tan} = (K_{ji}^{41})^{Tan} = (K_{ij}^{14})_L + 2(K_{ij}^{14})_{NL}$$

$$(K_{ij}^{15})^{Tan} = (K_{ji}^{51})^{Tan} = (K_{ij}^{15})_L + 2(K_{ij}^{15})_{NL}$$

$$(K_{ij}^{16})^{Tan} = (K_{ji}^{61})^{Tan} = (K_{ij}^{16})_L + 2(K_{ij}^{16})_{NL}$$

$$(K_{ij}^{22})^{Tan} = (K_{ij}^{22})_L$$

$$(K_{ij}^{23})^{Tan} = (K_{ji}^{32})^{Tan} = (K_{ij}^{23})_L + 2(K_{ij}^{23})_{NL}$$

$$(K_{ij}^{24})^{Tan} = (K_{ji}^{42})^{Tan} = (K_{ij}^{24})_L + 2(K_{ij}^{24})_{NL}$$

$$(K_{ij}^{25})^{Tan} = (K_{ji}^{52})^{Tan} = (K_{ij}^{25})_L + 2(K_{ij}^{25})_{NL}$$

$$(K_{ij}^{26})^{Tan} = (K_{ji}^{62})^{Tan} = (K_{ij}^{26})_L + 2(K_{ij}^{26})_{NL}$$

$$(K_{ij}^{33})^{Tan} = (K_{ij}^{33})_L + (K_{ij}^{33})_s +$$

$$\int_{\ell_e} \left(N_x + D_{11}\left(\frac{dw_0}{dx}\right)^2 + 2D_{12}\frac{dw_0}{dx}\mathcal{T}_0 + D_{22}(\mathcal{T}_0)^2\right)\frac{dH_i}{dx}\frac{dH_j}{dx}\,dx -$$

$$\int_{\ell_e} (D_{13}\frac{dw_0}{dx} + D_{23}\mathcal{T}_0)(\frac{d^2H_i}{dx^2}\frac{dH_j}{dx} + \frac{dH_i}{dx}\frac{d^2H_j}{dx^2})\,dx$$

$$(K_{ij}^{34})^{Tan} = (K_{ji}^{43})^{Tan} = (K_{ij}^{34})_L + (K_{ij}^{34})_s +$$

$$\int_{\ell_e} \left(N_x + D_{11}\left(\frac{dw_0}{dx}\right)^2 + 2D_{12}\frac{dw_0}{dx}\mathcal{T}_0 + D_{22}(\mathcal{T}_0)^2\right)\frac{dH_i}{dx}\frac{dH_j}{dx}\,dx -$$

$$\int_{\ell_e} (D_{13}\frac{dw_0}{dx} + D_{23}\mathcal{T}_0)\frac{d^2H_i}{dx^2}\frac{dH_j}{dx} + (D_{15}\frac{dw_0}{dx} + D_{25}\mathcal{T}_0)\frac{dH_i}{dx}\frac{d^2H_j}{dx^2})\,dx$$

$$(K_{ij}^{35})^{Tan} = (K_{ji}^{53})^{Tan} = (K_{ij}^{35})_L +$$

$$\int_{\ell_e} \left(N_{xy} + +\left((D_{12}\frac{dw_0}{dx} + D_{22}\mathcal{T}_0)\frac{dw_0}{dx}\right)\frac{dH_i}{dx}H_j\,dx -\right.$$

$$\int_{\ell_e} \left(D_{23}\frac{dw_0}{dx}\frac{d^2H_i}{dx^2}H_j + 2(D_{14}\frac{dw_0}{dx} + D_{24}\mathcal{T}_0)\frac{dH_i}{dx}\frac{dH_j}{dx}\right)\,dx$$

$$(K_{ij}^{36})^{Tan} = (K_{ji}^{63})^{Tan} = (K_{ij}^{36})_L +$$

$$\int_{\ell_e} \left(N_{xy} + \left((D_{12}\frac{dw_0}{dx} + D_{22}\mathcal{T}_0)\frac{dw_0}{dx}\right)\frac{dH_i}{dx}H_j\,dx -\right.$$

$$\int_{\ell_e} \left(D_{23}\frac{dw_0}{dx}\frac{d^2H_i}{dx^2}H_j + (D_{16}\frac{dw_0}{dx} + D_{26}\mathcal{T}_0)\frac{dH_i}{dx}\frac{dH_j}{dx}\right) dx$$

$$(K_{ij}^{44})^{Tan} = (K_{ij}^{44})_L + (K_{ij}^{44})_s +$$

$$\int_{\ell_e} \left(N_x + D_{11}\left(\frac{dw_0}{dx}\right)^2 + 2D_{12}\frac{dw_0}{dx}\mathcal{T}_0 + D_{22}(\mathcal{T}_0)^2\right)\frac{dH_i}{dx}\frac{dH_j}{dx}\,dx -$$

$$\int_{\ell_e} (D_{15}\frac{dw_0}{dx} + D_{25}\mathcal{T}_0)(\frac{d^2H_i}{dx^2}\frac{dH_j}{dx} + \frac{dH_i}{dx}\frac{d^2H_j}{dx^2})\,dx$$

$$(K_{ij}^{45})^{Tan} = (K_{ji}^{54})^{Tan} = (K_{ij}^{45})_L +$$

$$\int_{\ell_e} \left(N_{xy} + +\left((D_{12}\frac{dw_0}{dx} + D_{22}\mathcal{T}_0)\frac{dw_0}{dx}\right)\frac{dH_i}{dx}H_j - D_{25}\frac{dw_0}{dx}\frac{d^2H_i}{dx^2}H_j\,dx -\right.$$

$$2\int_{\ell_e} (D_{14}\frac{dw_0}{dx} + D_{24}\mathcal{T}_0)\frac{dH_i}{dx}\frac{dH_j}{dx}\,dx$$

$$(K_{ij}^{46})^{Tan} = (K_{ji}^{64})^{Tan} = (K_{ij}^{46})_L +$$

$$\int_{\ell_e} \left(N_{xy} + +\left((D_{12}\frac{dw_0}{dx} + D_{22}\mathcal{T}_0)\frac{dw_0}{dx}\right)\frac{dH_i}{dx}H_j - D_{25}\frac{dw_0}{dx}\frac{d^2H_i}{dx^2}H_j\,dx -\right.$$

$$2\int_{\ell_e} (D_{16}\frac{dw_0}{dx} + D_{26}\mathcal{T}_0)\frac{dH_i}{dx}\frac{dH_j}{dx}\,dx$$

$$(K_{ij}^{55})^{Tan} = (K_{ij}^{55})_L + \int_{\ell_e} \left(D_{22}\left(\frac{dw_0}{dx}\right)^2 H_iH_j - 2D_{24}\frac{dw_0}{dx}(H_i\frac{dH_j}{dx} + \frac{dH_i}{dx}H_j)\right) dx$$

$$(K_{ij}^{56})^{Tan} = (K_{ji}^{65})^{Tan} = (K_{ij}^{56})_L +$$

$$\int_{\ell_e} \left(D_{22}\left(\frac{dw_0}{dx}\right)^2 H_iH_j - 2\frac{dw_0}{dx}(D_{24}\frac{dH_i}{dx}H_j + D_{26}H_i\frac{dH_j}{dx})\right) dx$$

$$(K_{ij}^{66})^{Tan} = (K_{ij}^{66})_L + \int_{\ell_e} \left(D_{22}\left(\frac{dw_0}{dx}\right)^2 H_iH_j - 2D_{26}\frac{dw_0}{dx}(H_i\frac{dH_j}{dx} + \frac{dH_i}{dx}H_j)\right) dx$$

VITA

The author was born on May 5, 1965 in Hannover, Germany. He graduated from the Christophorus Gymnasium in Braunschweig, Germany, in June 1985. After completing his military service in September 1986, he began his engineering studies at the TU Braunschweig, Germany, where he received the Vordiplom in October 1988. Between October 1988 and August 1989 he studied aerospace engineering at the TU Braunschweig. In September 1989 he transferred to the Department of Aerospace and Ocean Engineering at Virginia Polytechnic Institute and State University, USA, where he completed his studies towards the Master of Science in December 1991.